Icarus **156**, 76–106 (2002)
doi:10.1006/icar.2001.6758, available online at http://www.idealibrary.com on IDEAL®

Photochemistry of a Volcanically Driven Atmosphere on Io: Sulfur and Oxygen Species from a Pele-Type Eruption

Julianne I. Moses

Lunar and Planetary Institute, 3600 Bay Area Blvd., Houston, Texas 77058-1113
E-mail: moses@lpi.usra.edu

Mikhail Yu. Zolotov

Department of Earth and Planetary Sciences, Washington University CB1169, One Brookings Drive, St. Louis, Missouri 63130-4899

and

Bruce Fegley, Jr.

Department of Earth and Planetary Sciences, Planetary Chemistry Laboratory, McDonnell Center for the Space Sciences, Washington University CB1169, One Brookings Drive, St. Louis, Missouri 63130-4899

Received November 15, 2000; revised September 17, 2001

To determine how active volcanism might affect the standard picture of sulfur dioxide photochemistry on Io, we have developed a one-dimensional atmospheric model in which a variety of sulfur-, oxygen-, sodium-, potassium-, and chlorine-bearing volatiles are volcanically outgassed at Io's surface and then evolve due to photolysis, chemical kinetics, and diffusion. Thermochemical equilibrium calculations in combination with recent observations of gases in the Pele plume are used to help constrain the composition and physical properties of the exsolved volcanic vapors. Both thermochemical equilibrium calculations (Zolotov and Fegley 1999, *Icarus* 141, 40–52) and the Pele plume observations of Spencer *et al.* (2000; *Science* 288, 1208–1210) suggest that S_2 may be a common gas emitted in volcanic eruptions on Io. If so, our photochemical models indicate that the composition of Io's atmosphere could differ significantly from the case of an atmosphere in equilibrium with SO_2 frost. The major differences as they relate to oxygen and sulfur species are an increased abundance of S, S_2, S_3, S_4, SO, and S_2O and a decreased abundance of O and O_2 in the Pele-type volcanic models as compared with frost sublimation models. The high observed SO/SO_2 ratio on Io might reflect the importance of a contribution from volcanic SO rather than indicate low eddy diffusion coefficients in Io's atmosphere or low SO "sticking" probabilities at Io's surface; in that case, the SO/SO_2 ratio could be temporally and/or spatially variable as volcanic activity fluctuates. Many of the interesting volcanic species (e.g., S_2, S_3, S_4, and S_2O) are short lived and will be rapidly destroyed once the volcanic plumes shut off; condensation of these species near the source vent is also likely. The diffuse red deposits associated with active volcanic centers on Io may be caused by S_4 radicals that are created and temporarily preserved when sulfur vapor (predominantly S_2) condenses around the volcanic vent. Condensation of SO across the surface and, in particular, in the polar regions might also affect the surface spectral properties. We predict that the S/O ratio in the torus and neutral clouds might be correlated with volcanic activity—during periods when volcanic outgassing of S_2 (or other molecular sulfur vapors) is prevalent, we would expect the escape of sulfur to be enhanced relative to that of oxygen, and the S/O ratio in the torus and neutral clouds could be correspondingly increased. © 2002 Elsevier Science (USA)

Key Words: **Io; photochemistry; atmospheres, composition; volcanism; geochemistry.**

1. INTRODUCTION

Jupiter's satellite Io has one of the most unusual atmospheres in our solar system (see the reviews of Lellouch 1996, Spencer and Schneider 1996), and our understanding of the composition and physical properties of Io's atmosphere has evolved rapidly in the past few years. Recent observations of SO_2, a molecule that has long been known to be present in the ionian atmosphere (Pearl *et al*. 1979), have helped constrain the surface pressure and the degree of atmospheric "patchiness" on Io (Lellouch *et al*. 1990, 1992, Ballester *et al*. 1990, 1994, Sartoretti *et al*. 1994, 1996, Lellouch 1996, Trafton *et al*. 1996, Hendrix *et al*. 1999, McGrath *et al*. 2000). Other molecular constituents such as SO and S_2 have recently been identified on the satellite (Lellouch *et al*. 1996, McGrath *et al*. 2000, Spencer *et al*. 2000), and atomic and molecular emissions from neutral O, S, Na, Cl, H, SO_2 (and/or SO) have been mapped on and about Io's disk from Galileo Orbiter, Hubble Space Telescope (HST), and ground-based observations (e.g., Belton *et al*. 1996; Geissler

0019-1035/02 $35.00

et al. 1999b; Roesler *et al*. 1999; Ballester *et al*. 1999; Bouchez *et al*. 2000; McGrath *et al*. 2000; Feldman *et al*. 2000a; Trafton 2000; Retherford *et al*. 2000a, 2000b; see also the Voyager observations of Cook *et al*. 1981). Continuing Io plasma torus and neutral cloud observations, including the recent detection of Cl^+ and Cl^{++} in the torus (Küppers and Schneider 2000, Schneider *et al*. 2000, Feldman *et al*. 2000b), confirm that Na, K, and Cl in atomic and/or molecular form must be present in Io's atmosphere (e.g., Spencer and Schneider 1996). These observations have refocused attention on the composition and chemistry of Io's atmosphere and on the importance of active volcanism in maintaining that atmosphere.

The three main proposed mechanisms for generating an atmosphere on Io include frost sublimation, surface sputtering, and active volcanism. Although the relative importance of each mechanism is not well understood, both frost sublimation and active volcanism appear to play a role. Wong and Smyth (2000) summarize the evidence for a sublimation-driven component. The role of active volcanism is demonstrated by several aspects of the observations. First, the sulfur dioxide vapor appears to be nonuniformly distributed over Io's surface; the observed patchiness does not have a subsolar latitude dependence nor does it appear to follow the surface SO_2 frost distribution as would be expected from a sublimation-driven atmosphere (e.g., Lellouch *et al*. 1992, 1994, 1996, Sartoretti *et al*. 1994, 1996, Ballester *et al*. 1994, Lellouch 1996, Trafton *et al*. 1996, Hendrix *et al*. 1999, McGrath *et al*. 2000). Second, the observed red shifts and the degree of broadening of the millimeter-wave SO_2 and SO lines suggest that energetic outgassing of gases from volcanic plumes may be responsible for these aspects of the microwave emission (Lellouch *et al*. 1994; see also Ballester *et al*. 1994, Strobel *et al*. 1994, Lellouch 1996). Third, visible-wavelength emissions from what is presumed to be neutral atomic oxygen, atomic sodium, and molecular SO_2 and/or SO were observed on Io when the satellite passed into Jupiter's shadow (e.g., McEwen *et al*. 1998a, Geissler *et al*. 1999b, Bouchez *et al*. 2000; see also the ultraviolet observations of Roesler *et al*. 1999). The correlation of many of the emission features in these eclipse images with known volcanic plumes or other centers of volcanic activity on Io suggests that volcanoes may be a major source of these neutral species (Geissler *et al*. 1999b). Finally, the H Lyman alpha emission observed near high latitudes on Io might be caused by diffuse reflection of the solar Ly α line from Io's surface when the overlying SO_2 atmosphere has collapsed due to condensation (e.g., Roesler *et al*. 1999, Ballester *et al*. 1999, Retherford *et al*. 2000b, Feldman *et al*. 2000a, Trafton 2000, Strobel and Wolven 2001). If so, then the temporal and spatial variability of the emission, combined with its lack of symmetry about the subsolar point (e.g., Roesler *et al*. 1999, Feldman *et al*. 2000a, Trafton 2000), suggest that volcanic sources are important in producing and maintaining Io's SO_2 atmosphere (see also the modeling of Strobel and Wolven 2001).

Although volcanoes clearly play an important role in the generation of an atmosphere on Io, previous photochemical models have concentrated on sublimation-generated or even sputtering-generated atmospheres (e.g., Kumar 1980, 1982, 1984, 1985, Summers 1985, Summers and Strobel 1996, Wong and Johnson 1996, Wong and Smyth 2000). The effects of active volcanism on ionian photochemistry have remained relatively unexplored. To determine how volcanic outgassing might affect the standard picture of SO_2 photochemistry on Io, we have developed a simple one-dimensional (1-D) model in which a variety of S-, O-, Na-, K-, Cl-, and H-bearing volatiles are volcanically outgassed from the surface and then evolve due to photolysis and subsequent chemical kinetics. Initial and boundary conditions for the volcanic outgassing are specified (with some modification) from the thermochemical equilibrium calculations of Zolotov and Fegley (2000a) and Fegley and Zolotov (2000). The former used recent HST observations (McGrath *et al*. 2000, Spencer *et al*. 2000) to constrain the temperature, pressure, and speciation of the exsolved sulfur- and oxygen-bearing gases in the vicinity of the Pele volcanic vent, and the latter calculated the equilibrium chemistry of Na-, K-, and Cl-bearing volcanic gases on Io. Eddy and molecular diffusion are assumed to dominate the vertical transport of the atmospheric constituents, and the atmosphere is assumed to be in hydrostatic equilibrium. Although our modeling is designed to represent average atmospheric density conditions within a large-scale quasi-hydrostatic region surrounding an active Pele-type eruption, we do not consider plume dynamics, and our "volcanic" models are thus zeroth-order approximations to the actual situation.

Dynamical studies by Ingersoll *et al*. (1985), Ingersoll (1989), Moreno *et al*. (1991), Wong and Johnson (1995, 1996), Wong and Smyth (2000), and Austin and Goldstein (1996, 2000), along with the observed heterogeneity of Io's atmosphere (e.g., McGrath *et al*. 2000), illustrate that the ionian atmosphere is complex, highly dynamic, and not likely to be in hydrostatic equilibrium. One-dimensional models will not be able to reproduce all the complexities. However, 1-D models are very useful for first-order predictions of the relative abundances of different atmospheric species and for determining the importance of photochemical processing of the volcanic gases. For the first time ever, our photochemical models include sulfur compounds such as S_3, S_4, and S_2O that have been proposed as surface coloring agents on Io (e.g., Nelson and Hapke 1978, Hapke 1979, Smith *et al*. 1979, Sagan 1979, Sill and Clark 1982, Hapke 1989, Spencer *et al*. 1997a) as well as chlorine and potassium compounds that must be available in the atmosphere and/or surface in order to feed the torus and neutral clouds. We also consider a larger variety of sodium-bearing compounds than previous models. The kinetics of such a large number of atmospheric constituents has never been included in multidimensional models due to the large computational expense.

In this paper, we will focus on the photochemistry of neutral sulfur and oxygen species. The results regarding sodium, potassium, and chlorine species will be considered in a companion

paper in this volume (Moses *et al*. 2002; hereafter called Paper 2). We will discuss the important production and loss schemes for the major sulfur- and oxygen-bearing volatiles released from a continuous Pele-like eruption, and we will examine the time-variable behavior of the atmospheric constituents after the volcanic source is turned off or turned on. We will also identify observable quantities that might help distinguish between a sublimation-driven atmosphere and a volcanic atmosphere, and we will discuss the implications of our modeling for the observed composition of Io's atmosphere, surface, neutral clouds, and plasma torus.

2. CONSTRAINTS ON COLUMN ABUNDANCE AND COMPOSITION OF VOLCANIC VAPOR

Sulfur dioxide vapor has been detected in specific plumes or in spatially resolved plume regions on Io by a variety of techniques (e.g., Pearl *et al*. 1979, Sartoretti *et al*. 1994, 1996, Spencer *et al*. 1997b, 2000, Hendrix *et al*. 1999, McGrath *et al*. 2000). Whole-disk observations can also provide information about maximum SO_2 column densities within volcanic plumes (e.g., Lellouch *et al*. 1992, 1994; Ballester *et al*. 1994; Lellouch 1996; Trafton *et al*. 1996). Other gases such as SO (e.g., Lellouch *et al*. 1996, McGrath *et al*. 2000) and S_2 (e.g., Spencer *et al*. 2000) have been identified in Io's atmosphere and/or within specific plume regions.

Based on the above observations, we conclude that typical SO_2 column densities in local atmospheres from large plume eruptions on Io should fall in the range $\sim 2 \times 10^{16}$ to $\sim 5 \times 10^{18}$ cm^{-2}. Other vapors such as S_2, SO, and S are important constituents in the plumes. If heavy ions in the Io plasma torus are supplied by atmospheric sputtering or other atmospheric escape processes (e.g., Spencer and Schneider 1996), then volcanic outgassing of sodium, potassium, and chlorine species might also be important on Io. Gases containing Na, K, or Cl are difficult to observe in Io's near-surface atmosphere, so torus and neutral-cloud or corona observations along with theoretical models of magma conditions are crucial for estimating the relative abundances of these gases.

The composition of an erupting Pele-type plume can be estimated based on the theoretical work of Zolotov and Fegley (2000a), who use thermochemical equilibrium calculations in combination with the simultaneous observations of SO_2, SO, and S in the Pele plume region (McGrath *et al*. 2000) to determine the temperature and oxidation state of the volcanic magma and exsolved volcanic gases at Pele. Their model can represent the true state of the volcanic gases erupting at Pele if the vapor can be assumed to be in thermochemical equilibrium in a high-temperature volcanic conduit and/or lava lake before eruption and if the gas chemistry is quenched rapidly in the vicinity of the vent during the eruption (e.g., Zolotov and Fegley 1998a, 1998b, 1999). The Pele magma temperature of $\sim$1440 K derived by Zolotov and Fegley (2000a) is consistent with the temperatures inferred from Galileo infrared and visible observations of the Pele hot spot (e.g., McEwen *et al*. 1998b, Lopes-Gautier *et al*. 1999, Davies *et al*. 1999, 2000a, 2000b). When combined with information on the S_2/SO_2 ratio in the Pele plume (Spencer *et al*. 2000), the vent pressures can also be constrained; Zolotov and Fegley (2000a) determine that vent pressures at Pele lie within the range $(0.4–2) \times 10^{-5}$ bars.

For our standard model, we assume that (a) the relative elemental abundances of O/S/Na/K/Cl/H in the volcanic gases are $1.521/1.0/0.05/0.005/0.05/10^{-20}$, (b) the magma temperature is 1440 K, and (c) the vent pressure is 6.9×10^{-6} bars (for input to the thermochemical equilibrium code)—these values represent the nominal case for the Pele model of Zolotov and Fegley (2000a), except sodium, potassium, and chlorine have been added to the model based on the thermochemical equilibrium specifications of Fegley and Zolotov (2000). The S/O ratio is constrained by the Pele plume observations of McGrath *et al*. (2000) and Spencer *et al*. (2000), as is described in Zolotov and Fegley (2000a). The relative elemental abundances of Na, Cl, and K are constrained by observations of the Io torus and neutral clouds and by chondritic abundances of S, Na, K, and Cl (see Fegley and Zolotov 2000 for more details). Here, the S/Na ratio of 20 is chosen to be consistent with the estimated relative abundances of sodium and sulfur ions in the Io plasma torus (e.g., Vogt *et al*. 1979, Bagenal and Sullivan 1981, Spencer and Schneider 1996), and chlorine is assumed to be 2% of all the elements based on the torus observations of Küppers and Schneider (2000). Note that these assumptions imply that the sodium abundance is equal to the chlorine abundance. Hydrogen is assumed to be unimportant in our standard model.

The thermochemical equilibrium code is run for the above assumptions regarding gas temperature, vent pressure, and elemental composition (see also Fegley and Zolotov 2000, Zolotov and Fegley 2000a). The resulting thermochemical equilibrium abundances for the different sulfur- and oxygen-bearing atomic and molecular vapor species are shown in Table I under the column labeled "Initial." As was determined by Zolotov and Fegley (2000a), SO_2 is the dominant volcanic vapor under these conditions, followed by S_2, and SO. Other important sulfur and oxygen species from the thermochemical equilibrium model include S, S_2O, S_3, O_2, and O. Alkali and halogen species such as NaCl, Na, KCl, Cl, and K are also important equilibrium constituents (see Paper 2).

Note that our initial volcanic abundances are relevant to a specific set of physical and compositional conditions believed to be representative of Pele-type eruptions (Zolotov and Fegley 2000a). Although S_2 is a major volcanic constituent for a variety of assumptions about pressure and temperatures of the exsolved volcanic gases (Zolotov and Fegley 1999, Fegley and Zolotov 2000), S_2 is not a major constituent under very oxidized conditions (i.e., if O/S $\gtrsim 2$; see Fegley and Zolotov 2000). Our models presented here are thus only relevant to S_2-rich Pele-type volcanism.

3. PHOTOCHEMICAL MODEL

The photochemistry of a sulfur dioxide atmosphere on Io was first investigated by Kumar (1980, 1982, 1984) and Summers (1985). Sodium species were added to some of the later models (e.g., Summers 1985, Kumar 1985, Summers and Strobel 1996, Wong and Smyth 2000). More complex three-dimensional models for Io were developed by Wong and Johnson (1996) and Wong and Smyth (2000) to investigate the simultaneous effects of SO_2 photochemistry and gas transport for a sublimation-driven atmosphere. Here, the most complete photochemical study to date, that of Summers and Strobel (1996), serves as the starting point for our photochemistry reaction list, but we have updated some of the reaction rate coefficients and photolysis cross sections, we have included Cl-, K-, and H-bearing species in the model to help explain several recent observations of the extended Io environment, and we have added other potentially important S-, O-, and Na-bearing species such as S_2O, S_3, S_4, $NaSO_2$, and NaOS that were not included in previous models. Appendix A contains a list of the important sulfur and oxygen reactions in our model. In order to reflect the full possible interaction between the increased number of atmospheric constituents, our reaction list is necessarily much larger than that of Summers and Strobel (1996). Not all the reactions in our model are important in our standard moderate-density model, however, and the discussion in Section 4 and the tables in Appendix A focus on the most important reactions.

To examine the fate of volcanic gases emitted in Pele-type plume eruptions on Io, we use the Caltech/JPL chemical kinetics and diffusion code (e.g., Allen *et al*. 1981) to solve the coupled 1-D continuity equations in spherical geometry for all the proposed constituents in Io's atmosphere (see Appendix A for more details concerning the numerical model and our adopted boundary conditions). Vertical transport proceeds by eddy and molecular diffusion; in our standard model, the eddy diffusion coefficient is fixed at 10^9 cm^2 s^{-1} at all altitudes. Both time-variable and steady-state models are considered.

One of the main inputs to the photochemical model is the assumed temperature and density structure of the atmosphere. As mentioned earlier, our model is designed to represent average conditions within a broad quasi-hydrostatic region centered near an active Pele-type plume. From the observations discussed in Section 2, the total column density of SO_2 within large volcanic plumes on Io or within broader regions assumed to be associated with large volcanic plumes (i.e., for the case of the whole-disk millimeter observations of Lellouch *et al*. 1992 or the regional observations of McGrath *et al*. 2000) appears to be lie in the range $\sim 2 \times 10^{16}$ to 5×10^{18} cm^{-2}, corresponding to SO_2 surface pressures of $\sim$0.4 to 100 nbars. For our standard model, we will adopt an SO_2 column abundance of 8×10^{16} cm^{-2}, which is close to the value derived from the Pele plume observations of Spencer *et al*. (2000) and is in between the values derived from the Pele-region observations of McGrath *et al*. (2000) and the Pele plume observations of Spencer *et al*. (1997b). Because SO_2 is not the only gas present in this model, the total atmospheric column density is $\sim 1.1 \times 10^{17}$ cm^{-2} and the surface pressure is $\sim$2 nbars. We call this model our standard "moderate density" case because it has a total atmospheric density intermediate between the high- and low-density models considered by Summers and Strobel (1996). We also examine the sensitivity of the results to a different atmospheric densities.

To obtain a temperature profile for our moderate-density $\sim$2-nbar atmosphere, we removed the lowest $\sim$4 km of the 3.5×10^{-9} bar model atmosphere of Strobel *et al*. (1994). In the particular model we adopted, Strobel *et al*. (1994) included solar heating, plasma heating, Joule heating, and nonlocal thermodynamic equilibrium cooling in their calculations (see their Fig. 12b). The resulting temperature profile is shown in Fig. 1. To determine a complete altitude–pressure–temperature profile, we assumed that the atmosphere is in hydrostatic equilibrium and that Io has a surface radius of 1815 km and a mass of 8.9354×10^{22} kg. The total atmospheric number density, temperature,

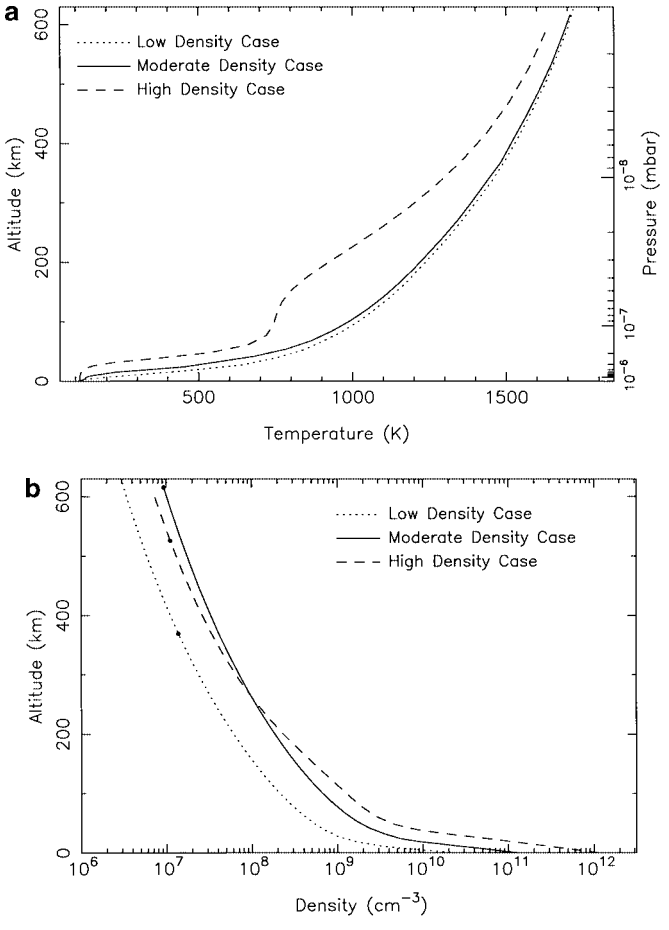

FIG. 1. The (a) temperature and (b) density profiles adopted for our low-density (dotted line), moderate-density (solid line), and high-density (dashed line) model atmospheres. The pressure scale on the right axis in Fig. 1a is for the moderate-density case only. Approximate exobase altitudes are shown in Fig. 1b as circles superimposed upon the density profiles.

and pressure at the surface of this moderate-density model are 1.35×10^{11} cm^{-3}, 113 K, and 2.1×10^{-9} bars, respectively.

For our high-density model, which could represent a region with more prolific outgassing than in our moderate-density model, we adopted the high-density case of Summers and Strobel (1996) (see Fig. 1). This high-density model has a surface number density, temperature, and pressure of 1.14×10^{12} cm^{-3}, 115 K, and 1.8×10^{-8} bars, respectively. For our low-density model, we again adopt a profile modified from Strobel *et al.* (1994). This model has a surface number density, temperature, and pressure of 2.44×10^{10} cm^{-3}, 110 K, and 3.7×10^{-10} bar, respectively (see Fig. 1).

Note that in the Strobel *et al.* (1994) thermal calculations that are adopted here, the moderate-density atmospheric model is warmer than the high-density model throughout the altitude range of interest (see Fig. 1a). Thus, the moderate-density model has a more extended atmosphere with a density at high altitudes that eventually exceeds that of the high-density model. The exobase (or "critical level" for atmospheric escape) is assumed to be located at the altitude where

$$n_c H_c Q K_c = 1, \tag{1}$$

where n_c is the atmospheric number density at this critical level, H_c is the scale height at this critical level, Q is the collisional cross section for the dominant atmospheric constituent ($Q \approx 4 \times 10^{-15}$ cm^{-2}), and K_c is a correction factor to account for atmospheric sphericity (see Chamberlain and Hunten 1987, pp. 340–345). The exobase altitudes are ~370 km, ~616 km, and ~526 km for the low-, moderate-, and high-density cases, respectively (see Fig. 1b). Note, however, that the number densities in our high-temperature upper atmospheres do not vary rapidly with height, and although the concept of a specific exobase level is a useful one, considerable atmospheric escape could occur more than ~100 km below these defined levels.

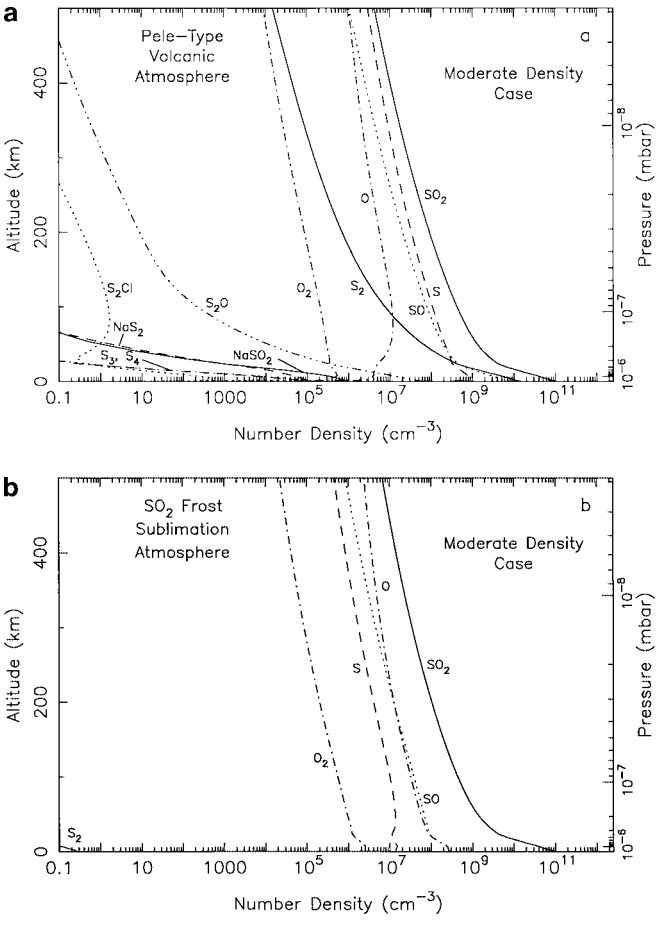

FIG. 2. The concentrations of several important sulfur and oxygen species in (a) our standard moderate-density Pele-type volcanic model (e.g., 2.1-nbar surface pressure, SO_2 column density 8.4×10^{16} cm^{-2}, $K_E = 10^9$ cm^2 s^{-1}) as a function of altitude and pressure, as compared with (b) a moderate-density model in which the atmosphere is generated solely by SO_2 frost sublimation (i.e., no emission of volcanic gases at the lower boundary).

4. MODEL RESULTS

4.1. General Considerations

The solutions to the steady-state continuity equations for the major sulfur and oxygen species in our standard moderate-density Pele-type volcanic model are shown in Fig. 2a, and the column-integrated mixing ratios for the sulfur and oxygen species are provided in Table I. Figure 2b shows the results for a model in which the atmosphere is generated solely by SO_2 frost sublimation (i.e., there is no emission of volcanic gases at the lower boundary) but in which the other important parameters (e.g., eddy diffusion coefficient, atmospheric density, reaction rate coefficients) are the same as in our standard moderate-density volcanic model. In the frost sublimation model, we fix the mixing ratio of SO_2 at the lower boundary to be the same (0.772) as is in our volcanic model; all other species are allowed to diffuse through the lower boundary at their maximum possible rate (see Appendix A). Because we assumed that alkali and halogen compounds are not released when the SO_2 frost sublimes, no alkali and halide species are present in the frost sublimation model. Other differences are readily apparent. The SO_2 frost sublimation model is much simpler—the only important sulfur- and oxygen-bearing constituents are O, O_2, S, SO, and SO_2. Important volcanic species such as S_2 and S_2O do not form readily from SO_2 photolysis under ionian conditions, and S_3 and S_4 formation is also negligible in the sublimation model. The relative abundances of the major species are also different for each of the models, with O much more abundant and S much less abundant in the sublimation model than in the volcanic model. In the discussion below, we focus on the results from our moderate-density Pele-type volcanic model.

Table I demonstrates that photochemistry can dramatically alter the composition of volcanic gases that are initially emitted from a Pele-type volcano. Although S_2 remains the second most abundant gas, photochemical processes have reduced

TABLE I
Abundance Relative to SO_2

Constituent	Initial	Moderate density case	High density case	Low density case
O	5.44×10^{-7}	3.05×10^{-3}	4.52×10^{-4}	4.61×10^{-3}
$O(^1D)$	0.	3.65×10^{-10}	2.94×10^{-11}	1.62×10^{-9}
O_2	5.50×10^{-7}	6.69×10^{-5}	6.78×10^{-6}	1.95×10^{-4}
O_3	1.67×10^{-21}	3.28×10^{-20}	3.30×10^{-21}	6.61×10^{-20}
S	3.18×10^{-3}	4.54×10^{-2}	1.51×10^{-2}	4.63×10^{-2}
S_2	1.43×10^{-1}	1.21×10^{-1}	1.36×10^{-1}	1.18×10^{-1}
S_3	1.59×10^{-6}	4.08×10^{-7}	1.49×10^{-5}	2.83×10^{-7}
S_4	5.53×10^{-11}	3.09×10^{-7}	2.22×10^{-5}	3.50×10^{-8}
S_5	3.50×10^{-16}	3.75×10^{-12}	5.78×10^{-8}	8.49×10^{-14}
S_6	5.79×10^{-20}	9.42×10^{-14}	7.59×10^{-10}	4.39×10^{-16}
S_7	5.01×10^{-24}	8.92×10^{-18}	1.52×10^{-11}	6.24×10^{-21}
S_8	8.67×10^{-29}	6.73×10^{-17}	3.25×10^{-11}	3.36×10^{-20}
$S_{8(con)}$	0.	1.54×10^{-18}	1.10×10^{-12}	4.25×10^{-22}
SO	7.28×10^{-2}	9.12×10^{-2}	7.79×10^{-2}	9.59×10^{-2}
SO_3	9.03×10^{-8}	8.45×10^{-8}	8.66×10^{-8}	8.05×10^{-8}
S_2O	5.82×10^{-4}	3.34×10^{-4}	7.91×10^{-4}	3.09×10^{-4}
$(SO)_2$	0.	5.29×10^{-9}	1.68×10^{-7}	1.73×10^{-10}
ClO	7.43×10^{-12}	3.41×10^{-10}	7.99×10^{-12}	1.48×10^{-10}
SCl	9.40×10^{-9}	3.00×10^{-9}	1.19×10^{-9}	2.35×10^{-9}
SCl_2	1.35×10^{-13}	2.06×10^{-14}	1.67×10^{-14}	3.03×10^{-14}
S_2Cl	8.65×10^{-10}	4.88×10^{-9}	2.95×10^{-7}	1.21×10^{-9}
OSCl	0.	3.73×10^{-9}	2.55×10^{-10}	3.86×10^{-9}
$ClSO_2$	0.	1.79×10^{-8}	2.18×10^{-9}	1.36×10^{-8}
SO_2Cl_2	7.13×10^{-22}	1.52×10^{-13}	2.12×10^{-13}	2.04×10^{-14}
NaO	3.37×10^{-9}	8.56×10^{-10}	7.71×10^{-10}	9.50×10^{-10}
NaO_2	0.	4.81×10^{-13}	5.81×10^{-12}	4.43×10^{-14}
NaS	0.	2.87×10^{-8}	7.75×10^{-7}	1.95×10^{-9}
NaS_2	0.	9.82×10^{-7}	7.19×10^{-5}	3.94×10^{-8}
Na_2S	0.	2.03×10^{-15}	8.17×10^{-12}	2.36×10^{-18}
NaOS	0.	6.33×10^{-7}	3.79×10^{-5}	3.38×10^{-8}
$NaSO_2$	0.	6.72×10^{-6}	3.37×10^{-4}	2.59×10^{-7}
KO	6.24×10^{-11}	1.10×10^{-10}	1.52×10^{-10}	8.51×10^{-11}
KO_2	0.	4.65×10^{-14}	3.93×10^{-13}	3.65×10^{-15}
KS	1.91×10^{-7}	3.57×10^{-8}	2.75×10^{-7}	4.73×10^{-8}
KS_2	0.	1.19×10^{-7}	8.39×10^{-6}	4.15×10^{-9}
KSO_2	0.	7.71×10^{-7}	4.30×10^{-5}	2.37×10^{-8}

Note. Only the most abundant sulfur and oxygen species are included in the table. Mixing ratios represent the column density of the constituent divided by the column density of SO_2. Mixing ratios of 0 in the "Initial" column indicate that the constituent was not included in the thermochemical equilibrium calculations, and the subscript (con) refers to the condensed phase. The SO_2 column density is 8.35×10^{16} cm^{-2} for the moderate-density case, 7.37×10^{17} cm^{-2} for the high-density case, and 1.48×10^{16} cm^{-2} for the low-density case. The total atmospheric column densities are 1.1×10^{17} cm^{-2} for the moderate-density case, 9.6×10^{17} cm^{-2} for the high-density case, and 2.0×10^{16} cm^{-2} for the low-density case.

its overall relative abundance. Photochemistry has also caused large increases in the abundances of S, O, O_2, S_2Cl, and sulfur molecules with four or more atoms, and a small increase in the abundance of SO, which remains the third most abundant gas in the photochemical model. Short-lived radicals such as S_3, S_2O, and KS exhibit mild decreases in abundance in our moderate-density model due to photochemical processes. Although sodium–sulfur and potassium–sulfur species such as $NaSO_2$, NaOS, NaS_2, NaS, KSO_2, and KS_2 were not included in the thermochemical equilibrium calculations due to a lack of information about their thermodynamic properties, we have estimated that these molecules could have photochemical sources (see also Summers and Strobel 1996, Schofield and Steinberg 1992). It is difficult to estimate whether the photochemical abundances of these molecules would be higher or lower than their thermochemical equilibrium abundances. The fact that little (or no) thermodynamic information exists for these molecules suggests that they might be relatively unstable under laboratory conditions; the equilibrium abundances would therefore not be expected to be grossly higher.

Most of the atomic and molecular species in our Pele-type volcanic model are produced photochemically from a small number of "parent" volcanic gases. Important parent molecules for the sulfur and oxygen species include S_2, SO_2, S_2O, SO, S_3, and KS. Because SO_2 is no longer solely responsible for initiating the photochemistry, the sulfur and oxygen photochemistry of a volcanically generated atmosphere on Io is considerably more complex (see Fig. 2) than that of the SO_2 frost sublimation atmospheres considered in the previous photochemical models of Kumar (1980, 1982, 1984), Summers and Strobel (1996), and Wong and Johnson (1996). Figure 3 shows the most important reaction pathways responsible for maintaining the abundances of the major sulfur and oxygen species in our standard Pele-type volcanic model. Most of the photochemical pathways described in Fig. 3 are initiated by the photolysis of S_2 and SO_2.

4.2. *Diatomic Sulfur*

Diatomic sulfur (S_2) is a major volcanic gas in the Pele plume (Spencer *et al*. 2000) and is either the first or second most abundant gas in thermochemical models of ionian volcanic gases

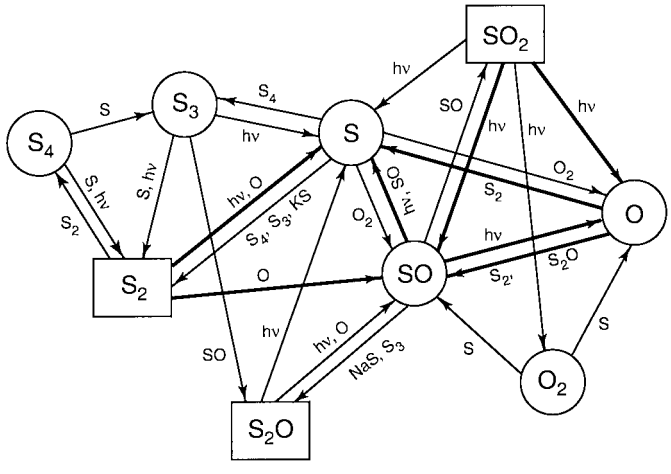

FIG. 3. A schematic diagram illustrating the important reaction pathways for sulfur and oxygen species in our standard moderate-density model. Important "parent" volcanic gases are outlined with rectangles, and "daughter" products are outlined as ovals. Thicker lines indicate more important reactions. The symbol hν corresponds to a solar ultraviolet photon.

(Zolotov and Fegley 1998a, 1998b, 1999, 2000a, Fegley and Zolotov 2000). Although S_2 has been included in some of the previous photochemical models (Kumar 1982, Summers and Strobel 1996), an independent (nonphotochemical) source of S_2 has never been considered, and the dominant previously considered photochemical source ($S + S + M \rightarrow S_2 + M$) is not effective because of the low density of Io's atmosphere (e.g., note that S_2 just barely appears within the density range shown in the lower left corner of Fig. 2b). Therefore, S_2 was at most a minor constituent in previous photochemical models. Our inclusion of a large volcanic source of S_2, along with the subsequent photochemistry initiated by S_2 destruction, is the primary reason for differences between our model and previous photochemical models.

Because of its large photoabsorption cross sections in the 240–310 nm region (R. V. Yelle, S. Langhoff, and H. Partridge, unpublished manuscript entitled "Absorption, photodissociation, and scattering in the $B^3\Sigma_u^- \leftarrow X^3\Sigma_g^+$ band system of S_2," 2000) and its highly reactive nature, S_2 will be very short lived in Io's atmosphere and would quickly be depleted if volcanic sources were not available to replenish it. The short photochemical lifetime for S_2 makes it the most important parent species for the sulfur compounds despite the greater abundance of SO_2 in the initial volcanic gas. In terms of the total column destruction rate, the dominant loss mechanisms for S_2 in our standard moderate-density model are reaction R11 ($S_2 + h\nu \leftarrow 2S$; ~63% of the total loss rate) and reaction R63 ($O + S_2 \leftarrow S + SO$; ~37% of the total loss rate), with reaction R268 ($2S_2 + M \rightarrow S_4 + M$) accounting for the bulk of the remainder (see Table II). The latter reaction (R268) becomes relatively more important in higher-density models and less important in lower-density models. The time scale for photolysis of S_2 in our model atmosphere ranges from ~3 h at the top of the atmosphere to ~4 h near the surface (see also Table A2 in the appendix). Because other loss processes besides photolysis are effective as well (e.g., R63), the overall lifetime of S_2 in our moderate-density model is ~2 h. Any observations of S_2 on Io (e.g., Spencer *et al*. 2000) would provide positive evidence that volcanoes are currently active.

Aside from volcanic activity, which is by far the main source of S_2 in our model, the main reactions that produce S_2 photochemically are recycling reactions (i.e., reactions that were initiated by the chemical destruction of volcanic S_2). However, S_2 is not efficiently recycled and is quickly lost from the atmosphere. The most effective recycling pathways involve other elemental sulfur species (see Table II). Most of the rate coefficients for the reactions that involve interchanges between the various elemental sulfur allotropes have not been measured in the laboratory and were estimated based on the structure of the molecules and on the exothermicity of the reactions.

4.3. Sulfur Dioxide

As in the previous photochemical models of Kumar (1980, 1982, 1984) and Summers and Strobel (1996), sulfur dioxide is lost primarily by photolysis, with the dominant branch being $SO_2 + h\nu \rightarrow SO + O$ (reaction R16; ~98% of the total loss). The other two possible neutral photolysis pathways, $SO_2 + h\nu \rightarrow S + O_2$ (R17) and $SO_2 + h\nu \rightarrow S + 2O$ (R18) account for only ~1% of the total column destruction rate of SO_2, and three-body reactions with K and Na (i.e., R342 and R344) account for ~0.7% of the total destruction rate (see Table II). Sulfur dioxide is produced predominantly by reaction R324 ($2SO \rightarrow SO_2 + S$; ~96% of the total SO_2 column production rate in our moderate-density model), with two-body reactions between sulfur-bearing radicals and $NaSO_2$ (e.g., R280, R339, R255) making up most of the remainder of the SO_2 production rate.

4.4. Sulfur Monoxide

Sulfur monoxide is produced volcanically (e.g., Zolotov and Fegley 1998b) as well as photochemically in our model. The photochemical production of SO results from both reaction of atomic oxygen with volcanic S_2 and from SO_2 photolysis (see Table II). Because S_2 is much more prevalent when active Pele-type volcanoes are present, reaction R63 will cause SO to be more abundant in atmospheres generated from Pele-type volcanic sources than in atmospheres generated from SO_2 frost sublimation. Sulfur monoxide is lost primarily by photodissociation into S + O (e.g., reaction R15; 72% of column loss rate) and by self reaction to form SO_2 and atomic S (i.e., reaction R324; 26% of column loss rate). Other loss processes such as photoionization (reaction R529), charge-exchange reactions (e.g., reaction R636), or reaction with sodium species (e.g., reactions R338 and R339) collectively account for only ~2% of the total column loss rate of SO.

4.5. Disulfur Monoxide

Disulfur monoxide (S_2O) is an important gas that is produced both photochemically and volcanically (see Table II). Volcanic production of S_2O was proposed and qualitatively discussed by Sill and Clark (1982). The thermochemical equilibrium models of Zolotov and Fegley (1998a) show that up to 6% S_2O may be produced in gases emitted by high-temperature silicate magmas on Io. Previous photochemical models have not included this interesting molecule. The photochemistry of S_2O is very uncertain. The molecule absorbs strongly in the 260–340 nm region; however, the photoabsorption cross sections are only known to within a factor of ~10 (Mills 1998). Hapke (1979) and Hapke and Graham (1989) predicted that S_2O would be present on Io due to photochemical schemes similar to the following:

$$3(SO_2 \xrightarrow{h\nu} SO + O) \qquad \text{R16}$$

$$2SO \xrightarrow{M} (SO)_2 \qquad \text{R325}$$

$$SO + (SO)_2 \rightarrow S_2O + SO_2 \qquad \text{R327}$$

$$\text{Net: } 2SO_2 \rightarrow S_2O + 3O, \qquad (2)$$

TABLE II
Important Photochemical Production and Loss Mechanisms

Species		Reaction	Column-integrated rate (cm^{-2} s^{-1})	% of total rate
S_2	Production	R12: $S_3 + h\nu \rightarrow S_2 + S$	1.41×10^9	24.8
		R205: $S + S_3 \rightarrow 2S_2$	1.33×10^9	23.4
		R207: $S + S_4 \rightarrow S_2 + S_3$	1.31×10^9	23.0
		R252: $S + NaS_2 \rightarrow NaS + S_2$	4.13×10^8	7.3
		R251: $S + NaS \rightarrow Na + S_2$	2.99×10^8	5.3
		R262: $S + KS \rightarrow K + S_2$	2.20×10^8	3.9
		R293: $S_3 + SO \rightarrow S_2O + S_2$	2.12×10^8	3.7
		R13: $S_4 + h\nu \rightarrow 2S_2$	1.67×10^8	2.9
		R641: $S_2^+ + Na \rightarrow Na^+ + S_2$	1.21×10^8	2.1
		All other reactions	2.06×10^8	3.6
	Loss	R11: $S_2 + h\nu \rightarrow 2S$	7.86×10^{11}	62.6
		R63: $O + S_2 \rightarrow S + SO$	4.63×10^{11}	36.9
		R268: $2S_2 + M \rightarrow S_4 + M$	5.38×10^9	0.4
		All other reactions	1.04×10^9	0.1
SO_2	Production	R324: $2SO \rightarrow SO_2 + S$	3.25×10^{10}	96.1
		R280: $S_2 + NaSO_2 \rightarrow NaS_2 + SO_2$	6.10×10^8	1.8
		R339: $SO + NaSO_2 \rightarrow NaOS + SO_2$	3.58×10^8	1.1
		R255: $S + NaSO_2 \rightarrow NaS + SO_2$	9.12×10^7	0.3
		All other reactions	2.54×10^8	0.8
	Loss	R16: $SO_2 + h\nu \rightarrow SO + O$	4.55×10^{11}	98.3
		R17: $SO_2 + h\nu \rightarrow S + O_2$	4.58×10^9	1.0
		R342: $SO_2 + Na + M \rightarrow NaSO_2 + M$	2.79×10^9	0.6
		All other reactions	6.35×10^8	0.1
SO	Production	R63: $O + S_2 \rightarrow S + SO$	4.63×10^{11}	47.9
		R16: $SO_2 + h\nu \rightarrow SO + O$	4.55×10^{11}	47.1
		R23: $S_2O + h\nu \rightarrow SO + S$	4.49×10^{10}	4.6
		All other reactions	4.13×10^9	0.4
	Loss	R15: $SO + h\nu \rightarrow S + O$	8.92×10^{10}	71.8
		R324: $2SO \rightarrow SO_2 + S$	3.25×10^{10}	26.2
		R529: $SO + h\nu \rightarrow SO^+ + e^-$	1.02×10^9	0.8
		R338: $SO + NaS \rightarrow S_2O + Na$	4.41×10^8	0.4
		All other reactions	1.00×10^9	0.8
S_2O	Production	R338: $SO + NaS \rightarrow S_2O + Na$	4.41×10^8	66.6
		R293: $S_3 + SO \rightarrow S_2O + S_2$	2.12×10^8	32.1
		R333: $SO + SCl \rightarrow S_2O + Cl$	8.02×10^6	1.2
		All other reactions	8.64×10^5	0.1
	Loss	R23: $S_2O + h\nu \rightarrow SO + S$	4.49×10^{10}	99.7
		R76: $O + S_2O \rightarrow 2SO$	1.13×10^8	0.3
		R227: $S + S_2O \rightarrow S_2 + SO$	1.88×10^7	0.04
S	Production	R11: $S_2 + h\nu \rightarrow 2S$	7.86×10^{11}	55.3
		R63: $O + S_2 \rightarrow S + SO$	4.63×10^{11}	32.5
		R15: $SO + h\nu \rightarrow S + O$	8.92×10^{10}	6.3
		R23: $S_2O + h\nu \rightarrow SO + S$	4.49×10^{10}	3.2
		R324: $2SO \rightarrow SO_2 + S$	3.25×10^{10}	2.3
		All other reactions	7.26×10^9	0.5
	Loss	R134: $O_2 + S \rightarrow SO + O$	2.70×10^9	38.2
		R205: $S + S_3 \rightarrow 2S_2$	1.33×10^9	18.7
		R207: $S + S_4 \rightarrow S_2 + S_3$	1.31×10^9	18.5
		R252: $S + NaS_2 \rightarrow NaS + S_2$	4.13×10^8	5.8
		R251: $S + NaS \rightarrow Na + S_2$	2.99×10^8	4.2
		R254: $S + NaOS \rightarrow NaS + SO$	2.77×10^8	3.9
		R528: $S + h\nu \rightarrow S^+ + e^-$	2.63×10^8	3.7
		R262: $S + KS \rightarrow K + S_2$	2.20×10^8	3.1
		All other reactions	2.66×10^8	3.8
O	Production	R16: $SO_2 + h\nu \rightarrow SO + O$	4.55×10^{11}	83.1
		R15: $SO + h\nu \rightarrow S + O$	8.92×10^{10}	16.3
		R134: $O_2 + S \rightarrow SO + O$	2.70×10^9	0.5
		All other reactions	8.71×10^8	0.2

TABLE II—*Continued*

	Species	Reaction	Column-integrated rate (cm^{-2} s^{-1})	% of total rate
	Loss	R63: $O + S_2 \rightarrow S + SO$	4.63×10^{11}	99.97
		R76: $O + S_2O \rightarrow 2SO$	1.13×10^{8}	0.02
		All other reactions	2.75×10^{7}	trace
O_2	Production	R17: $SO_2 + h\nu \rightarrow S + O_2$	4.58×10^{9}	98.9
		R534: $SO_2 + h\nu \rightarrow S^+ + O_2 + e^-$	3.01×10^{7}	0.7
		All other reactions	1.99×10^{7}	0.4
	Loss	R134: $O_2 + S \rightarrow SO + O$	2.70×10^{9}	99.72
		R135: $O_2 + SO \rightarrow SO_2 + O$	6.73×10^{6}	0.25
		All other reactions	9.46×10^{5}	0.03

or

$$2(SO_2 \xrightarrow{h\nu} SO + O) \quad \text{R16}$$
$$2SO \xrightarrow{M} (SO)_2 \quad \text{R325}$$
$$S_2 + (SO)_2 \rightarrow 2S_2O \quad \text{R275}$$
$$\text{Net: } 2SO_2 + S_2 \rightarrow 2S_2O + 2O, \quad (3)$$

Because the SO concentration and the overall atmospheric density on Io is very low, however, reaction R325 is not efficient, and the schemes (2) and (3) do not produce S_2O in significant quantities. This result would be true even if we were to consider the largest observed atmospheric densities on Io—the above schemes were proposed for laboratory conditions at much higher densities, and the rate coefficient for R325 as measured by Herron and Huie (1980) indicates that reaction R325 will be relatively unimportant at low ionian densities (see Section 8.2 for further details).

Instead of being produced by the above reaction schemes, the S_2O in our model has both a volcanic source (e.g., Zolotov and Fegley 1998a) and a photochemical source, with photochemical production resulting from reaction R293 ($S_3 + SO \rightarrow S_2O + S_2$) and from some speculative reactions involving interactions between sodium and sulfur species, e.g.,

$$SO_2 + Na \xrightarrow{M} NaSO_2 \quad \text{R342}$$
$$S + NaSO_2 \rightarrow NaS + SO_2 \quad \text{R255}$$
$$SO + NaS \rightarrow S_2O + Na \quad \text{R338}$$
$$\text{Net: } SO + S \rightarrow S_2O. \quad (4)$$

The S_3 and NaS required for S_2O production are derived from volcanically produced S_2. There are no efficient production mechanisms for S_2O that result solely from SO_2 photolysis. Therefore, S_2O would not be an important component in a low-density SO_2 frost sublimation-driven atmosphere on Io (see Fig. 2b) but could become more important in a volcanically driven atmosphere because of direct outgassing of S_2O and indirect production via reactions with volcanic S_2.

In our moderate-density model, the photolysis of S_2O into SO and S (reaction R23) accounts for greater than 99% of the total column destruction of S_2O. The photochemical lifetime of S_2O in our model is ~10 min (e.g., see Table A2), and S_2O would quickly be depleted from Io's atmosphere if volcanic sources were not active.

4.6. Atomic Sulfur and Heavy Sulfur Molecules

Elemental sulfur allotropes, such as S_3 and S_4, are produced both volcanically and photochemically. The chemical kinetics of these sulfur radicals has been poorly studied in the laboratory but is likely to be highly complex, with interconversion between the different elemental forms being prevalent. The photochemical production of S_3 in our model results primarily from reaction R207 ($S + S_4 \rightarrow S_2 + S_3$); note, however, that the rate coefficient for this reaction has never been measured. The photochemical production of S_4 proceeds mainly via the three-body recombination of S_2 (reaction R268: $2S_2 + M \rightarrow S_4 + M$). Considerable scatter in the measured low-pressure limiting rate coefficient (k_0) for this reaction exists in the literature, with the measured rates appearing highly dependent on the background temperature, gas composition, and assumptions about other sulfur vapor reactions. Our adopted room-temperature value of $k_0 = 8 \times 10^{-30}$ cm^6 s^{-1} is intermediate between values given in Langford and Oldershaw (1972, 1973), Fowles *et al*. (1967), and Nicholas *et al*. (1979). The temperature dependence is assumed to parallel that of $2S + M \rightarrow S_2 + M$ (reaction R203, see Table A3).

The dominant loss pathway for S_3 in our moderate-density model is photolysis (R12: $S_3 + h\nu \rightarrow S_2 + S$; ~48% of loss rate), followed by R205 ($S + S_3 \rightarrow 2S_2$; ~45% of total column loss rate) and R293 ($S_3 + SO \rightarrow S_2O + S_2$; ~7% of loss rate). The dominant loss pathway for S_4 is reaction R207 ($S + S_4 \rightarrow S_2 + S_3$; ~87% of the total column loss rate), followed by R13 ($S_4 + h\nu \rightarrow 2S_2$; ~11% of loss rate) and R307 ($S_4 + Cl \rightarrow S_2 + S_2Cl$; ~1.5% of loss rate). Recycling among different sulfur molecules is rampant, and atomic sulfur is an important byproduct. Io's atmosphere is not dense enough for gas-phase three-body production of the heavier sulfur rings such as S_8 and S_7 to be important, but solid S_8 will eventually be created upon condensation of any of the different gas-phase elemental forms.

Atomic sulfur is produced much more readily than it is destroyed photochemically (see Table II), and the S abundance

increases well above its initial volcanic abundance (see Table I). Photolysis of S_2 (reaction R11) dominates the column production rate of S (~55% of total production rate), followed by reaction R63 ($O + S_2 \rightarrow S + SO$; ~33% of total production), SO photolysis (R15; 6% of total production), and S_2O photolysis (R23; ~3% of total production). Reaction R134 ($O_2 + S \rightarrow SO + O$) accounts for ~38% of the total column loss rate of atomic sulfur, sulfur interchange reactions (e.g., R205, R207) account for another ~37%, and reactions with sodium and potassium compounds (e.g., reactions R252, R251, R254, R262, and R255) account for ~19%, and photoionization (e.g., R528) accounts for ~4% of the total loss rate.

4.7. Atomic and Molecular Oxygen

Atomic oxygen is produced almost entirely by photolysis of SO_2 and SO (see Table II). Ionospheric reactions account for $\ll$1% of the O production. The dominant O loss process is reaction R63 ($O + S_2 \rightarrow S + SO$), which accounts for almost 100% of the total column loss rate. Because S_2 is only prevalent when reduced (i.e., low O/S ratio) Pele-type volcanic sources are active (see Zolotov and Fegley 2000a, Fegley and Zolotov 2000), our volcanically generated model atmosphere has much less atomic oxygen than the pure SO_2-generated photochemical models of Kumar (1982), Summers and Strobel (1996), Wong and Johnson (1996), and Wong and Smyth (2000).

Molecular oxygen is produced almost entirely by reaction R17 ($SO_2 + h\nu \rightarrow S + O_2$; ~99% of the total column production rate), with ionospheric reactions (e.g., R534, R594, R596) being responsible for the bulk of the remainder. The main photochemical loss mechanism for O_2 is reaction R134 ($O_2 + S \rightarrow SO + O$).

4.8. Other Sulfur- and Oxygen-Containing Species

Little interaction between oxygen species and sodium, potassium, or chlorine species is seen in our standard model. Chlorine oxides are not important. However, some interaction between sulfur species and alkali or halogen species does exist. Because the photochemistry of sulfur chlorides and sodium–sulfur or potassium–sulfur species is discussed fully in Paper 2, only a brief discussion is presented here. The dominant sulfur chloride, S_2Cl, is produced from reaction R307 ($S_4 + Cl \rightarrow S_2 + S_2Cl$). The main loss pathway for S_2Cl is reaction R455 ($S_2Cl + Na \rightarrow NaCl + S_2$). Neither of these reactions have ever been suggested or studied in the laboratory, so both are speculative. Sodium–sulfur species such as $NaSO_2$, NaS_2, and NaOS are not particularly important in our moderate-density model (see Table I), but they become more important for higher atmospheric densities. The most abundant sodium–sulfur species, $NaSO_2$, is produced from three-body addition of Na and SO_2 (reaction R342) and is lost from interaction with S_2, SO, S, Na, and Cl (see reactions R280, R339, R255, R471, and R377). The above reactions are suspected to be important in flame-chemistry experiments (e.g., Schofield and Steinberg 1992). Because of a lack of information on photochemical reactions of Na_2SO_4 and K_2SO_4, we do not include the photochemical production and loss of these species in our model, although we do allow their profiles to be affected by diffusion.

5. SENSITIVITY STUDIES

The results described above are sensitive to certain assumptions about atmospheric properties, kinetic rate constants, or boundary conditions. Some of these issues have been discussed by previous photochemical modelers (e.g., Kumar 1982, 1985, Summers 1985, Summers and Strobel 1996, Wong and Johnson 1996). In Appendix B, we consider how the results for our volcanically driven atmosphere change when specific aspects of the above standard moderate-density model are altered. In particular, we focus on the sensitivity of the model results to changes in the total atmospheric density, the eddy diffusion coefficient, and certain key reaction rates. The sensitivity of the results to the assumed elemental composition of the volcanic gases is discussed in Paper 2. Although we do not examine the sensitivity of the results to the assumed temperature, pressure, and O/S ratio in the emitted volcanic gas, these parameters could also have an important effect on the results (e.g., Fegley and Zolotov 2000). For example, the assumption of an O/S ratio of ~2 would result in SO_2-dominated volcanic atmospheres (Fegley and Zolotov 2000) that would behave more like the case of a pure SO_2 frost sublimation-driven atmosphere.

From the sensitivity studies described in Appendix B, we find that an increase in the volcanic emission rate (such that the total atmospheric density is increased) can affect both the absolute and relative abundances of the different atmospheric constituents (see Table I and Fig. 4). A decrease in the assumed eddy diffusion coefficient causes several changes in the predicted column abundances and concentration profiles of the constituents (see Fig. 5), including an increased relative importance of atomic species as opposed to molecular species (especially at high altitudes). Changes in the rate coefficients for uncertain (i.e., unmeasured or unstudied) reactions can also affect our results (see Tables B1 and B2 in Appendix B), but the results seem less sensitive to changes in reaction rates than they are to variations in eddy diffusion coefficients or atmospheric density.

6. TEMPORAL EVOLUTION

All the results discussed above and in Appendix B are steady-state models for atmospheres generated from Pele-type eruptions. A volcanic atmosphere on Io will never truly be in steady state because volcanic eruptions are not continuous and uniform, because the atmosphere will respond to plume eruptions in a complex dynamical way (e.g., Ingersoll 1989, Moreno *et al.* 1991, Austin and Goldstein 1996), because Io's heterogeneous surface will complicate atmosphere–surface interactions, and because photochemical reactions are dependent on time-variable effects such as the change in solar zenith angle throughout the

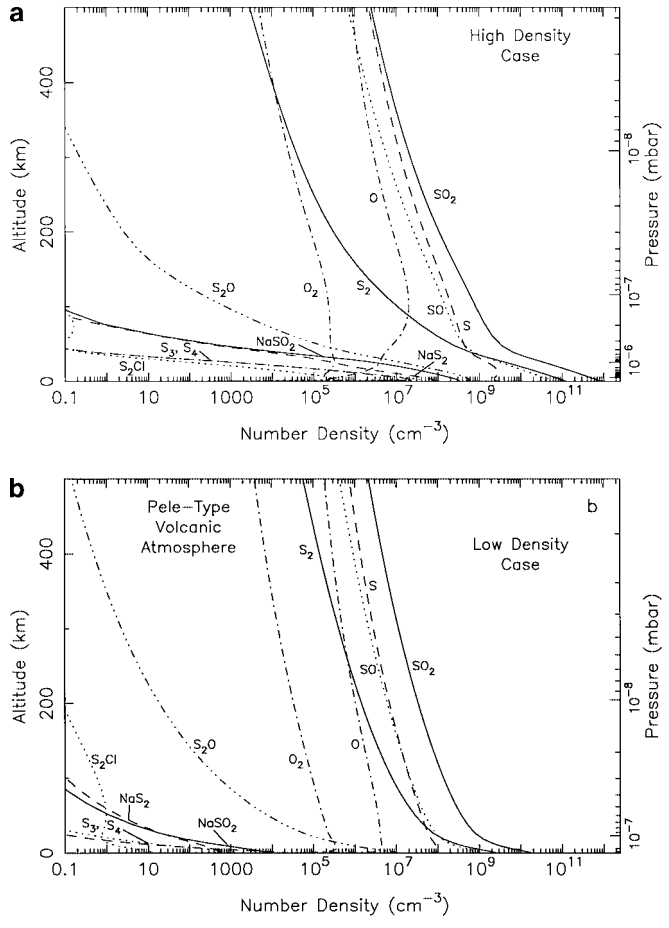

FIG. 4. The concentrations of several important atmospheric constituents in (a) our high-density model (e.g., 18-nbar surface pressure, SO_2 column density 7.4×10^{17} cm^{-2}, $K_E = 10^9$ cm^2 s^{-1}) and (b) our low-density model (e.g., 0.37-nbar surface pressure, SO_2 column density 1.5×10^{16} cm^{-2}, $K_E = 10^9$ cm^2 s^{-1}) as a function of altitude and pressure.

day. Therefore, it is useful to examine the time variability of photochemistry and to compare the photochemical time constants with other time scales of interest.

The first thing we want to examine is how rapidly the volcanic vapors are processed by photochemistry. For their thermochemical equilibrium calculations, Zolotov and Fegley (2000a) have assumed that the abundances of SO_2, S_2, SO, and S seen in the Pele plume region by McGrath *et al*. (2000) and Spencer *et al*. (2000) reflect equilibrium volcanic abundances. If photochemical processing of the plume vapors occurs on very short time scales relative to the lifetime of fresh volcanic gas that is being supplied to the plume, then the above assumption will be incorrect, and the magma temperature or vent pressure derived for the Pele volcanic region from the thermochemical equilibrium calculations could be suspect. Note, however, that based on the observed plume abundances and thermochemical equilibrium calculations, Zolotov and Fegley (2000a) derive a magma temperature (~1440 K) that is consistent with independent Galileo infrared and visible observations of *minimum* temperatures of ~1280–1400 K for the hottest component observed in the Pele region (McEwen *et al*. 1998b, 2000; Davies *et al*. 1999, 2000a), and both the temperature and oxygen fugacity (3.3 log fO_2 units below the Ni-NiO buffer) derived by Zolotov and Fegley (2000a) are consistent with the possible presence of Mg-rich silicates (orthopyroxene) in pyroclastic deposits around Pele (Geissler *et al*. 1999a, 2000).

To determine the rate of photochemical processing of the volcanic vapors, we first set up a model in which the initial volcanic vapor abundances are consistent with the thermochemical equilibrium abundances shown in Table I and in which the volcanic species are assumed to be uniformly mixed with altitude. We then allow photochemistry and diffusion to act upon the gas-phase species. The model is exactly the same as our standard moderate-density model, except we now record the state of the atmosphere at various points in time as the abundances approach steady state. Figure 6 shows how the column densities of the major sulfur and oxygen species vary with time. Note from both Table I and Fig. 6 that the SO_2, S_2, and S_2O abundances decrease slightly with time, while the S, O, and O_2 abundances increase dramatically and the SO abundance increases slightly as photochemical reactions take place. Although conditions within a real plume will differ considerably from our simple 1-D hydrostatic equilibrium description presented here, the vapor column densities should be similar (because we used actual plume observations to set the column densities), and a comparison between the photochemical time constants and dynamical time scales for a plume eruption should give us a first-order indication of whether photochemical processes could alter the initial gas abundances.

The reduction in the sulfur dioxide column abundance with time shown in Fig. 6 is mainly due to photolysis. The photochemical time constant for SO_2, as defined by the initial column density of SO_2, divided by the integral of the difference between the initial photochemical production and loss rates

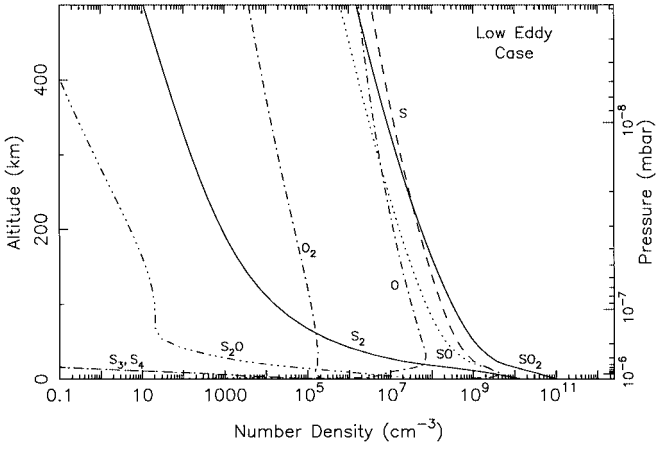

FIG. 5. The concentrations of several important atmospheric constituents in our moderate-density low-eddy-diffusion model (e.g., for an assumed altitude-independent eddy diffusion coefficient of $K_E = 10^8$ cm^2 s^{-1}) as a function of altitude and pressure.

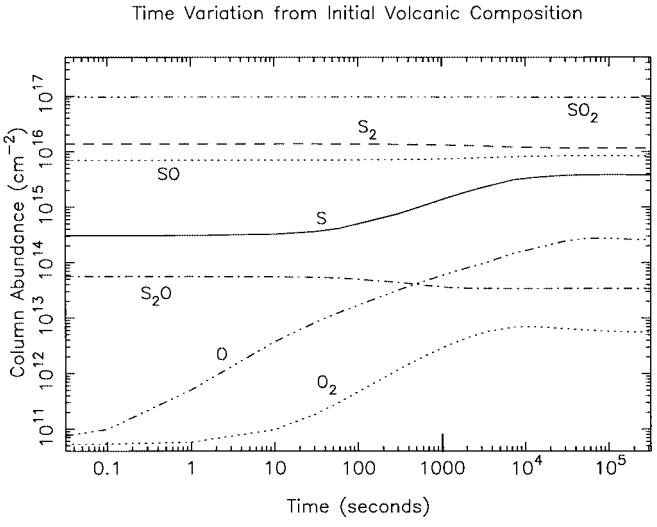

FIG. 6. The photochemical evolution of volcanic vapors in our standard moderate-density model. Each curve represents the time variation of the column density of an important sulfur or oxygen species (as marked) from its initial thermochemical equilibrium abundance at time zero. The thick vertical line segment near 1000 seconds illustrates the typical dynamical time scales for a large plume eruption on Io (see text).

(integrated over altitude), is ~50 h. This time constant is long compared to possible dynamical (gas flow) time scales (e.g., ~17 min for an assumed horizontal scale length L of 100 km and a flow speed of 100 m s^{-1}; see Ingersoll 1989) or to ballistic lifetimes within a large plume eruption (~20 min for an assumed initial ejection velocity of 1.1 km s^{-1}, such as would produce a typical Pele plume height of ~350 km; see McEwen and Soderblom 1983, McEwen *et al*. 1998a, Spencer *et al*. 2000). Therefore, volcanically produced SO_2 is expected to survive a plume eruption in abundances relatively unaltered by photochemistry. The photochemical time constant for SO is ~4 h; the observed increase with time shown in Fig. 6 is due to both SO_2 photolysis and to reaction of atomic oxygen with S_2 (reaction R63). Like SO_2, SO should survive a plume eruption relatively unaltered by photochemistry. The same can be said for S_2, whose photochemical time constant is also ~4 h. The reduction in the S_2 abundance with time is due to both photolysis and to reaction R63. Because SO_2, SO, and S_2 have long photochemical lifetimes compared with typical dynamical lifetimes within the plume, the relative abundances of these species as determined by McGrath *et al*. (2000) and Spencer *et al*. (2000) should provide reliable indicators of the volcanic gas composition coming from the vent.

All the other species shown in Fig. 6 can be altered appreciably by photochemistry. The photochemical time constants for S_2O, S, O_2, and O are 10 min, 2 min, 9 s, and <1 s, respectively. Therefore, observations of these species within volcanic plumes might not provide reliable indications of thermochemical equilibrium conditions within the volcanic conduit or caldera-confined lava lake. The observed S_2 column abundance in the Pele plume (Spencer *et al*. 2000) is quite large, and even a small amount of S_2 photolysis within a ~20-min plume eruption would create a considerable column of sulfur atoms. For example, if the initial column-integrated S_2 photolysis rate of 9.54×10^{11} cm^{-2} s^{-1} in our moderate-density model is assumed to be constant over a 20-min period (with each photolysis event producing two sulfur atoms), then a column of 2.3×10^{15} cm^{-2} sulfur atoms could be produced during a Pele-type eruption (cf. Fig. 6), an amount of sulfur quite a bit higher than the 3×10^{14} cm^{-2} observed by McGrath *et al*. (2000). The above calculations are quite sensitive to the assumed column density of S_2 in the plume, and no S_2 observations are available from the time of the McGrath *et al*. observations. Photochemical processing of sulfur atoms will be less important for smaller plumes (because of the shorter ballistic lifetimes for the gas molecules), for lower S_2/S ratios in the freshly emitted volcanic gases (because the initial abundances will then be closer to the final steady-state photochemical abundances), and for lower total S_2 column abundances in the plume (because loss processes for S might then compete with S production, see Table II). Atomic sulfur production will also be reduced if plume dust particles help shield the S_2 (although observations by Spencer *et al*. (1997b, 2000) and McGrath *et al*. (2000) suggest that the Pele plume dust is not optically thick).

Because sulfur atoms are produced readily from photochemistry in our model of an S_2-rich Pele-type atmosphere, it is possible that the ~0.3% S/SO_2 ratio observed by McGrath *et al*. (2000) in the Pele volcanic region could include sulfur atoms that were generated from photochemistry as well as from equilibrium thermochemistry within the magma chamber or lava lake. If so, then the equilibrium S/SO_2 ratio would have been lower than was indicated by the observations, and the Pele magma temperature could be higher than was derived by Zolotov and Fegley (2000a) (see their Fig. 1). As noted by Zolotov and Fegley (2000a), a 10–30% change in the S abundance leads to temperature changes of 60–150 K. The only sure way to deconvolve the relative contributions of photochemistry and thermochemistry in determining the abundances of the volcanic plume gases would be to make simultaneous observations of plume composition (e.g., S, SO, SO_2, S_2) and vent temperature. Failing that, simultaneous observations of S, along with S_2 and/or SO_2 in a known active plume, would greatly aid in determining whether the photochemical processing as outlined above might actually be occurring. Determinations of whether the ultraviolet emission lines for atomic sulfur observed by McGrath *et al*. (2000) and others represent excitation from the entire column of sulfur atoms or whether the electrons responsible for the excitation lose too much energy before they have penetrated the entire gas column is also critical for our understanding of the thermochemical and photochemical processes taking place on Io.

The second time-variable model we consider is the evolution of the Pele-type volcanic vapor once the volcanic source is shut off. In this case, we start from the steady-state model shown in Fig. 2, but the boundary conditions are changed such that the

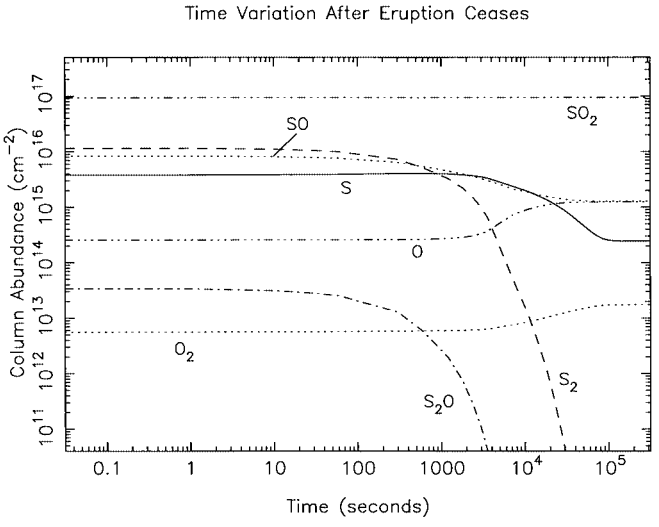

FIG. 7. The photochemical evolution of volcanic vapors in our moderate-density model after the volcanic source is shut off. Each curve represents the time variation of the column density of an important sulfur or oxygen species (as marked) from its initial steady-state photochemical abundance at time zero.

volcanic input at the lower boundary is eliminated. Instead, all species except SO_2 are assumed to be lost to the lower boundary at a maximum possible rate. Sulfur dioxide, which still has a frost sublimation source, is assumed to have a constant mixing ratio of 0.772 at the lower boundary (i.e., the same as in our standard model). Figure 7 shows the secular variation of the column densities of the major sulfur and oxygen species once the volcanic source has been turned off. Sulfur dioxide remains the most important vapor, and as the volcanic gases are removed from the atmosphere, SO_2 photolysis initiates all atmospheric chemistry. The abundances of S_2 and S_2O decrease dramatically with time because they no longer have a volcanic source and because they are not important products of SO_2 photochemistry. Both SO and S, on the other hand, are important SO_2 photodissociation products, and although their abundances decrease with time, the decrease is not as drastic as seen for S_2 and S_2O. The abundances of O and O_2 actually increase with time because they are important SO_2 photolysis products and because they are no longer destroyed efficiently by S_2 and S.

Note that after the volcanic species have completely diffused out of the atmosphere, the column-integrated SO/SO_2 ratio is reduced to $\sim$1.5% (see Fig. 2b; $SO/SO_2 \approx 2.0 \times 10^{-3}$ at the surface, but lighter species like SO become relatively more important at high altitudes). The column-integrated abundances of O and S relative to SO_2 become 1.5% and 2.9×10^{-3}, respectively. These results are consistent with the high-eddy diffusion ($K_E = 10^9$ cm^2 s^{-1}) models of Summers and Strobel (1996) (see their Fig. 6 and 9).

In our steady-state moderate-density model, the photochemical time constants (as defined above) for SO_2, SO, S_2, O, O_2, and S are 54 h, 2.6 h, 2.2 h, 50 min, 49 min, and 29 min, respectively. The S_2O molecule has a very short 10-min time constant against photolysis. However, the evolutionary profiles shown in Fig. 7 do not solely reflect the photochemical lifetimes. Both eddy and molecular diffusion help transport the vapor to the surface, where the atoms or molecules are assumed to "stick." The diffusion time constant within the lowest atmospheric level is $\sim$7 min for all of the species (eddy diffusion dominates at low altitudes). Diffusion therefore contributes to the overall lifetime of the molecules shown in Fig. 7. For example, the SO, S_2, and S_2O column densities drop to $1/e$ of their initial values in $\sim$55 min, $\sim$13 min, and $\sim$5 min, respectively. Note that the atmospheric composition changes considerably in the time period of a couple hours. Active plumes should thus have very different atomic and molecular abundances than ambient regions well away from centers of active volcanic activity. Molecules such as S_2 and S_2O will only be present in areas where relatively reduced volcanoes are actively outgassing, and S and SO abundances will generally be larger in regions with active outgassing from such volcanoes.

The third time-variable model we consider is the diurnal variation of an atmosphere whose volcanic source is constant over the course of a day. For this model, we keep the boundary conditions the same as in our standard moderate-density Pele-type volcanic model, but we allow the solar zenith angle to change with time. Figure 8 shows the results for a model of the equatorial region at vernal or autumnal equinox. Note that SO_2, which has a constant large supply rate regardless of time of day and whose time constant against photolysis is relatively long (see Table A2 in Appendix A), exhibits only mild changes in column density over the course of an ionian day ($\sim$42 h). Both S_2 and S_2O have photolysis lifetimes shorter than an ionian day,

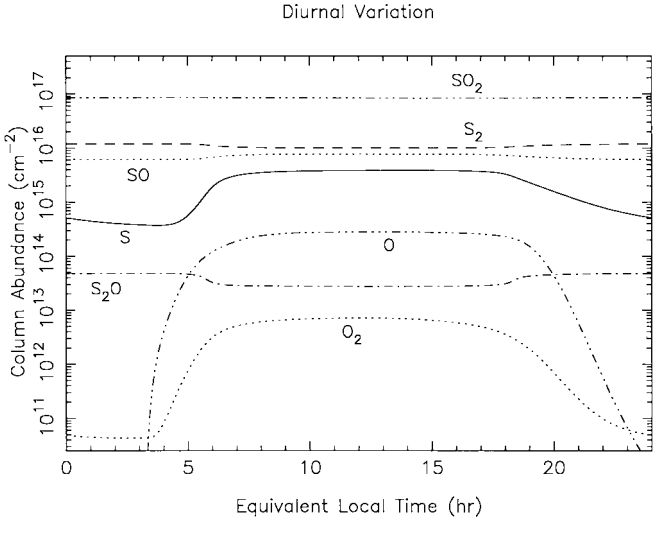

FIG. 8. The diurnal variation of important sulfur and oxygen species in our moderate-density model. The volcanic emission (and total atmospheric density) is assumed to be constant with time; all variation is caused by short-term photochemical processes. Column densities for the important sulfur and oxygen species (as marked) are plotted as a function of local time such that 0 represents midnight and 12 represents noon.

and these molecules will be more prevalent at night. However, the constant volcanic supply of S_2 and S_2O at the lower boundary moderates the overall diurnal variation of these species. Both the production and loss mechanisms for SO are reduced at night, and time constants are relatively long, so sulfur monoxide does not exhibit much diurnal variation. Atomic and molecular oxygen, who are produced almost exclusively by photolysis and who have efficient and rapid photochemical loss processes (see Fig. 3 and Table II), exhibit dramatic diurnal variation. Atomic sulfur also has production mechanisms (e.g., photolysis of S_2 and reaction R63) whose efficiency is much greater during daylight hours; thus, atomic S experiences moderate diurnal variation. A reduction in ultraviolet emission from atomic O and S as Io passes into Jupiter's shadow has been noted from HST observations (e.g., Clarke *et al*. 1994, Ballester *et al*. 1996, 1997), and a rapid decrease in the photochemical sources of these atoms as solar photons are lost might contribute to this behavior (although other dissociative sources such as torus electron impact are still operative at night, and the observed emission behavior is highly variable and not consistent from one eclipse entrance to another).

The model shown in Fig. 8 is highly simplified in that we ignore dynamical effects that could allow vapor to flow from the dayside to the nightside (e.g., Wong and Johnson 1996, Wong and Smyth 2000, Austin and Goldstein 2000), and we neglect other sources of energy (such as impacts from torus electrons) that could dissociate molecules (even at night). The possibility that electron impact could be occurring at night is clearly demonstrated in Galileo eclipse and nighttime images of Io (e.g., McEwen *et al*. 1998a, Geissler *et al*. 1999b) in which visible gas emissions are observed both in localized regions associated with known volcanic centers and in broad regions of diffuse emission across the whole disk. The emission is believed to be caused by electron impact of SO_2 and/or SO (prominent at blue wavelengths), atomic oxygen (prominent at red and green wavelengths), and atomic sodium (prominent at green wavelengths) (see Bouchez *et al*. 2000, Geissler *et al*. 1999b; see also the theoretical descriptions of the "equatorial spots" and other emissions, e.g., Retherford *et al*. 2000a, Saur *et al*. 2000, Michael and Bhardwaj 2000). The fact that Io's disk-integrated brightness decreases with time after Io has passed behind Jupiter's shadow in these images suggests that SO_2 might be condensing (and the atmosphere collapsing) as the surface temperature drops (Geissler *et al*. 1999b). Interestingly, the localized plume glows at low latitudes actually increase in brightness with time in shadow (Geissler *et al*. 1999b), perhaps due to the plumes conducting a greater share of the current through Io (or the electrons penetrate deeper into the plumes) as the atmosphere collapses at night (Geissler *et al*. 1999b, Wong and Smyth 2000).

7. IMPLICATIONS FOR IO'S PLASMA TORUS AND NEUTRAL CLOUDS

The upward flux of volcanic species (especially SO_2, S_2, S_2O, and S_3) in our standard model is balanced by the diffusion of photochemically produced species to the surface (especially SO, S, and O) and by escape of all species to space (see Table A1 in Appendix A). Although we have not attempted to accurately model atmospheric escape, several generalizations can be made on the basis of our simple one-dimensional models. Most importantly, our Pele-type volcanic models have a much different atmospheric composition at high altitudes than pure SO_2 frost sublimation-driven atmospheres (cf. Figs. 2a and 2b). For example, in our moderate-density volcanic model, atomic sulfur is the second most abundant consituent (other than SO_2) at the exobase ($\sim$616 km), and the overall O/S ratio at the exobase is 1.27. In contrast, the moderate-density frost sublimation model has atomic O as the second-most abundant species at the exobase because it is a major product of SO_2 photolysis, because its lighter mass allows it to diffuse to high altitudes more readily than some of the other species, and because there are no longer efficient loss mechanisms for O at high altitudes (e.g., R63 is not efficient when there is no volcanic S_2). The overall O/S ratio in the sublimation model is 2.23. This difference in high-altitude composition could lead to differences in the supply rate to the Io torus and neutral clouds of sulfur-bearing species as opposed to oxygen-bearing species.

Our models suggest that long-lived volcanic sources with high S_2 emission rates (i.e., either one source or several sources erupting intermittently in such a way that emission is roughly continuous over long time periods) will produce atmospheres in which the high-altitude abundance (and hence relative escape rate) of sulfur as compared with oxygen is higher than that in pure SO_2 frost sublimation-driven atmospheres; the S/O ratio in the neutral clouds and plasma torus will be correspondingly enhanced. The key phrase here is "long-lived" when referring to the volcanic sources. As shown in Section 6, S_2 is very photochemically reactive and will only remain in the atmosphere as long as the volcanoes are actually outgassing (erupting). Similarly, the lifetime of ions in the torus is long enough (weeks to months) that obvious changes in the torus composition would only be evident if atmospheric variations (e.g., due to changing volcanic input) persisted over long time scales (Schneider *et al*. 1989).

The possibility of active sulfur-rich volcanism causing sulfur to be a major neutral constituent in Io's extended atmosphere (corona) and sulfur ions to be the dominant ions in the Io torus was first suggested by Smith and Strobel (1985) and Summers *et al*. (1989; see also Moreno *et al*. 1985) in an attempt to explain the differences in the luminosity, energetics, and composition of the torus at various times as compared with that of the Voyager era. Smith and Strobel (1985) claim that the very low O^{++} density inferred by Brown *et al*. (1983) and the low O^+ density inferred by Morgan and Pilcher (1982) during, respectively, 1981 and winter 1979 is inconsistent with an oxygen-rich torus and appears to require a sulfur-rich torus. Because of the shorter life-times of sulfur ions within the torus, they expect that a sulfur-dominated torus would be transient and would only persist for short periods during and after major sulfur-driven eruptions. Shemansky (1987, 1988) argues, however, that

oxygen/sulfur partitioning within the torus was largely invariant between the Voyager 1 and 2 encounters, despite a significant change in the plasma electron temperature and number density; as emphasized by Shemansky (1988), this result is not consistent with the neutral-cloud theory for the origin of the torus (such as was considered by Smith and Strobel 1985 and many others). Shemansky (1987, 1988) suggests that variations in electron temperature near Io may stabilize the neutral supply rate; a sudden increase in the supply of neutrals due to increased volcanic activity would then affect densities within the neutral clouds but not ion densities within the torus (see Schneider *et al*. 1989).

The physics and chemistry of the plasma torus and the atmosphere-torus interactions are very complicated and not completely understood. However, Smith and Strobel (1985) suggest several observational tests for their hypothesis (and ours) that major episodes of active S_2-rich volcanism could significantly (and temporarily) alter the observed properties of Io's extended neutral clouds and plasma torus. These suggestions deserve more study. Whenever possible, torus and neutral cloud observations should be compared with ground-based and spacecraft observations that monitor the intensity, duration, and preferably composition of volcanic activity on Io.

8. IMPLICATIONS FOR SURFACE COMPOSITION

Many of the volcanically and photochemically produced gases discussed in this paper will condense upon contact with Io's cold surface. The vapor erupting from "balanced" umbrella-shaped volcanic plumes might be expected to condense in a concentric ring of debris surrounding the vent. Simple ballistic trajectories, however, may not be adequate for explaining the behavior of gases within a plume—plume models indicate that very complex and perhaps turbulent gas flow can carry vapor large distances from the source (e.g., Smythe *et al*. 2000, Cataldo and Wilson 1999, Austin and Goldstein 1996, Moreno *et al*. 1991)—and the resulting condensation regions may be broad and complex.

8.1. Sulfur

The discovery by Spencer *et al*. (2000) of large amounts of S_2 vapor in the Pele plume reinforces the suggestion that the diffuse red deposits that surround the Pele vent (as well as the red deposits associated with other volcanic centers) could be composed of elemental sulfur that has condensed from a high temperature vapor or liquid (e.g., Spencer *et al*. 2000, McEwen *et al*. 1998a, Spencer *et al*. 1997a; see also Nelson and Hapke 1978, Smith *et al*. 1979, Sagan 1979, Soderblom *et al*. 1980, Sill and Clark 1982, Nelson *et al*. 1990, Moses and Nash 1991, Johnson 1997, Zolotov and Fegley 1998a, Geissler *et al*. 1999a). Volcanic vapor that was in contact with hot silicate magma on Io will contain a variety of sulfur molecules (see Fegley and Zolotov 2000); although S_2 should dominate for Pele-type eruptions, the vapor should also contain sulfur atoms, and $S_3, S_4, \ldots, S_{10}$ molecules. The condensation of once-hot sulfur vapor is very complicated, as the smaller molecules are not stable within the condensed phase. When these sulfur molecules condense on a cold surface, some are initially preserved while other recombine to form larger molecules, which in turn can recombine to form even larger, more stable molecules (e.g., Meyer 1964, 1976; Brewer *et al*. 1965). The stable form of elemental sulfur at Io's surface temperature and pressure is orthorhombic α-sulfur, or S_8 molecules arranged in an orthorhombic crystalline lattice. Elemental sulfur that has condensed from a hot vapor can contain S_3 and S_4 molecules that can be preserved at typical Io surface temperatures of $\leq$130 K, but these radicals will eventually disappear as the solid converts to orthorhombic sulfur (e.g., Young 1984, Meyer 1976, Meyer and Stroyer-Hansen 1972, Radford and Rice 1960, Meyer and Schumacher 1960, and references therein). Sulfur polymers may also form and be preserved as the condensate converts to the stable form (see Moses and Nash 1991). Because of strong broad electronic absorption bands at $\sim$390 nm and $\sim$530 nm (Meyer *et al*. 1972, Meyer 1976; see also Billmers and Smith 1991), S_3 imparts a yellow–green color and S_4 imparts a red color to the condensed solid.

Hot sulfur vapor that contains a large percentage of S_2 molecules, when condensed on a cold (e.g., $\leq$77 K) surface, most often appears purple or violet (e.g., Rice and Sparrow 1953, Brewer *et al*. 1965). However, the condensate can appear yellow, green, violet, purple, maroon, or red depending on the percentage of the highly colored metastable molecules like S_3 and S_4 that are initially preserved in the solid; that percentage in turn depends on the composition of the initial vapor, the temperature of the surface upon which the vapor condenses, and the rate of vapor deposition (see Rice and Sparrow 1953, Rice and Ditter 1953, Rice and Ingalls 1959, Meyer and Shumacher 1960, Radford and Rice 1960, Brewer *et al*. 1965, Meyer 1964, 1976). Judging from the absorption spectra of Rice and Ingalls (1959), the purple color of "condensed S_2" may be due to small amounts of S_4 and S_3, whose characteristic absorption bands appear to be superimposed upon a "yellow sulfur" (presumably an amorphous mixture of polymeric sulfur and S_8) spectrum. This interpretation is not definitive, however, as the observed $\sim$550–620 nm absorption band in the Rice and Ingalls spectrum of purple sulfur seems to lie at longer wavelengths than the S_4 band. The purple color seems to appear when the condensate reaches a certain thickness (Brewer *et al*. 1965). Meyer and Stoyer-Hansen (1972) find that the 530-nm band of S_4 is observed when S_2 condensed at 20 K is exposed to visible light; they claim that the larger the amount of S_4 that the condensate contains, the redder the condensate appears and the more pronounced an infrared band at 668 cm^{-1}. The presence of S_4 and a variety of metastable sulfur molecules is clearly indicated in samples of "condensed S_2" that are exposed to light. Such molecules will probably be able to form in condensed S_2 volcanic deposits on Io. It is not clear whether more S_4 radicals would be preserved on Io from condensation of S_2 vapor or from direct condensation of volcanically or photochemically produced S_4 vapor; however, the sheer amount of the S_2 vapor observed in the Pele plume

suggests the former (compare the S_4 and S_2 mixing ratios listed in Table I).

Sulfur radicals such as S_3 and S_4 can also be preserved from the quenching of hot liquid sulfur (e.g., Meyer 1964, 1976, Meyer *et al*. 1972), but the liquid must be quenched very rapidly. Young (1984) emphasizes that the low thermal conductivity of sulfur will prevent large bodies of liquid sulfur (such as in volcanic flows or lakes) from cooling rapidly enough to preserve S_3 and S_4 radicals. Only very small droplets of liquid sulfur, say from plume eruptions, might be quenched rapidly enough to preserve the unstable radicals (e.g., Moses and Nash 1991). Thus, S_4 absorption bands should not be seen in volcanic sulfur flows on Io's surface but might be present in diffuse plume deposits.

The colored sulfur radicals that are preserved from condensed vapor or quenched liquid droplets would not be stable indefinitely at typical daytime temperatures on Io (e.g., Young 1984), and any red deposits that formed by these mechanisms would eventually fade to white or pale yellow over time. Any S_3 would recombine very quickly, and S_4 more slowly (e.g., Hopkins *et al*. 1973, Young 1984). Therefore, if S_4 is responsible for the diffuse red deposits seen near active volcanoes at Pele, Marduk, Culann, Isum, Zamama, Zal, Euboea, Ulgen, Tupan, Prometheus, and Amirani (McEwen *et al*. 1998a; and now there are new red deposits seen by Galileo covering a broad region centered at Tvashtar), then the red coloration might be expected to fade over time. Indeed, McEwen *et al*. (1998a) find that the color of reddish areas near volcanic centers that are not currently active on Io tends to be more muted, and they suggest (from comparing Voyager and Galileo observations) that the red plume deposits at low latitudes of Io fade on time scales of years to decades. Furthermore, because S_4 is observed to disappear from samples held at temperatures of 130–180 K (Hopkins *et al*. 1973), S_4 would not be present in warmer regions on Io (i.e., hot spots). This restriction is consistent with the observed distribution of red deposits on Io (McEwen *et al*. 1998a, A. S. McEwen, personal communication, 2000).

In summary, the diffuse red deposits observed near active volcanic centers on Io have characteristics that are consistent with the presence of S_4 radicals that are preserved when S_2 vapor from active volcanic plumes condenses on cold surfaces; however, other explanations are possible. For example, different impurities can impart colors to elemental sulfur (e.g., Kargel *et al*. 1999), or S_4 radicals and/or other red chromophores could be preserved from the condensation of other vapors besides sulfur (see below).

8.2. S_2O and Polysulfur Oxides

Disulfur monoxide (S_2O) and polysulfur oxides $(S_mO)_n$ with $m > 2$ have also been proposed as surface coloring agent on Io (Hapke 1979, Sill and Clark 1982, Hapke 1989, Spencer *et al*. 1997a). Both of these substances can be formed in environments in which SO_2 vapor is being dissociated to form SO (e.g., Schenk and Steudel 1965, 1968, Hapke and Graham 1989, Hapke 1989). In typical laboratory experiments at "low" temperatures and pressures (but not as low as typical Io temperatures and pressures), the highly reactive SO vapor molecules undergo addition and disproportionation reactions to form a dimer, $(SO)_2$ (e.g., R324), which then reacts with another SO molecule to form S_2O and SO_2 (e.g., R326). When exposed to a cold surface with a temperature below ~115 K, the S_2O condenses to form an orange-red to dark-red solid (Schenk and Steudel 1965, 1968, Hapke and Graham 1989). When the condensate is heated above ~120 K, its color changes to a pale yellow as the S_2O polymerizes into a polysulfur oxide; SO_2 gas is released during the process. The color change is irreversible, and the yellow polysulfur oxide is stable for months at room temperature (Hapke and Graham 1989). Because strong absorption bands at ~420 and ~530 nm are seen in the spectra of the condensate, the red color of condensed S_2O is believed to be due to the presence of S_3 and S_4 radicals trapped within the solid (e.g., Tsang and Brown 1975, Hapke 1989, Hapke and Graham 1989).

As discussed in Section 4, the typical method for forming S_2O in a laboratory environment (and the method that has been proposed by Hapke (1989) for forming S_2O on Io) is not effective on Io because of the satellite's low atmospheric density. Schenk and Steudel (1965) suggest that the reaction $SO + SO \rightarrow (SO)_2$ is second order because of the "low heat of reaction involved"; however, the experimental study of Herron and Huie (1980) indicates that the reaction is pressure dependent and is most likely third order. With the low-pressure limiting rate constant of 4.4×10^{-31} cm^6 s^{-1} determined by Herron and Huie (1980), we find that SO dimerization is not effective in Io's low-density atmosphere, and S_2O is not formed via these proposed reactions. Instead, S_2O could be a primary volcanic product, as was initially suggested by Sill and Clark 1982 (see also Spencer *et al*. 1997a) and was quantitatively demonstrated by Zolotov and Fegley (1998a), or could form photochemically by reaction of SO with volcanic S_3 or NaS (see Section 4). In either case, condensation of S_2O would be expected specifically around active volcanic plumes, as is consistent with the observations of diffuse red deposits near centers of active volcanism (McEwen *et al*. 1998a). Note from Table I, however, that the S_2O abundance predicted from thermochemical and photochemical models for Pele-type eruption is much smaller than that of SO_2 or S_2, and in the absence of a temperature gradient permitting fractional condensation, any condensed S_2O would most likely be intimately mixed with or perhaps even covered by condensed sulfur (which is less volatile than S_2O) and, at sufficiently low temperatures, by SO_2 frost (which is more volatile than S_2O). In addition, S_2O would rapidly convert to yellow polysulfur oxide at daytime temperatures in the equatorial regions of Io. Such short-term changes in the appearance of the red Pele deposits, which extend to the equator, have not been observed by Galileo (e.g., McEwen *et al*. 1998a, Geissler *et al*. 1999a).

Hapke (1989) also suggests that S_2O or polysulfur oxides will form at Io's surface from the condensation of SO, although

he provides no experimental evidence on SO condensation to back up this claim. As with sulfur, sulfur monoxide condensation is clearly complex and not well understood, and laboratory investigations are hampered by the fact that SO vapor is very reactive. Early attempts to isolate solid SO were not successful due to its rapid vapor-phase conversion to $(SO)_2$ and S_2O, followed by condensation of S_2O or polysulfur oxides; Schenk and Steudel (1965) report anecdotal evidence for the formation of a yellow solid at low temperatures that presume is condensed SO. Until the condensation of SO is better characterized, it is difficult to determine whether S_2O and polysulfur oxides could be widespread on Io due to SO condensation.

We note, however, that SO is not just a volcanic product but is a primary product of SO_2 photolysis, and we would expect SO to condense (or adsorb) all over Io's surface where temperatures are sufficiently low (especially on the nightside or at the poles). It therefore seems unlikely that the diffuse red deposits seen near active volcanic centers in Galileo and HST images (Spencer *et al*. 1997a, McEwen *et al*. 1998a, Geissler *et al*. 1999a) are caused by SO condensation or such deposits would be seen all over Io and not just around active volcanoes. On the other hand, our photochemical calculations and the thermochemical equilibrium work of Zolotov and Fegley (1998b, 2000a) and Fegley and Zolotov (2000) indicate that SO on Io might be produced predominantly from volcanic sources, in which case deposits of condensed SO might be much thicker around volcanoes than elsewhere across the planet (depending on the uncertain volatility of SO). Interestingly, Io's polar regions are darker and redder than planetary average (e.g., Geissler *et al*. 1999a, McEwen *et al*. 1998a, Spencer *et al*. 1997a). If SO partially condenses into S_2O (with possible S_3 and S_4 production during the process), then condensed SO might help explain the appearance of the polar regions. If SO condenses into polysulfur oxides, then polysulfur oxides are still viable candidates for the yellow regions seen all over Io (Geissler *et al*. 1999a, McEwen *et al*. 1998a), as is elemental sulfur (S_8) that has been irradiated by ultraviolet light; see Steudel *et al*. (1986).

9. DISCUSSION

As mentioned in the previous sections, our models indicate that atmospheres generated by Pele-type volcanic outgassing on Io should differ in several important ways from atmospheres generated purely by SO_2 frost sublimation. Several observational tests might help distinguish the relative importance of these sources. For example, species such as S_2 and S_2O are not major products of SO_2 photolysis and would only be present when volcanoes are active (see Fig. 2), and both S and SO should exhibit enhanced abundances relative to SO_2 when active volcanism is prevalent. High-quality simultaneous observations of S and/or SO along with SO_2, such as were presented by McGrath *et al*. (2000), might help indicate whether active volcanoes are affecting the atmospheric abundances in the regions observed. For instance, McGrath *et al*. (2000) used HST/FOS to obtain spectra in three separate target regions on Io, one centered at Pele, one at Ra, and one in a "control" region they call T3. McGrath *et al*. found evidence for SO_2 and SO absorption at all three locations and S emission at Pele and T3 (but not at Ra). The enhanced SO_2 abundance at Pele as compared to Ra (a factor of $\sim$2.2 difference in the vertical column density) led McGrath *et al*. (2000) to conclude that the Pele plume may have been active at the time of the observations—roughly equal SO_2 abundances at the two sites would have been expected from the three-dimensional azimuthally symmetric SO_2 frost sublimation/photochemistry models of Wong and Johnson (1996). Note that when comparing the models of Wong and Johnson to observations, we compare only those models that assume SO to be condensible; given the highly reactive nature of SO, we believe that SO should more readily stick to Io's surface than is allowed by the noncondensible assumption.

Wong and Johnson (1996) predict that the SO/SO_2 ratio will be 2–4% at the solar zenith angles relevant to the observations of McGrath *et al*. (2000). Low SO/SO_2 ratios (perhaps even $<2\%$) are also derived for one-dimensional SO_2 frost sublimation models with high vertical mixing (e.g., Summers and Strobel 1996 and our nonvolcanic model shown in Fig. 2). While the observed $\sim$3.3% SO/SO_2 ratio at Ra falls within the range predicted for frost sublimation, the $\sim$7.7% SO/SO_2 ratio observed at Pele provides further evidence that Pele may have been active at the time of the McGrath *et al*. observations (see Sections 4 and 6 above). In fact, although McGrath *et al*. (2000) do not emphasize this point, the very high $\sim$21% SO/SO_2 ratio suggested from the T3 observations suggests that this region also may have contained active volcanoes at the time of the observations (cf. Zolotov and Fegley 1998b). Although Wong and Johnson (1996) predict that the SO/SO_2 ratio can be enhanced with flow away from the subsolar point (the main source of SO_2 in their model), the SO/SO_2 ratio for the subsolar latitude relevant to T3 does not approach 21% even in models in which SO is assumed to be incondensible at the surface (see also Wong and Smyth 2000).

Volcanic emission with an SO/SO_2 ratio of 21% is possible but requires either high magma temperatures or low vent pressures, as can be seen in Fig. 2 of Zolotov and Fegley (1998b). However, the ratios between S, SO, and SO_2 inferred by McGrath *et al*. (2000) at T3 cannot be explained in terms of thermochemical equilibria in volcanic gases (Zolotov and Fegley 2000b), perhaps indicating that both volcanic and photochemical sources of SO might be present at T3 (e.g., more SO can be produced photochemically from photolysis of S_2 in a low density atmosphere). Alternatively (or additionally), as McGrath *et al*. (2000) point out, the column abundance of atomic sulfur as determined from ultraviolet emission lines could simply reflect the amount of sulfur that has been exposed to torus electrons that are energetic enough to cause excitation. If these electrons do not penetrate all the way to the surface (i.e., lose energy rapidly at they proceed), the derived S column density could be a lower limit.

The possibility of the sulfur column abundances derived from ultraviolet emission lines being lower limits complicates

interpretations of the McGrath *et al*. (2000) data. The S/SO_2 ratios observed by McGrath *et al*. are consistent with the ratios predicted by the frost sublimation models of Wong and Johnson (1996). However, the abundance of atomic sulfur is clearly not correlated with the abundance of SO_2 (e.g., no S emission was seen at Ra despite its inferred SO_2 column density intermediate between Pele and T3), causing McGrath *et al*. (2000) to conclude that SO_2 dissociation is not responsible for generating the atomic sulfur. This result is intriguing because it suggests that atomic S might be correlated with volcanic emission (either from direct outgassing or from photolysis of volcanic S_2). If so, disk-resolved observations of atomic sulfur could possibly be used to monitor the strength and ubiquitousness of volcanic emission across Io. The high SO/SO_2 ratios and the detection of S emission at Pele and T3 and the low SO/SO_2 abundance and lack of S emission at Ra is consistent with the hypothesis that active S_2-emitting volcanoes might be present at Pele and T3, but not at Ra. Even if this interpretation is incorrect (and note that Zolotov and Fegley 2000b show that the observed SO and SO_2 abundances at Ra can be explained by volcanic emission of gases with oxygen fugacity values similar to Pele and with reasonable derived magma temperatures in the range 1400–1500 K), the spatial heterogeneity in the SO_2 abundance observed by McGrath *et al*. (2000) indicates that frost sublimation models alone are not adequate for explaining Io's patchy atmosphere. Volcanic sources are clearly important.

The importance of widespread S_2-rich volcanism, however, is not evident because reliable data on the number of plumes that are S_2 rich vs those that are SO_2 dominant (and every possibility in between) are not available. Building on earlier work by McEwen and Soderblom (1983), McEwen *et al*. (1998a) suggest that several different classes of volcanic plumes may exist on Io. Prometheus-type plumes are the most common in the Voyager and Galileo images; they are characterized by plume heights of 50–150 km (in reflected light) and long eruption lifetimes. McEwen *et al*. (1998a) believe that these plumes may be associated with lateral migration of silicate magma that has come into contact with surface or near-surface volatiles such as SO_2 frost (e.g., plumes generated at the margins of silicate flows as they vaporize local SO_2 frost deposits). High-resolution Galileo images (McEwen *et al*. 2000) support this hypothesis. Such plumes may not contain much S_2 if SO_2 frost deposits are more prevalent than sulfur deposits in the surrounding terrain, if the encroaching silicate lava can cause melting and mobilization of liquid sulfur before the sulfur can be vaporized, or if the vaporization could occur at low enough temperatures that S_8 rather than S_2 is the dominant sulfur gas. Most of the interesting photochemistry discussed in this paper occurs because of the presence of S_2. The other plume types discussed by McEwen *et al*. (1998a), intermediate-sized plumes, stealth plumes, and unique individual plumes (e.g., Pele), may contain varying amounts of S_2. We simply have no way of telling right now.

Thermochemical equilibrium calculations by Zolotov and Fegley (1998a, 1998b, 1999, 2000a) and Fegley and Zolotov (2000) suggest that S_2 should be the second or first most abundant volcanic vapor on Io for a wide variety of assumptions about magma temperatures and vent pressures. However, in these papers, the S_2 abundance is shown to be quite sensitive to the O/S ratio of the exsolved volcanic gases. For Pele, the inferred O/S atomic ratio of 1.2 to 1.7 leads to S_2 concentrations of 24% to 7%. If for some reason more oxidized volcanism is the norm across Io, then then Pele-type plumes that are rich in S_2 might be rare. Further observations designed to search for S_2 in other plumes besides Pele are warranted. If the diffuse red deposits seen near active volcanic centers on Io (e.g., Spencer *et al*. 1997a, McEwen *et al*. 1998a) are caused by the generation of S_4 radicals upon condensation of S_2 vapor (see Section 8 above and Spencer *et al*. 2000), then S_2 emission might be common (but perhaps not continuous with time) on Io.

Aside from searching for S_2, future simultaneous or near-simultaneous observations of large plumes (such as at Pele) at a variety of ultraviolet wavelengths (e.g., with HST/STIS) would better define the relative abundances of S, SO, S_2, and SO_2 in plume eruptions. Such information would provide important constraints for thermochemical equilibrium models and would help characterize the temperature of the magma (and exsolved gases) and the pressure at which these gases were last equilibrated (see Zolotov and Fegley 2000a). If simultaneous observations are not possible, the determination of the S/SO_2 ratio in volcanic regions and the determination of whether S emission is correlated with volcanic plumes would be very helpful in constrainting the relative contribution of photochemistry and thermochemistry to the production of atomic S. Microwave monitoring of SO and SO_2 would better define the average SO/SO_2 ratio on Io and would help confirm or refute our suggestion that the SO/SO_2 ratio could be correlated with volcanic activity. Far-infrared observations from ground-based telescopes, Earth-orbiting satellites, or the Cassini Composite Infrared Spectrometer (CIRS) instrument might aid in the search for signatures of S_2O, polysulfur oxides, S_8, or any surface constituent other than SO_2 frost. Our photochemical modeling reinforces earlier suggestions that the O/S ratio in Io's plasma torus may be correlated with volcanic activity (e.g., Smith and Strobel 1985). Existing or future observations that monitor the time-variability of the O/S ratio of the neutral cloud or torus ions and are then compared with ground-based or Galileo observations of volcanic activity on Io may confirm or refute this suggestion.

Additional laboratory and theoretical investigations would help in the quest to fully understand the complex nature of Io's atmosphere and surface. Better theoretical or experimental cross sections for S_2, SO, and S_2O would be useful in constraining the atmospheric photochemistry, as would better kinetic rate constants for reactions involving S_2 (e.g., $S_2 + S_2 + M \rightarrow S_4 + M$, $O + S_2 \rightarrow SO + S$) and reactions involving sulfur–sulfur and sodium–sulfur interactions (see Table II for a list of the most important reactions). Modern laboratory investigations into the behavior of condensed S_2 and condensed SO at conditions relevant to Io would shed light on possible atmosphere–surface

interactions and on the surface composition near active plumes and across Io's entire surface.

The one-dimensional hydrostatic equilibrium models described here are gross oversimplifications to the actual situation on Io, in which volcanic gases will rapidly flow away from the source regions. The models were designed to highlight the important potential qualitative differences between volcanically generated atmospheres and frost-sublimation driven atmospheres on Io. To derive a more realistic description of the composition and chemistry of Io's atmosphere, multidimensional models similar to the powerful three-dimensional atmospheric models of Wong and Johnson (1996) and Wong and Smyth (2000) should be expanded to include volcanic sources. In addition, a more realistic description of photochemistry and condensation within an actual plume eruption (as opposed to a simple 1-D model with volcanic gases being released at the surface) would highlight specific interesting short-term photochemical behavior.

Although we are still far from acquiring a complete understanding of the chemistry of Io's atmospheric and surface environment, each new bit of evidence brings us closer to unraveling the mysteries of this enigmatic moon.

APPENDIX A: PHOTOCHEMICAL MODEL DESCRIPTION

A.1. Numerical Approach

Using the Caltech/JPL chemical kinetics and diffusion code (e.g., Allen *et al*. 1981, Yung *et al*. 1984, Gladstone *et al*. 1996), we solve the coupled one-dimensional continuity equations in spherical geometry as a function of time t and radius r for all of the proposed constituents in Io's atmosphere:

$$\frac{\partial n_i}{\partial t} + \frac{1}{r^2}\frac{\partial (r^2 \Phi_i)}{\partial r} = P_i - L_i, \tag{5}$$

where n_i is the concentration of the i-th constituent (cm^{-3}), $r = R_0 + z$ is the radius at altitude z above Io's surface radius R_0, Φ_i is the radial flux of the i-th constituent (cm^{-2} s^{-1}), and P_i and L_i are the local chemical production and loss rates of the i-th constituent (cm^{-3} s^{-1}). In most cases, we allow the solutions to the coupled equations (5) to reach steady state, so that $\partial n_i/\partial t \rightarrow 0$, and we keep the solar zenith angle fixed at a hemispherically averaged value of 60°. Both eddy and molecular diffusion are considered in the transport terms for the neutral species:

$$\Phi_i = -n_i D_i \left(\frac{1}{n_i}\frac{dn_i}{dr} + \frac{1}{H_i} + \frac{1}{T}\frac{dT}{dr} \right) - n_i K_E \left(\frac{1}{n_i}\frac{dn_i}{dr} + \frac{1}{H_a} + \frac{1}{T}\frac{dT}{dr} \right), \tag{6}$$

where D_i is the molecular diffusion coefficient of the i-th constituent, $H_i = kT/m_i g$ is the pressure scale height of the i-th constituent, T is the neutral atmospheric temperature, $H_a = kT/\mu g$ is the average atmospheric pressure scale height, K_E is the eddy (turbulent) diffusion coefficient, k is the Boltzmann constant, m_i is the mass of the i-th constituent, μ is the mean molecular mass of the atmosphere, and g is the gravitational acceleration at radius r. The effects from thermal diffusion will be small and are ignored.

The coupled equations (5) are solved using an implicit finite-difference Eulerian method, with a vertical resolution of at least three altitude levels per scale height. Calculations are performed until successive iterations differ by no more than 0.1%. The extinction of solar radiation is calculated in 5-nm wavelength bins for wavelengths greater than 125 nm and with a finer wavelength grid below 125 nm. For most models, we adopt solar flux values representative of low solar activity (as described in Mills 1998). A total of 109 different S-, O-, Na-, K-, Cl, and H-bearing neutral and ionized species are allowed to vary with vertical transport and with 766 different chemical reactions. Condensation of supersaturated vapor about atmospheric aerosols is included using the technique of Moses *et al*. (2000). Although ion chemistry and diffusion are considered in the model, a full discussion of ion transport and chemistry (as well as the chemistry of hydrogen-bearing species) is deferred to a future paper. Ion chemistry will only be mentioned when it plays an important role in controlling neutral abundances. As with the models of Summers and Strobel (1996), we make the simplifying assumption that solar ultraviolet radiation is the only ionization source in the atmosphere—photoelectron impact (e.g., Bhardwaj and Michael 1999) and bombardment by corotating jovian magnetospheric electrons (e.g., Kumar 1980, 1984, 1985) are ignored despite their obvious potential importance as ionization sources. The neglect of these ionization sources, however, should have relatively little effect on our predictions regarding the relative column densities of the neutral constituents (although the concentrations at high altitudes could be greatly affected).

Appropriate boundary conditions for Io photochemical models are difficult to characterize definitively. Jovian magnetospheric plasma, which is locked to and rotates with Jupiter's magnetic field, continually bombards Io. Although a large but currently uncertain fraction of the corotating plasma may be diverted around Io due to the thickness of Io's atmosphere, due to ionospheric currents within Io's atmosphere, or due to a possible intrinsic magnetic field of the satellite, some portion of the corotating ions will impact the neutral atmosphere (e.g., Spencer and Schneider 1996). This plasma–atmosphere interaction leads to momentum and energy transfer (and hence atmospheric sputtering), charge–exchange reactions, heating of the atmosphere, and other effects that enhance the escape of ions, atoms, and molecules from Io's upper atmosphere. Because these interaction processes depend in a complex way on the poorly defined geometry and characteristics of the plasma flow past Io, we follow the lead of Summers and Strobel (1996) in making the simplifying assumption that escape from the top of our model atmosphere is highly efficient.

Our upper boundary condition for all neutral and ionic species represents a maximum "limiting flux" condition (see Chamberlain and Hunten 1987) in which escape occurs as rapidly as the species can be replaced by vertical transport (with appropriate modifications to account for the fact that an escaping constituent can become a major component of the atmosphere at high altitudes). For SO_2, we assume an escape flux of zero at the top boundary to remain consistent with our hydrostatic equilibrium assumption. In reality, SO_2 will also be escaping due to sputtering and other processes; in that situation, the "background" gas will not be completely stationary, and our assumptions are no longer valid. In addition, we neglect mutual drag forces between the constituents. Hunten (1985) shows that mutual drag forces operating on the escaping atmospheric species could offset diffusive separation to some extent, so that differences in the scale heights of the various species would be minimized. Our simplifying assumptions will adversely affect the predictions for species concentrations at high altitudes. Note, however, that escape out the top boundary is generally a minor component of mass loss from the system compared with the flux to the surface in our models, and although our simplifying assumptions will affect the high-altitude concentrations, the overall predictions regarding the column abundances of the important constituents will not be greatly affected.

At the lower boundary of our model (Io's surface), we use fixed mixing ratio boundary conditions for those species that are produced volcanically from the thermochemical equilibrium calculations (see Table I). Thus, our model differs dramatically from previous photochemical models of Io (e.g., Kumar 1982, Summers and Strobel 1996, Wong and Johnson 1996, Wong and Smyth 2000) in that we assume a volcanic source continually resupplies vapor at the lower boundary. For species that are not included in the thermochemical equilibrium calculations (i.e., ions and several minor neutral species), we again follow the lead of Summers and Strobel (1996) and adopt a maximum flux boundary condition at the lower boundary. Such a boundary condition is similar to the assumption that these species flow as rapidly as is possible by diffusion to the surface and then react chemically or "stick" to the surface upon contact. Note that for these conditions, species such as SO that have a column-integrated

TABLE A1
Boundary Fluxes in Standard Moderate Density Model

Species	Flux at bottom (cm^{-2} s^{-1})	Flux at top (cm^{-2} s^{-1})	Species	Flux at bottom (cm^{-2} s^{-1})	Flux at top (cm^{-2} s^{-1})
O	-4.745×10^{10}	$+2.787 \times 10^{10}$	NaO_2	-7.382×10^{1}	$+7.632 \times 10^{-7}$
$O(^1D)$	-1.167×10^{1}	$+1.204 \times 10^{4}$	NaS	-1.431×10^{6}	$+8.831 \times 10^{-1}$
O_2	-1.578×10^{9}	$+3.231 \times 10^{8}$	NaS_2	-1.633×10^{8}	$+1.086 \times 10^{-4}$
O_3	-8.212×10^{-6}	$+3.608 \times 10^{-11}$	Na_2S	-2.806×10^{-1}	$+4.164 \times 10^{-7}$
S	-2.147×10^{12}	$+5.087 \times 10^{10}$	NaOS	-9.277×10^{7}	$+2.036 \times 10^{-2}$
S_2	$+1.255 \times 10^{12}$	$+2.355 \times 10^{8}$	$NaSO_2$	-1.483×10^{9}	$+1.587 \times 10^{-2}$
S_3	$+1.339 \times 10^{9}$	$+2.076 \times 10^{-2}$	KO	$+4.038 \times 10^{4}$	$+1.124 \times 10^{-3}$
S_4	-3.096×10^{9}	$+1.336 \times 10^{-8}$	KO_2	-6.529×10^{0}	$+1.216 \times 10^{-7}$
S_5	-5.273×10^{3}	$+2.977 \times 10^{-14}$	KS	$+1.596 \times 10^{8}$	$+4.079 \times 10^{-2}$
S_6	-1.037×10^{2}	$+4.622 \times 10^{-16}$	KS_2	-1.724×10^{7}	$+2.145 \times 10^{-5}$
S_7	-7.447×10^{-3}	$+2.439 \times 10^{-19}$	K_2S	$+2.663 \times 10^{0}$	$+4.890 \times 10^{-9}$
S_8	-7.329×10^{-2}	$+1.796 \times 10^{-20}$	KSO_2	-1.441×10^{8}	$+2.496 \times 10^{-3}$
SO	-7.979×10^{11}	$+1.776 \times 10^{10}$	O^+	-1.064×10^{2}	$+3.170 \times 10^{4}$
SO_2	$+4.274 \times 10^{11}$	$+0.0$	O_2^+	-2.089×10^{3}	$+2.328 \times 10^{4}$
SO_3	$+2.559 \times 10^{5}$	$+5.979 \times 10^{2}$	S^+	-5.476×10^{2}	$+1.725 \times 10^{6}$
S_2O	$+4.364 \times 10^{10}$	$+8.303 \times 10^{2}$	S_2^+	-6.180×10^{4}	$+1.236 \times 10^{4}$
$(SO)_2$	-6.712×10^{5}	$+2.369 \times 10^{1}$	SO^+	-5.375×10^{3}	$+1.870 \times 10^{6}$
ClO	$+4.132 \times 10^{4}$	$+1.410 \times 10^{3}$	SO_2^+	-3.343×10^{3}	$+7.341 \times 10^{4}$
SCl	$+4.326 \times 10^{7}$	$+2.352 \times 10^{3}$	NaO^+	-5.677×10^{3}	$+9.725 \times 10^{3}$
SCl_2	$+2.820 \times 10^{2}$	$+4.166 \times 10^{-5}$	NaS^+	-1.866×10^{3}	$+2.006 \times 10^{1}$
S_2Cl	-3.379×10^{6}	$+1.793 \times 10^{1}$	$NaSO_2^+$	-2.553×10^{3}	$+4.091 \times 10^{-4}$
OSCl	-1.646×10^{3}	$+4.850 \times 10^{3}$	KO^+	-1.648×10^{2}	$+4.793 \times 10^{2}$
$ClSO_2$	-1.296×10^{4}	$+3.385 \times 10^{4}$	KS^+	-4.667×10^{1}	$+9.556 \times 10^{-1}$
NaO	$+1.501 \times 10^{7}$	$+8.000 \times 10^{-3}$	KSO_2^+	-2.875×10^{2}	$+3.863 \times 10^{-5}$

Note. See text for further discussion. Only the most abundant sulfur and oxygen species are included in the table. Negative fluxes are downward, positive fluxes are upward. All fluxes are relative to a square centimeter at Io's surface radius. The zero flux for SO_2 at the top boundary is due to model assumptions. With the exception of SO_2, the fluxes listed in the table are actually calculated for the middle of the bottom layer and middle of the top layer in the model (i.e., values were printed out at half grid points rather than at the boundaries themselves).

photochemical production rate that is greater than than the combined rates of their volcanic influx and escape to space will have a net downward flux at the lower boundary [see Table A1 and Eqs. (5) and (6)]. This situation does not imply that the volcanic source is unimportant for such species—the downward flux is smaller than it would outherwise be without the volcanic source.

The upward flux of the major volcanic species (particularly S_2, SO_2, NaCl, KCl, S_2O, S_3, KS, SCl, NaO, Cl_2, KO, and ClO) at the lower boundary is balanced to within better than 0.1% by the downward flux of species such as SO, S, Na, Cl, $NaCl_{(con)}$, O, K, $KCl_{(con)}$, Na^+, O_2, K^+, and $NaSO_2$ at the lower boundary and the upward flux of species such as S, O, SO, Na, and Cl at the upper boundary (see Table A1). Conservation of mass is maintained for all our models (as can be seen by comparing the fluxes of the elements sulfur and oxygen into and out of the system; see Table A1), and the initial S/O/Na/K/Cl ratios are preserved to within better than 1% in the final steady-state models. Note that the high flux of S_2 as compared with SO_2 at the lower boundary in Table A1 does not imply that S_2 is dominating the volcanic input. The model is a one-dimensional Eulerian calculation, not a Lagrangian calculation or a zero-dimensional model. The fluxes and concentration gradients in the model adjust as a result of diffusion and chemistry [see Eqs. (5) and (6)]. The greater the column-integrated rate of photochemical loss or the larger the escape rate to space, the larger the upward flux at the lower boundary must become to preserve mass balance. Similarly, heavier species will tend to have steeper (more negative) concentration gradients because of molecular diffusion, and the upward fluxes of heavy inert species will be larger than light inert species. The flux at the lower boundary simply reflects a balance between loss (or gain) due to photochemistry and loss due to escape to space, and the values shown in Table A1 and Fig. 2, 4, and 5 represent the steady-state solution to Eqs. (5) and (6)—the resulting fluxes at the lower boundary are not linear (i.e., different by a factors of X_i, as they would be in a zero-dimensional model), even though the mixing ratios at the lower boundaries are fixed at factors of X_i apart.

We have not attempted to accurately model atmospheric escape. The fluxes given in Table A1 are limiting flux values and represent upper limits to atmospheric escape. Escape processes are efficient on Io, and the total escape rate will be limited by how rapidly gas species can be transported to altitude regions where they can be more efficiently lost. Because the quasi-hydrostatic local atmospheres we are attempting to model here are not expected to be of global extent and because we do not include the physics of atmospheric escape, we do not compare our results with estimated escape fluxes from Io. Instead, we simply note that if our moderate-density model were to uniformly cover Io, the global escape rate of oxygen (in all forms) would be 1.9×10^{28} atoms s^{-1} and the global escape rate of sulfur (in all forms) would be 2.9×10^{28} atoms s^{-1}. As in other recent photochemical models (e.g., Summers and Strobel 1996, Wong and Johnson 1996, Wong and Smyth 2000), molecular escape is important. If we had allowed SO_2 to escape from the model, both the total escape rate and the O/S escape ratio would have been higher. The observed properties of Io's plasma torus and neutral clouds, combined with models of atmospheric loss processes and energy budgets within the torus, indicate that Io is losing atmospheric constituents at a rate of $\sim 3 \times 10^{28}$ atoms s^{-1} (e.g., Spencer and Schneider 1996). The escape rates from our moderate-density model in Table A1 are somewhat higher than this value, suggesting that a moderately dense atmosphere of the type shown here does not uniformly cover Io's surface. Ultraviolet and microwave observations of SO_2 support this conclusion (e.g., Lellouch *et al*. 1992, 1994, 1996, Sartoretti *et al*. 1994, 1996, Ballester *et al*. 1996, Trafton *et al*. 1996, Hendrix *et al*. 1999, McGrath *et al*. 2000).

A.2. Diffusion Coefficients

In our model atmosphere, we include vertical transport caused by both molecular diffusion and "eddy" diffusion. If turbulence generated by such processes as high-Reynolds-number gas flow across the surface or mixing caused by the breaking of upwardly propagating atmospheric waves is strong enough on Io, chemically inert species could be mixed uniformly with altitude, at least at lower atmospheric levels, helping to homogenize the composition of Io's lower atmosphere and allowing heavier molecular species to be transported to higher altitudes (see Summers and Strobel 1996). As the atmospheric density decreases with increasing altitude, however, molecular diffusion will quickly begin to dominate, and species will become diffusively separated. Although some laboratory and theoretical data exist for the determination of molecular diffusion coefficients appropriate for Io's atmosphere, the eddy diffusion coefficient profile is a free parameter in our modeling. Using mixing length theory for a turbulent boundary layer, Wong and Johnson (1996) estimate that $K_E \approx 10^8$ cm^2 s^{-1} at low altitudes on Io. Using several similar arguments, Summers and Strobel (1996) derive $K_E \approx 10^9$ cm^2 s^{-1} at low altitudes, but they further emphasize that the near-neutral stability criterion assumed in the boundary-layer analysis might not be applicable the situation on Io.

In Io's atmosphere as well as in the low-density stably stratified upper atmospheres of Earth and the other planets, eddy diffusion most likely arises from such processes as gravity-wave dissipation (e.g., Lindzen 1971). For atmospheric mixing generated by these upwardly propoagating waves, one might expect K_E to increase roughly inversely with the square root of atmospheric pressure, and values of $K_E = 10^6$ to 10^9 cm^{-2} s^{-1} are not unreasonable based on the inferred values for K_E at similar pressures on Earth and the giant planets (e.g., Chamberlain and Hunten 1987, Moses *et al*. 2000). However, without better knowledge of how strongly these waves might be generated on Io, it is not possible to constrain K_E in Io's atmosphere without the aid of a chemical tracer from which K_E might be inferred. No such chemical tracers have been identified for Io's lower atmosphere. For a lack of more definitive information (including the altitude variation of K_E), we assume an altitude-independent eddy diffusion coefficient of 10^9 cm^{-2} s^{-1} in our standard model (see the similar modeling by Summers and Strobel 1996)—in that situation, the SO_2 homopause (i.e., the altitude at which the SO_2 self-diffusion coefficient equals K_E) is located at ~34 km in our standard moderate-density model. We also examine how the results change for an assumption of $K_E = 10^8$ cm^{-2} s^{-1} at all altitudes (e.g., homopause level at ~16 km).

For the molecular diffusion coefficients, we adopt the binary diffusion parameters given in Table 2 of Summers (1985). However, for a species X other than S, O, O_2, and SO_2, we assume that the X-SO_2 binary diffusion coefficients are

$$D_i = 8.1 \times 10^{15} \frac{T^{0.943}}{n} \sqrt{\frac{32.06}{m_i}\left(\frac{m_i + 64.06}{96.12}\right)}, \quad (7)$$

where D_i is in cm^2 s^{-1}, m_i is in amu, T is in kelvins, n is in cm^{-3}, and all the other symbols are defined above. Based on information provided in Reid *et al*. (1987), the self diffusion coefficient of SO_2 is assumed to be

$$D_i = 2.6 \times 10^{16} \frac{T^{0.75}}{n}, \quad (8)$$

where all units are cgs. At the surface of our moderate-density model, the most abundant species SO_2, S_2, and SO have diffusion coefficients $D_{SO_2} = 6.7 \times 10^6$ cm^2 s^{-1}, $D_{S_2} = 4.2 \times 10^6$ cm^2 s^{-1}, and $D_{SO} = 4.6 \times 10^6$ cm^2 s^{-1}. These values increase rapidly with height. At 24 km, $D_{SO_2} = 4.7 \times 10^8$ cm^2 s^{-1}, $D_{S_2} = 3.9 \times 10^8$ cm^2 s^{-1}, and $D_{SO} = 4.2 \times 10^8$ cm^2 s^{-1}.

A.3. Photochemical Reactions

Our model contains the species listed in Table I, along with SO_2, Cl, Cl_2, ClOO, OClO, ClO_3, Cl_2O, Cl_2O_2, S_2Cl_2, Na, Na_2, NaO_3, Na_2O, Na_2SO_4, NaCl, $NaCl_{(con)}$, $(NaCl)_2$, $(NaCl)_3$, K, K_2, K_2O, K_2S, K_2SO_4, KCl, $KCl_{(con)}$, $(KCl)_2$, KNa, neutral hydrogen-bearing species, and the ions H^+, H_2^+, H_3^+, O^+, O_2^+, OH^+, H_2O^+, H_3O^+, HO_2^+, S^+, S_2^+, SO^+, SO_2^+, HSO_2^+, Cl^+, Cl^-, HCl^+, Na^+, Na_2^+, NaO^+, NaO_2^+, Na_2O^+, NaS^+, $NaSO_2^+$, $NaCl^+$, K^+, KO^+, KO_2^+, KS^+, KSO_2^+, KCl^+, and electrons. Many of the species listed above and in Table I (e.g., the hydrogen compounds and the chlorine oxides) are not important in the current model; however, they were included to ensure that any future changes to our initial conditions (i.e., based on new observations or changes in the assumptions of the thermochemical model) would still provide as complete a picture as possible of the potential photochemical pathways in Io's atmosphere.

Table A2 lists the photodissociation reactions for the neutral sulfur and oxygen species considered in this paper. Also shown in the table are the photolysis rates (J values) in free space at 1 AU for low solar activity (for ease in comparison with other studies), the photolysis rates at 490 and 10 km in our standard Io model atmosphere, and the references for the photoabsorption cross sections and photolysis quantum yields. Most of the cross sections used in our modeling are taken from the Venus study of Mills (1998). Branching ratios for the different photolysis pathways are generally poorly known as a function of wavelength, and often had to be estimated. The total photoabsorption cross sections for SO_2 used in this paper are discussed fully in Mills (1998). The photodissociation and photoionization quantum yields for SO_2 are not completely known. We use the quantum yields provided by F. P. Mills (personal communication, 1999). Mills estimated the quantum yields for the three primary branches for netural photolysis based on the known structure of the SO_2 molecule, on qualitative measurements of the relative importance of the different photolysis pathways, on limited information regarding the vibrational modes that are likely to be excited at different wavelengths, and on the measured fluorescence efficiencies.

For S_2, we use theoretical cross sections and photolysis rates provided by Yelle *et al*. (unpublished manuscript, 2000). The S_2 cross sections are very temperature- and pressure-dependent. For a total S_2 column density of 10^{16} molecules cm^{-2}, Yelle *et al*. find that the photolysis rates at 1 AU in free space are ~2.4×10^{-3} s^{-1}, ~4.0×10^{-3} s^{-1}, and ~5.8×10^{-3} s^{-1} for S_2 molecules at 100 K, 300 K, and 1000 K, respectively, and the J values also change with the assumed total column density of S_2. We use this information combined with the actual low-temperature cross sections, a dissociation threshold of 278 nm, and an assumed photodissociation efficiency of ~77% to determine roughly appropriate photolysis cross sections for our model (see also A'Hearn *et al*. 1983, de Almeida and Singh 1986, and Kim *et al*. 1990 for further information about the photolysis lifetime of S_2). For S_3, we use the measured photoabsorption cross sections of Billmers and Smith (1991), and we assume that photolysis into the branch $S_3 \rightarrow S_2 + S$ occurs with 100% efficiency at wavelengths below the threshold 455 nm. For S_4, the cross sections also come from Billmers and Smith (1991). Based on the photodissociation thresholds for the $S_4 \rightarrow 2S_2$ versus $S_4 \rightarrow S_3 + S$ (1080 nm vs 439 nm), we assume that the former pathway dominates, and we arbitrarily adopt an 80% dissociation efficiency when determining the photolysis cross sections. For further information on the S_3 and S_4 cross sections, see Krasnopolsky (1987). Other details on the cross sections used in this model can be found in the references given in Table A2.

The list of neutral reactions for the S- and O-bearing species in our model is provided in Table A3. As is obvious from the table, the rate coefficients for many sulfur, alkali, and halogen reactions are not well determined and needed to be estimated. The kinetics databases and compilations of Mallard *et al*. (1998), DeMore *et al*. (1997), Atkinson *et al*. (1997), Baulch *et al*. (1994), and Singleton and Cvetanović (1988) were useful in creating this list, as were the flame chemistry studies of Schofield and Steinberg (1992) and Jensen and Jones (1978). Many of the sulfur reactions were taken from Moses *et al*. (1995), Moses (1996), and Mills (1998).

TABLE A2
Photolysis Reactions

	Reaction	Photolysis rate J (s^{-1}) at 1 AU	at 490 km	at 10 km	Wavelength (nm)	Reference
R2	$O_2 \xrightarrow{h\nu} 2O$	1.1×10^{-6}	4.1×10^{-8}	9.4×10^{-9}	$3 \leq \lambda \leq 242$	a
R3	$O_2 \xrightarrow{h\nu} O + O(^1D)$	3.0×10^{-6}	1.1×10^{-7}	8.3×10^{-8}	$117 \leq \lambda \leq 175$	a
R4	$O_3 \xrightarrow{h\nu} O_2 + O$	1.4×10^{-3}	4.4×10^{-5}	4.1×10^{-5}	$158 \leq \lambda \leq 800$	b
R5	$O_3 \xrightarrow{h\nu} O_2 + O(^1D)$	7.3×10^{-3}	2.7×10^{-4}	2.5×10^{-4}	$53 \leq \lambda \leq 411$	b
R6	$O_3 \xrightarrow{h\nu} 3O$	6.1×10^{-6}	2.3×10^{-7}	5.0×10^{-8}	$53 \leq \lambda \leq 203$	b
R11	$S_2 \xrightarrow{h\nu} 2S$	2.5×10^{-3}	9.4×10^{-5}	8.5×10^{-5}	$238 \leq \lambda \leq 278$	c
R12	$S_3 \xrightarrow{h\nu} S_2 + S$	1.1	4.1×10^{-2}	4.1×10^{-2}	$350 \leq \lambda \leq 455$	d
R13	$S_4 \xrightarrow{h\nu} 2S_2$	1.7×10^{-1}	6.4×10^{-3}	6.4×10^{-3}	$425 \leq \lambda \leq 575$	d
R15	$SO \xrightarrow{h\nu} S + O$	4.4×10^{-4}	1.6×10^{-5}	1.1×10^{-5}	$113 \leq \lambda \leq 230$	b
R16	$SO_2 \xrightarrow{h\nu} SO + O$	2.2×10^{-4}	8.3×10^{-6}	5.9×10^{-6}	$63 \leq \lambda \leq 220$	b, e
R17	$SO_2 \xrightarrow{h\nu} S + O_2$	6.6×10^{-6}	2.4×10^{-7}	4.7×10^{-8}	$63 \leq \lambda \leq 210$	b, e
R18	$SO_2 \xrightarrow{h\nu} S + 2O$	2.2×10^{-7}	8.0×10^{-9}	2.3×10^{-10}	$63 \leq \lambda \leq 112$	b, e
R19	$SO_3 \xrightarrow{h\nu} SO_2 + O$	4.6×10^{-5}	1.7×10^{-6}	8.1×10^{-7}	$99 \leq \lambda \leq 193$	a
R20	$SO_3 \xrightarrow{h\nu} SO_2 + O(^1D)$	8.7×10^{-4}	3.2×10^{-5}	2.5×10^{-5}	$99 \leq \lambda \leq 270$	a
R21	$SO_3 \xrightarrow{h\nu} SO + O_2$	1.3×10^{-4}	4.8×10^{-6}	4.6×10^{-6}	$218 \leq \lambda \leq 305$	a
R22	$SO_3 \xrightarrow{h\nu} SO + 2O$	1.6×10^{-5}	5.7×10^{-7}	4.5×10^{-8}	$99 \leq \lambda \leq 135$	a
R23	$S_2O \xrightarrow{h\nu} SO + S$	5.0×10^{-2}	1.8×10^{-3}	1.7×10^{-3}	$260 \leq \lambda \leq 335$	b
R26	$ClO \xrightarrow{h\nu} Cl + O$	6.1×10^{-3}	2.2×10^{-4}	2.1×10^{-4}	$228 \leq \lambda \leq 325$	b
R33	$SCl \xrightarrow{h\nu} S + Cl$	2.5×10^{-2}	9.3×10^{-4}	9.3×10^{-4}	$335 \leq \lambda \leq 505$	b
R36	$S_2Cl \xrightarrow{h\nu} S_2 + Cl$	6.6×10^{-2}	2.5×10^{-3}	2.5×10^{-3}	$325 \leq \lambda \leq 485$	b
R37	$S_2Cl \xrightarrow{h\nu} SCl + S$	1.8×10^{-4}	6.6×10^{-6}	6.6×10^{-6}	$325 \leq \lambda \leq 345$	b
R43	$NaO_2 \xrightarrow{h\nu} Na + O_2$	5.8×10^{-3}	2.1×10^{-4}	2.0×10^{-4}	$148 \leq \lambda \leq 325$	f
R48	$NaS_2 \xrightarrow{h\nu} Na + S_2$	—	3.2×10^{-4}	3.0×10^{-4}		Est. $= 1.5 \times J_{43}$
R51	$KO_2 \xrightarrow{h\nu} K + O_2$	—	2.1×10^{-4}	2.0×10^{-4}		Est., i

Note. Photolysis rates for low solar activity (see Mills 1998 for details about the adopted solar flux). Only the photodissociation reactions for the important sulfur and oxygen species are included in the table. The first column of J values corresponds to the photolysis rate in free space at 1 AU for low solar activity; the second and third columns correspond to the photolysis rates at 490 and 10 km altitude in our standard moderate-density Io model for a 60° solar zenith angle and low solar activity. Although the photodissociation reactions for the pure alkali and halogen species are not included in the list (see Paper 2), the full numbering system is maintained for consistency between papers. References: (a) Moses *et al*. (2000) and references therein; (b) Mills (1998) and references therein; (c) Roger V. Yelle, personal communication, 2000; (d) Billmers and Smith (1991); (e) Franklin P. Mills, personal communication, 1999; (f) Rajasekhar *et al*. (1989); (g) Helmer and Plane (1993); (h) Summers and Strobel (1996); (i) Eska *et al*. (1999).

APPENDIX B: SENSITIVITY TESTS

B.1. Sensitivity to Atmospheric Density

If we assume that volcanic outgassing is more (or less) prolific than in our moderate-density model such that the total atmospheric density is increased (or decreased), we find that both the absolute and relative abundances of the various atmospheric constituents change noticeably. For example, Fig. 4 shows the concentrations of the major sulfur and oxygen species in our high- and low-density atmospheric models as a function of altitude and pressure. Other properties, such as the eddy diffusion coefficient and the relative abundances of the volcanic gases at the lower boundary, are kept the same in these models as compared with our standard moderate-density model (cf. Fig. 2a).

Note from Fig. 4 that the column abundance of most of the atmospheric constituents increases (or decreases) when the total atmospheric density is increased (or decreased). This result is straightforward. Because the relative abundances of the thermochemical equilibrium species are kept the same at the lower boundary, the absolute abundances of the parent volcanic gases at the lower boundary are much greater in the higher density model, resulting in overall higher volcanic gas abundances and correspondingly greater photochemical production rates for most atmospheric constitutents. Similarly, production rates are generally reduced for the low-density model. Because of the complicated nature of the photochemistry, however, the increase (or decrease) in column abundances is not linear. Some species (such as $NaSO_2$) exhibit enormous increases going from the low-density to the high-density case while others (such as O_2) stay relatively unchanged (to within a factor of $\sim$2) in terms of total column abundance between the three models. Although production rates tend to increase in the high-density model, photochemical loss rates generally increase as well. For some of the species (O_2 is a prominent example), the increased production and loss rates balance each other such that there is little difference in the total column density between the three models.

TABLE A3
Neutral Chemical Reactions

	Reaction	Rate constant[a]	Reference
R57	$2O \xrightarrow{M} O_2$	$k_0 = 5.2 \times 10^{-35}\, e^{(900/T)}$	Tsang and Hampson (1986)
R58	$O + O_2 \xrightarrow{M} O_3$	$k_0 = 5.08 \times 10^{-27} T^{-2.8}$	Atkinson *et al*. (1997)
R62	$O + S \xrightarrow{M} SO$	$k_0 = 1.5 \times 10^{-34}\, e^{(900/T)}$	Est., Muller *et al*. (1979)
R63	$O + S_2 \rightarrow S + SO$	$2.2 \times 10^{-11}\, e^{(-84/T)}$	Craven and Murrell (1987)
R64	$O + S_3 \rightarrow S_2 + SO$	8.0×10^{-11}	Estimate, Moses (1996)
R65	$O + S_4 \rightarrow S_3 + SO$	8.0×10^{-11}	Estimate, Moses (1996)
R66	$O + S_5 \rightarrow S_4 + SO$	$8.0 \times 10^{-11}\, e^{(-200/T)}$	Estimate, Moses (1996)
R67	$O + S_6 \rightarrow S_5 + SO$	$8.0 \times 10^{-11}\, e^{(-300/T)}$	Estimate, Moses (1996)
R68	$O + S_7 \rightarrow S_6 + SO$	$8.0 \times 10^{-11}\, e^{(-200/T)}$	Estimate
R69	$O + S_8 \rightarrow S_7 + SO$	$8.0 \times 10^{-11}\, e^{(-400/T)}$	Estimate
R73	$O + SO \xrightarrow{M} SO_2$	$k_0 = 4.5 \times 10^{-27}\, T^{-1.59}$	Singleton and Cvetanović (1988) and Grillo *et al*. (1979)
R74	$O + SO_2 \xrightarrow{M} SO_3$	$k_0 = 4.0 \times 10^{-32}\, e^{(-1000/T)}$	Atkinson *et al*. (1997)
R75	$O + SO_3 \rightarrow SO_2 + O_2$	$2.32 \times 10^{-16}\, e^{(-487/T)}$	Jacob and Winkler (1972)
R76	$O + S_2O \rightarrow 2SO$	1.5×10^{-12}	Singleton and Cvetanović (1988)
R77	$O + (SO)_2 \rightarrow S_2O + O_2$	3.0×10^{-14}	Est., Yung and DeMore (1982)
R78	$O + (SO)_2 \rightarrow SO + SO_2$	3.0×10^{-15}	Est., Mills (1998)
R80	$O + Cl_2 \rightarrow ClO + Cl$	$4.17 \times 10^{-12}\, e^{(-1368/T)}$	Baulch *et al*. (1981)
R82	$O + ClO \rightarrow O_2 + Cl$	$3.0 \times 10^{-11}\, e^{(70/T)}$	DeMore *et al*. (1997)
R88	$O + SCl \rightarrow SO + Cl$	1.2×10^{-10}	Murrells (1988)
R90	$O + S_2Cl \rightarrow SO + SCl$	1.0×10^{-13}	Estimate
R91	$O + OSCl \rightarrow SO_2 + Cl$	$5.0 \times 10^{-11}\, e^{(-600/T)}$	Estimate
R92	$O + OSCl \rightarrow SO + ClO$	$2.0 \times 10^{-11}\, e^{(-600/T)}$	Estimate
R93	$O + ClSO_2 \rightarrow SO_2 + ClO$	1.0×10^{-11}	Est., Mills (1998)
R95	$O + Na_2 \rightarrow NaO + Na$	$4.0 \times 10^{-10}\, e^{(-800/T)}$	Estimate
R98	$O + NaO \rightarrow Na + O_2$	$1.56 \times 10^{-11}\, T^{0.5}$	Plane and Husain (1986)
R103	$O + NaS \rightarrow Na + SO$	3.7×10^{-10}	Assume same as O + NaO
R104	$O + NaS_2 \rightarrow NaS + SO$	$2.0 \times 10^{-10}\, e^{(-940/T)}$	Est. based on $O + NaO_2$
R105	$O + NaS_2 \rightarrow NaO + S_2$	$3.0 \times 10^{-10}\, e^{(-940/T)}$	Est. based on $O + NaO_2$
R108	$O + NaOS \rightarrow Na + SO_2$	$3.0 \times 10^{-10}\, e^{(-940/T)}$	Est. based on $O + NaO_2$
R109	$O + NaOS \rightarrow NaO + SO$	$2.0 \times 10^{-10}\, e^{(-940/T)}$	Est. based on $O + NaO_2$
R110	$O + NaSO_2 \rightarrow NaO + SO_2$	$8.5 \times 10^{-10}\, e^{(-800/T)}$	Est. based on Schofield and Steinberg (1992)
R114	$O + KO \rightarrow K + O_2$	$1.56 \times 10^{-11} T^{0.5}$	Est. based on O + NaO
R115	$O + KO_2 \rightarrow KO + O_2$	$5.0 \times 10^{-10}\, e^{(-940/T)}$	Est. based on $O + NaO_2$
R116	$O + KS \rightarrow K + SO$	$1.56 \times 10^{-11} T^{0.5}$	Est. based on O + NaO
R117	$O + KS_2 \rightarrow KS + SO$	$2.0 \times 10^{-10}\, e^{(-940/T)}$	Est. based on $O + NaO_2$
R118	$O + KS_2 \rightarrow KO + S_2$	$3.0 \times 10^{-10}\, e^{(-940/T)}$	Est. based on $O + NaO_2$
R121	$O + KSO_2 \rightarrow KO + SO_2$	$8.5 \times 10^{-10}\, e^{(-800/T)}$	Est. based $O + NaSO_2$
R128	$O(^1D) + SO_2 \rightarrow SO_2 + O$	7.0×10^{-11}	Estimate
R129	$O(^1D) + SO_2 \rightarrow SO + O_2$	1.3×10^{-10}	Estimate
R134	$O_2 + S \rightarrow SO + O$	2.3×10^{-12}	DeMore *et al*. (1997)
R135	$O_2 + SO \rightarrow SO_2 + O$	$2.6 \times 10^{-13}\, e^{(-2400/T)}$	DeMore *et al*. (1997)
R138	$O_2 + Na \xrightarrow{M} NaO_2$	$k_0 = 9.32 \times 10^{-27} T^{-1.4}$	DeMore *et al*. (1997)
R140	$O_2 + K \xrightarrow{M} KO_2$	$k_0 = 8.8 \times 10^{-27}\, T^{-1.23}$	DeMore *et al*. (1997)
R144	$O_3 + S \rightarrow SO + O_2$	1.2×10^{-11}	DeMore *et al*. (1997)
R147	$O_3 + Cl \rightarrow ClO + O_2$	$2.9 \times 10^{-11}\, e^{(-260/T)}$	DeMore *et al*. (1997)
R150	$O_3 + Na \rightarrow NaO + O_2$	$1.1 \times 10^{-9}\, e^{(-116/T)}$	Plane *et al*. (1993)
R153	$O_3 + K \rightarrow KO + O_2$	$1.15 \times 10^{-9}\, e^{(-120/T)}$	Plane and Helmer (1994)
R203	$2S \xrightarrow{M} S_2$	$k_0 = 5.0 \times 10^{-32}\, e^{(900/T)}$	Est. based on Fowles *et al*. (1967), Basco and Pearson (1967), and Langford and Oldershaw (1972, 1973)
R204	$S + S_2 \xrightarrow{M} S_3$	$k_0 = 1.0 \times 10^{-25}\, T^{-2}$	Estimate
R205	$S + S_3 \rightarrow 2S_2$	8.0×10^{-11}	Estimate, Moses (1996)
R206	$S + S_3 \xrightarrow{M} S_4$	$k_0 = 1.0 \times 10^{-25}\, T^{-2}$	Estimate
R207	$S + S_4 \rightarrow S_2 + S_3$	8.0×10^{-11}	Estimate, Moses (1996)
R208	$S + S_4 \xrightarrow{M} S_5$	$k_0 = 1.0 \times 10^{-25}\, T^{-2}$	Estimate

TABLE A3—*Continued*

	Reaction	Rate constant[a]	Reference
R209	$S + S_5 \rightarrow S_2 + S_4$	$5.0 \times 10^{-11}\, e^{(-200/T)}$	Estimate
R210	$S + S_5 \rightarrow 2S_3$	$3.0 \times 10^{-11}\, e^{(-200/T)}$	Estimate
R211	$S + S_5 \xrightarrow{M} S_6$	$k_0 = 1.0 \times 10^{-25}\, T^{-2}$	Estimate
R212	$S + S_6 \rightarrow S_2 + S_5$	$5.0 \times 10^{-11}\, e^{(-300/T)}$	Estimate
R213	$S + S_6 \rightarrow S_3 + S_4$	$3.0 \times 10^{-11}\, e^{(-300/T)}$	Estimate
R214	$S + S_6 \xrightarrow{M} S_7$	$k_0 = 1.0 \times 10^{-25}\, T^{-2}$	Estimate
R215	$S + S_7 \rightarrow S_2 + S_6$	$4.0 \times 10^{-11}\, e^{(-200/T)}$	Estimate
R216	$S + S_7 \rightarrow S_3 + S_5$	$2.0 \times 10^{-11}\, e^{(-200/T)}$	Estimate
R217	$S + S_7 \rightarrow 2S_4$	$2.0 \times 10^{-11} e^{(-200/T)}$	Estimate
R218	$S + S_7 \xrightarrow{M} S_8$	$k_0 = 1.0 \times 10^{-25}\, T^{-2}$	Estimate
R219	$S + S_8 \rightarrow S_2 + S_7$	$4.0 \times 10^{-11}\, e^{(-400/T)}$	Estimate
R220	$S + S_8 \rightarrow S_3 + S_6$	$2.0 \times 10^{-11}\, e^{(-400/T)}$	Estimate
R221	$S + S_8 \rightarrow S_4 + S_5$	$2.0 \times 10^{-11}\, e^{(-400/T)}$	Estimate
R225	$S + SO \xrightarrow{M} S_2O$	$k_0 = 1.0 \times 10^{-26}\, T^{-2}$	Estimate
R226	$S + SO_3 \rightarrow SO_2 + SO$	1.0×10^{-16}	Estimate
R227	$S + S_2O \rightarrow S_2 + SO$	$1.0 \times 10^{-12}\, e^{(-1200/T)}$	Estimate
R228	$S + Cl \xrightarrow{M} SCl$	$k_0 = 1.0 \times 10^{-29}\, T^{-1}$	Est. based on O + Cl
R229	$S + ClO \rightarrow SO + Cl$	4.0×10^{-11}	Estimate
R237	$S + SCl \rightarrow S_2 + Cl$	3.0×10^{-11}	Estimate
R239	$S + OSCl \rightarrow S_2O + Cl$	$5.0 \times 10^{-11}\, e^{(-600/T)}$	Estimate
R240	$S + OSCl \rightarrow SO + SCl$	$2.0 \times 10^{-11}\, e^{(-600/T)}$	Estimate
R241	$S + ClSO_2 \rightarrow SO_2 + SCl$	1.0×10^{-11}	Est. based on $O + ClSO_2$
R242	$S + Na \xrightarrow{M} NaS$	$k_0 = 1.6 \times 10^{-24}\, T^{-2}$	Est., Schofield and Steinberg (1992)
R243	$S + Na_2 \rightarrow NaS + Na$	$4.0 \times 10^{-10}\, e^{(-800/T)}$	Estimate
R246	$S + NaO \rightarrow Na + SO$	$1.56 \times 10^{-11}\, T^{0.5}$	Est. based on O + NaO
R247	$S + NaO_2 \rightarrow NaO + SO$	$4.0 \times 10^{-10}\, e^{(-940/T)}$	Est. based on $O + NaO_2$
R248	$S + NaO_2 \rightarrow NaS + O_2$	$1.0 \times 10^{-10}\, e^{(-940/T)}$	Est. based on $O + NaO_2$
R251	$S + NaS \rightarrow Na + S_2$	$1.56 \times 10^{-11}\, T^{0.5}$	Est. based on O + NaO
R252	$S + NaS_2 \rightarrow NaS + S_2$	$6.8 \times 10^{-13}\, T^{0.5}$	Est., Schofield and Steinberg (1992)
R254	S +NaOS → NaS + SO	$7.0 \times 10^{-13}\, T^{0.5}$	Est., Schofield and Steinberg (1992)
R255	$S + NaSO_2 \rightarrow NaS + SO_2$	$7.2 \times 10^{-11}\, e^{(-800/T)}$	Est. based on Schofield and Steinberg (1992)
R256	$S + K \xrightarrow{M} KS$	$k_0 = 1.6 \times 10^{-24}\, T^{-2}$	Est. based on S + Na
R259	$S + KO \rightarrow K + SO$	$1.56 \times 10^{-11}\, T^{0.5}$	Est. based on O + NaO
R260	$S + KO_2 \rightarrow KO + SO$	$4.0 \times 10^{-10}\, e^{(-940/T)}$	Est. based on $O + NaO_2$
R261	$S + KO_2 \rightarrow KS + O_2$	$1.0 \times 10^{-10}\, e^{(-940/T)}$	Est. based on $O + NaO_2$
R262	$S + KS \rightarrow K + S_2$	$1.56 \times 10^{-11}\, T^{0.5}$	Est. based on O + NaO
R263	$S + KS_2 \rightarrow KS + S_2$	$6.8 \times 10^{-13}\, T^{0.5}$	Est. based on $S + NaS_2$
R265	$S + KSO_2 \rightarrow KS + SO_2$	$7.2 \times 10^{-11}\, e^{(-800/T)}$	Est. based on $S + NaSO_2$
R268	$2S_2 \xrightarrow{M} S_4$	$k_0 = 4.0 \times 10^{-31}\, e^{(900/T)}$	Est. based on Fowles *et al*. (1967), Nicholas *et al*. (1979), and Langford and Oldershaw (1972, 1973)
R269	$S_2 + S_3 \xrightarrow{M} S_5$	$k_0 = 1.0 \times 10^{-25}\, T^{-2}$	Estimate
R270	$S_2 + S_4 \xrightarrow{M} S_6$	$k_0 = 1.0 \times 10^{-25}\, T^{-2}$	Estimate, Moses (1996)
R271	$S_2 + S_5 \xrightarrow{M} S_7$	$k_0 = 1.0 \times 10^{-25}\, T^{-2}$	Estimate
R272	$S_2 + S_6 \xrightarrow{M} S_8$	$k_0 = 1.0 \times 10^{-25}\, T^{-2}$	Estimate, Moses (1996)
R273	$S_2 + S_8 \rightarrow 2S_5$	$1.0 \times 10^{-11}\, e^{(-1400/T)}$	Estimate
R274	$S_2 + SO_3 \rightarrow S_2O + SO_2$	2.0×10^{-16}	Estimate
R275	$S_2 + (SO)_2 \rightarrow 2S_2O$	3.3×10^{-14}	Est. based on $SO + (SO)_2$
R276	$S_2 + ClO \rightarrow S_2O + Cl$	2.8×10^{-11}	Est. based on SO + ClO
R277	$S_2 + SCl \rightarrow S_3 + Cl$	2.0×10^{-11}	Estimate
R278	$S_2 + ClSO_2 \rightarrow S_2Cl + SO_2$	$5.0 \times 10^{-11}\, e^{(-800/T)}$	Estimate
R279	$S_2 + Na \xrightarrow{M} NaS_2$	$k_0 = 1.6 \times 10^{-24}\, T^{-2}$	Est., Schofield and Steinberg (1992)
R280	$S_2 + NaSO_2 \rightarrow NaS_2 + SO_2$	$6.3 \times 10^{-11} e^{(-800/T)}$	Est. based on Schofield and Steinberg (1992)
R281	$S_2 + K \xrightarrow{M} KS_2$	$k_0 = 1.6 \times 10^{-24}\, T^{-2}$	Est. based on $S_2 + K$
R282	$S_2 + KSO_2 \rightarrow KS_2 + SO_2$	$6.3 \times 10^{-11} e^{(-800/T)}$	Est. based on $S_2 + KSO_2$
R283	$2S_3 \xrightarrow{M} S_6$	$k_0 = 1.0 \times 10^{-25}\, T^{-2}$	Estimate, Moses (1996)

TABLE A3—*Continued*

	Reaction	Rate constant[a]	Reference
R284	$S_3 + S_4 \rightarrow S_2 + S_5$	$4.0 \times 10^{-11}\, e^{(-200/T)}$	Estimate
R285	$S_3 + S_4 \xrightarrow{M} S_7$	$k_0 = 1.0 \times 10^{-25}\, T^{-2}$	Estimate
R286	$S_3 + S_5 \rightarrow S_2 + S_6$	$4.0 \times 10^{-11}\, e^{(-200/T)}$	Estimate
R287	$S_3 + S_5 \xrightarrow{M} S_8$	$k_0 = 1.0 \times 10^{-25}\, T^{-2}$	Estimate
R288	$S_3 + S_6 \rightarrow S_2 + S_7$	$4.0 \times 10^{-12}\, e^{(-300/T)}$	Estimate
R289	$S_3 + S_7 \rightarrow S_2 + S_8$	$3.0 \times 10^{-11}\, e^{(-200/T)}$	Estimate
R290	$S_3 + S_7 \rightarrow S_4 + S_6$	$1.0 \times 10^{-11}\, e^{(-200/T)}$	Estimate
R291	$S_3 + S_7 \rightarrow 2S_5$	$1.0 \times 10^{-11}\, e^{(-200/T)}$	Estimate
R293	$S_3 + SO \rightarrow S_2O + S_2$	1.0×10^{-12}	Estimate
R299	$2\,S_4 \xrightarrow{M} S_8$	$k_0 = 4.0 \times 10^{-31}\, e^{(900/T)}$	Est. based on $2S_2$
R300	$S_4 + S_5 \rightarrow S_2 + S_7$	$2.0 \times 10^{-12}\, e^{(-200/T)}$	Estimate
R301	$S_4 + S_5 \rightarrow S_3 + S_6$	$2.0 \times 10^{-12}\, e^{(-200/T)}$	Estimate
R302	$S_4 + S_6 \rightarrow S_2 + S_8$	$2.0 \times 10^{-12}\, e^{(-300/T)}$	Estimate
R303	$S_4 + S_6 \rightarrow 2S_5$	$2.0 \times 10^{-12}\, e^{(-300/T)}$	Estimate
R304	$S_4 + S_7 \rightarrow S_3 + S_8$	$5.0 \times 10^{-12}\, e^{(-200/T)}$	Estimate
R305	$S_4 + S_7 \rightarrow S_5 + S_6$	$5.0 \times 10^{-12}\, e^{(-200/T)}$	Estimate
R307	$S_4 + Cl \rightarrow S_2 + S_2Cl$	1.0×10^{-11}	Estimate
R324	$2SO \rightarrow SO_2 + S$	$1.0 \times 10^{-12}\, e^{(-1700/T)}$	Martinez and Herron (1983)
R325	$2SO \xrightarrow{M} (SO)_2$	$k_0 = 4.4 \times 10^{-31}$	Herron and Huie (1980)
R326	$SO + SO_3 \rightarrow 2SO_2$	2.0×10^{-15}	Chung *et al*. (1975)
R327	$SO + (SO)_2 \rightarrow S_2O + SO_2$	3.3×10^{-14}	Herron and Huie (1980)
R328	$SO + Cl \xrightarrow{M} OSCl$	$k_0 = 7.3 \times 10^{-21}\, T^{-5}$	Mills (1998)
R329	$SO + ClO \rightarrow SO_2 + Cl$	2.8×10^{-11}	DeMore *et al*. (1997)
R333	$SO + SCl \rightarrow S_2O + Cl$	1.0×10^{-11}	Estimate
R334	$SO + OSCl \rightarrow SCl + SO_2$	6.0×10^{-13}	Est., Mills (1998)
R335	$SO + ClSO_2 \rightarrow OSCl + SO_2$	$5.0 \times 10^{-11}\, e^{(-800/T)}$	Estimate
R336	$SO + Na \xrightarrow{M} NaOS$	$k_0 = 1.6 \times 10^{-24}\, T^{-2}$	Est., Schofield and Steinberg (1992)
R337	$SO + NaO \rightarrow SO_2 + Na$	6.0×10^{-11}	Estimate
R338	$SO + NaS \rightarrow S_2O + Na$	6.0×10^{-11}	Estimate
R339	$SO + NaSO_2 \rightarrow NaOS + SO_2$	$6.3 \times 10^{-11}\, e^{(-800/T)}$	Est. based on Schofield and Steinberg (1992)
R340	$SO_2 + Cl \xrightarrow{M} ClSO_2$	$k_0 = 1.3 \times 10^{-34}\, e^{(940/T)}$	Est., Mills (1998)
R342	$SO_2 + Na \xrightarrow{M} NaSO_2$	$k_0 = 1.58 \times 10^{-23}\, T^{-2}$	Est. based on Shi and Marshall (1991)
R343	$SO_2 + NaO \rightarrow SO_3 + Na$	1.0×10^{-19}	Estimate
R344	$SO_2 + K \xrightarrow{M} KSO_2$	$k_0 = 4.4 \times 10^{-23}\, T^{-2}$	Est. based on Goumri *et al*. (1993)
R358	$Cl + S_2Cl \rightarrow S_2 + Cl_2$	1.0×10^{-12}	Estimate
R360	$Cl + OSCl \rightarrow SO + Cl_2$	3.0×10^{-11}	Estimate
R361	$Cl + ClSO_2 \xrightarrow{M} SO_2Cl_2$	$k_0 = 1.0 \times 10^{-23}\, T^{-2}$	Est. based on Goumri *et al*. (1993)
R362	$Cl + ClSO_2 \rightarrow SO_2 + Cl_2$	1.0×10^{-20}	Estimate
R363	$Cl + SO_2Cl_2 \rightarrow ClSO_2 + Cl_2$	$1.0 \times 10^{-11}\, e^{(-1000/T)}$	Estimate
R368	$Cl + NaO \rightarrow NaCl + O$	2.0×10^{-10}	Estimate
R369	$Cl + NaO_2 \rightarrow NaCl + O_2$	$5.0 \times 10^{-10}\, e^{(-700/T)}$	Est. based on $O + NaO_2$
R372	$Cl + NaS \rightarrow NaCl + S$	2.0×10^{-10}	Estimate
R373	$Cl + NaS_2 \rightarrow NaCl + S_2$	$5.0 \times 10^{-10}\, e^{(-700/T)}$	Est. based on $O + NaO_2$
R376	$Cl + NaOS \rightarrow NaCl + SO$	$1.0 \times 10^{-10}\, e^{(-800/T)}$	Estimate
R377	$Cl + NaSO_2 \rightarrow NaCl + SO_2$	$1.0 \times 10^{-10}\, e^{(-800/T)}$	Estimate
R382	$Cl + KO \rightarrow KCl + O$	2.0×10^{-10}	Estimate
R383	$Cl + KO_2 \rightarrow KCl + O_2$	$5.0 \times 10^{-10}\, e^{(-700/T)}$	Est. based on $O + NaO_2$
R386	$Cl + KS \rightarrow KCl + S$	2.0×10^{-10}	Estimate
R387	$Cl + KS_2 \rightarrow KCl + S_2$	$5.0 \times 10^{-10}\, e^{(-700/T)}$	Est. based on $O + NaO_2$
R389	$Cl + KSO_2 \rightarrow KCl + SO_2$	$1.0 \times 10^{-10}\, e^{(-800/T)}$	Est. based on $Cl + NaSO_2$
R410	$ClO + Na \rightarrow NaCl + O$	$2.0 \times 10^{-10}\, e^{(-300/T)}$	Estimate
R412	$ClO + K \rightarrow KCl + O$	$2.0 \times 10^{-10}\, e^{(-300/T)}$	Estimate
R445	$SCl + Na \rightarrow NaCl + S$	2.0×10^{-10}	Estimate
R446	$SCl + Na \rightarrow NaS + Cl$	1.0×10^{-12}	Estimate
R449	$SCl + K \rightarrow KCl + S$	2.0×10^{-10}	Estimate
R450	$SCl + K \rightarrow KS + Cl$	1.0×10^{-12}	Estimate
R455	$S_2Cl + Na \rightarrow NaCl + S_2$	1.0×10^{-10}	Estimate

TABLE A3—*Continued*

	Reaction	Rate constant[a]	Reference
R459	$OSCl + Na \rightarrow NaCl + SO$	$1.0 \times 10^{-10}\, e^{(-400/T)}$	Estimate
R460	$OSCl + K \rightarrow KCl + SO$	$1.0 \times 10^{-10}\, e^{(-400/T)}$	Estimate
R462	$2\,ClSO_2 \rightarrow SO_2Cl_2 + SO_2$	5.0×10^{-11}	Estimate
R463	$2\,ClSO_2 \rightarrow Cl_2 + 2\,SO_2$	5.0×10^{-13}	Estimate
R464	$ClSO_2 + Na \rightarrow NaCl + SO_2$	1.0×10^{-11}	Estimate
R465	$ClSO_2 + K \rightarrow KCl + SO_2$	1.0×10^{-11}	Estimate
R466	$SO_2Cl_2 + Na \rightarrow NaCl + ClSO_2$	$5.0 \times 10^{-11}\, e^{(-1000/T)}$	Estimate
R471	$Na + NaSO_2 \rightarrow Na_2 + SO_2$	1.0×10^{-13}	Estimate
R500	$S_8 + \text{dust} \rightarrow S_8(s)$	condensation	
R501	$S_8(s) \rightarrow S_8$	evaporation	

[a] Two-body rate constants are in units of $cm^3\ s^{-1}$. Low-pressure limiting rate constants for three-body reactions (k_0) are in units of $cm^6\ s^{-1}$.
[b] M represents any third body, prod represents higher-order products.

The relative abundance of the constituents also changes when the atmospheric density changes. The column-integrated mixing ratios for our high-, moderate-, and low-density models are listed in Table I. One result apparent from the table is that molecules that directly or indirectly rely on termolecular reactions for their formation (e.g., $S_3, S_4, \ldots, S_8$, alkali-sulfur species) often exhibit a considerable increase (or decrease) in their relative abundances when the atmospheric density is increased (or decreased). As the atmospheric density increases, three-body reactions become more important because the abundance of all three reactants generally increases, and the column-integrated rates of reactions such as R268 ($2S_2 + M \rightarrow S_4 + M$) and R342 ($SO_2 + Na + M \rightarrow NaSO_2 + M$) can increase by several orders of magnitude. Most of the effects from the three-body reactions are limited to lower altitudes where the atmospheric density is highest.

As the concentration of molecular species increases, two-body reactions also become more important, and these reactions contribute to the observed relative decrease in monatomic S and O with increasing atmospheric density. For example, reactions R207 and R205 that destroy atomic S are greatly enhanced and reaction R63 that destroys atomic O are moderately enhanced when molecular densities are increased. Unlike the situation in the low- and moderate-density models, the loss rates for atomic sulfur and oxygen in the high-density model can then compete with the production rates, and O and S become relatively less important in the high-density model.

Recycling reactions, in general, tend to become more important when the atmospheric density is increased, keeping the abundances of the major volcanic gases high in the high-density model. Diatomic sulfur is more important as the densitiy is increased because reactions R207, R205, and R12 can better compete with S_2 photolysis. Disulfur monoxide is more abundant because reactions R338 and R293 can better compete with S_2O photolysis. Both the reactions that produce and destroy SO are increased when the atmospheric density is increased; the net result is a slight reduction in the relative abundance of SO as the atmospheric density is increased (see Table I).

B.2. Sensitivity to Eddy Diffusion Coefficient

It is difficult to estimate the degree of eddy mixing in Io's atmosphere based on first principles (see Summers and Strobel 1996, Wong and Johnson 1996, and Appendix A.2 above). Gravity waves initiated by atmospheric thermal tides, volcanic eruptions, or gas flow across the heterogeneous surface could quickly become damped as they propagate upward in Io's low-density atmosphere. If the generation mechanisms are strong, then the damped waves could cause significant vertical mixing.

The sensitivity of Io photochemical models to the assumed eddy diffusion coefficient profile has been discussed extensively by Summers and Strobel (1996). However, because our volcanically driven atmosphere is considerably different from the situations considered by Summers and Strobel, we now reexamine the effects of variable eddy diffusion coefficients on our photochemical model results. The eddy diffusion coefficient K_E in our standard model is assumed to be $10^9\ cm^2\ s^{-1}$ at all altitudes based on arguments in Summers and Strobel (1996). With this value for K_E, the SO_2 homopause is located at ~34 km. Figure 5 shows how the results from our standard moderate-density model would change for an assumed altitude-independent eddy diffusion coefficient of $K_E = 10^8\ cm^2\ s^{-1}$ (e.g., Wong and Johnson 1996) rather than $K_E = 10^9\ cm^2\ s^{-1}$. The homopause in this lower eddy diffusion coefficient model is ~16 km. For steady-state models that do not include chemistry (i.e., $P_i - L_i = 0$ and $\partial n_i/\partial t = 0$ in Eq. 5), a reduction in K_E causes species that are heavier than SO_2 to have larger density gradients than in models with higher K_E (see Eq. 6). The situation is exacerbated by photochemistry, especially when the photochemical lifetimes of some of the volcanic species become similar to or smaller than the diffusion time scales. For instance, it is clear from a comparison of Figs. 2 and 5 that the S_2 and S_2O drop off very sharply with altitude when the eddy diffusion coefficient is reduced. In contrast, light species that have strong photochemical sources such that their net flux is downward at the lower boundary (e.g., S, O, SO) experience a reduction in the downward flux when the eddy diffusion coefficient is reduced. These species tend to exhibit an increase in their column abundances when K_E is reduced because they are not lost as rapidly to the surface. Atomic species, which tend to be lighter than molecular species and which tend to be produced predominantly from photochemistry rather than volcanic processes, are able to diffuse more readily to higher altitudes both because of the decreased surface loss and the increased importance of molecular diffusion.

Note that in the low eddy diffusion case, atomic S becomes the dominant species at altitudes above ~240 km, and the total column abundance of S relative to the column abundance of SO_2 increases dramatically from $S/SO_2 \approx 4.5\%$ in the $K_E = 10^9\ cm^2\ s^{-1}$ model to $S/SO_2 \approx 13\%$ in the $K_E = 10^8\ cm^2 s^{-1}$ model. The column abundance of SO increases slightly relative to SO_2, changing from $SO/SO_2 \approx 9.1\%$ in the $K_E = 10^9\ cm^2\ s^{-1}$ model to 13% in the $K_E = 10^8\ cm^2\ s^{-1}$ model. Note that this trend of an increased SO abundance for decreasing eddy diffusion coefficient in our volcanically driven atmosphere is similar to the trend found in the sublimation-driven atmospheres of Summers and Strobel (1996) and is caused by a decreased loss due to diffusion to the surface. In contrast, the column-integrated S_2/SO_2 ratio decreases from ~12.1% to ~8.2% and the S_2O/SO_2 ratio decreases from $\sim 3.3 \times 10^{-4}$ to $\sim 1.8 \times 10^{-4}$ when K_E is decreased from 10^9 to $10^8\ cm^2\ s^{-1}$.

These changes are slight. It would be difficult to use observations such as the SO/SO_2 ratio to help constrain eddy diffusion coefficients in Io's atmosphere (as was attempted by Lellouch *et al*. 1996), especially since other parameters such as volcanic outgassing (e.g., Zolotov and Fegley 1998b) or gas transport (e.g., Wong and Johnson 1996, Wong and Smyth 2000) can have a large influence on the SO/SO_2 ratio. The change in the S/SO_2 ratio is more pronounced, but ultraviolet emission by atomic S can only be observed when sulfur is excited by processes such as electron impact. It is not clear that McGrath *et al*. (2000) are sampling an atomic sulfur column all the way down to the surface (because torus electrons may not penetrate all the way to the surface), and McGrath *et al*.'s observed S/SO_2 ratio of ~0.3% for the Pele plume may be a lower limit.

B.3. Sensitivity to Key Reaction Rates

Photoabsorption cross sections for sulfur dioxide and the rate coefficients for oxygen–oxygen and oxygen–sulfur reactions have been well constrained by laboratory measurements. However, the rate coefficients for many of the other reactions in our list have not been measured in the laboratory or calculated theoretically (see Table A2). Information is particularly sparse for reactions involving sulfur molecules (e.g., S_2, S_3, S_4, . . . , S_8), S_2O molecules, and chlorine–sulfur or sodium–sulfur interactions. We now examine the sensitivity of our results to the rate coefficients or photolysis cross sections adopted for certain important reactions that do not have well-constrained rates.

As discussed in Appendix A, we adopt S_2 cross sections that are modified from calculations provided by Yelle *et al*. (unpublished manuscript, 2000). Because the S_2 cross sections are pressure- and temperature-dependent and because conditions within Io's atmosphere are uncertain, we estimate that our adopted cross sections could be uncertain by a factor of ∼2. Although our assumption of a constant S_2 mixing ratio at the lower boundary moderates the effects of any changes in the S_2 photolysis loss rate, Table B1 shows that factor-of-2 changes in the adopted S_2 cross sections can noticeably affect the results of our standard moderate-density model. When σ_{11}, the cross section for reaction R11, is increased by a factor of 2, the S_2 abundance decreases by 4.1%. When σ_{11} is decreased by a factor of 2, the S_2 abundance increases by 2.5%. Species that depend on S_2 for their production or loss (see Fig. 3 and Section 4) are also affected (usually to a larger degree). For example, atomic O becomes more abundant when σ_{11} is increased because reaction R63 ($O + S_2 \rightarrow S + SO$) now operates at a reduced rate due to the reduced S_2 abundance. Sulfur atoms become more abundant when σ_{11} is increased due to the increased photolysis rate of S_2; the increase is not as great as one might expect because the resulting lower overall S_2 abundance limits the rate of important S production reactions such as R63, R15, R23, R324 (see Table II). The photochemical responses can be nonlinear and quite complicated. Sulfur molecules containing more than three atoms and those species (such as S_2Cl) that depend on heavy sulfur molecules for their production are particularly affected by factor-of-2 changes in σ_{11} (see Table B1) because of their dependence on three-body reactions for their formation.

The S_2O cross sections are even more uncertain than those of S_2. Table B1 shows that factor-of-5 changes in the cross sections for reaction R23 ($S_2O \xrightarrow{h\nu} SO + S$) mainly affect the S_2O abundance itself while having little effect on other species. Again, the effects on the S_2O abundance are not linear because S_2O is continually being resupplied from volcanic sources and because other production and loss mechanisms are operating. Because moderate changes in the S_2O abundance have at most a minor influence on the abundances of the other sulfur-bearing molecules, it is clear that S_2O is not an important parent molecule.

In our standard moderate-density model, three-body recombination of S_2 to form S_4 (reaction R268) is the third most important loss process for S_2 (the first two most important are reaction R11 and reaction R63; see Table II). Although reaction R268 has been studied extensively in the laboratory (e.g., Fowles *et al*. 1967, Elbanowski 1970, Langford and Oldershaw 1972, 1973), there is no consensus concerning the rate constant at room temperature, and the rate constant has never been measured at the low temperatures typical near the surface of Io. Part of the difficulty may be the highly reactive nature of all the sulfur molecules and atoms produced in these flash-photolysis experiments (e.g., Langford and Oldershaw 1973)—isolating the rate for reaction R268 in these experiments is difficult. Based on the discussions in the above papers, we estimate that the rate coefficient k_{268} for reaction R268 is uncertain by at least an order of magnitude, and we examine how factor-of-10 changes in k_{268} affect our standard moderate-density model. We find (see Table B1) that although the abundance of heavy sulfur molecules is quite sensitive to k_{268}, the S_2 abundance itself is unaffected, and few other molecules depend on k_{268}. One exception is S_2Cl, whose primary production mechanism in our model is R307 ($S_4 + Cl \rightarrow S_2 + S_2Cl$).

Although atomic sulfur and all the small sulfur molecules are believed to react readily with each other, very few direct measurements of the rate constants for these interconversion reactions have been obtained. Langford and Oldershaw (1973) provide indirect evidence that reactions such as R205 ($S + S_3 \rightarrow 2S_2$) and R207 ($S + S_4 \rightarrow S_2 + S_3$) are rapid. In our standard moderate-density model, we adopt a temperature-independent rate constant of 8×10^{-11} cm^3 s^{-1} for both these reactions. We estimate that the rate constants for these reactions could be as much as four times higher or eight times lower than the above value. Table B2 shows how sensitive our results are to such changes in k_{205} and k_{207}.

TABLE B1
Change Relative to Standard Moderate-Density Model

Constituent	$\sigma_{11} \times 2$	$\sigma_{11} \div 2$	$\sigma_{23} \times 5$	$\sigma_{23} \div 5$	$k_{268} \times 10$	$k_{268} \div 10$
O	+17%	−11%	+0.0%	+0.0%	+0.0%	+0.0%
O_2	−12%	+11%	+0.0%	+0.1%	+0.1%	+0.0%
S	+28%	−18%	+0.2%	−0.4%	−0.2%	+0.0%
S_2	−4.1%	+2.5%	+0.0%	+0.0%	+0.0%	+0.0%
S_3	−6.1%	+3.9%	−0.2%	+0.2%	+310%	−31%
S_4	−24%	+21%	−1.0%	+0.6%	+900%	−90%
S_5	−41%	+44%	−2.1%	+1.1%	+6300%	−95%
S_6	−36%	+36%	−1.6%	+0.8%	+930%	−90%
S_7	−49%	+63%	−2.6%	+1.5%	+27000%	−99%
S_8	−44%	+48%	−2.2%	+1.2%	+9900%	−99%
SO	−0.8%	+0.4%	+0.1%	−0.1%	+0.0%	+0.0%
S_2O	+0.0%	+0.0%	−38%	+35%	+0.3%	+0.0%
S_2Cl	−28%	+26%	−1.0%	+0.4%	+830%	−83%
NaS_2	−25%	+22%	−0.8%	+0.5%	+0.2%	−0.1%
NaOS	−26%	+24%	−0.6%	+0.5%	+0.1%	+0.0%
$NaSO_2$	−0.7%	+0.4%	+0.0%	+0.1%	+0.0%	+0.0%
KS_2	−27%	+24%	−0.8%	+0.8%	+0.0%	+0.0%
KSO_2	−1.0%	+0.6%	+0.0%	+0.1%	+0.1%	+0.0%

Note. Numbers in this table represent the change in the column-integrated mixing ratios (i.e., the column density of the constituent divided by the SO_2 column denisty). Changes of less than 1% are not significant.

TABLE B2
Change Relative to Standard Moderate-Density Model

Constituent	$k_{205} \times 4$	$k_{205} \div 8$	$k_{207} \times 4$	$k_{207} \div 8$	$k_{307} \times 10$	$k_{307} \div 10$
O	+0.0%	+0.0%	+0.0%	+0.0%	+0.0%	+0.0%
O_2	+0.0%	+0.0%	+0.0%	+0.0%	+0.0%	+0.0%
S	+0.0%	+0.0%	+0.1%	+0.0%	+0.0%	+0.0%
S_2	+0.0%	+0.0%	+0.0%	+0.0%	+0.0%	+0.0%
S_3	−29%	+35%	+9.8%	−21%	−3.4%	+0.5%
S_4	+0.0%	+0.0%	−66%	+180%	−9.4%	+1.0%
S_5	−54%	+58%	−54%	+38%	−13%	+1.3%
S_6	+0.0%	+0.1%	−65%	+150%	−8.6%	+1.0%
S_7	−24%	+24%	−81%	+330%	−16%	+1.9%
S_8	+0.1%	+0.0%	−86%	+410%	−15%	+1.8%
SO	+0.0%	+0.0%	+0.0%	+0.0%	+0.0%	+0.0%
S_2O	+0.0%	+0.0%	+0.0%	+0.0%	+0.0%	+0.0%
S_2Cl	+0.0%	−0.2%	−64%	+230%	+720%	−83%
NaS_2	+0.0%	−0.1%	+0.0%	−0.1%	+0.0%	+0.0%
NaOS	+0.0%	+0.0%	+0.0%	+0.0%	+0.0%	+0.0%
$NaSO_2$	+0.0%	+0.0%	+0.0%	+0.0%	+0.0%	+0.0%
KS_2	+0.0%	+0.0%	+0.0%	+0.0%	+0.0%	+0.0%
KSO_2	+0.0%	+0.0%	+0.0%	+0.0%	+0.0%	+0.0%

Note. Numbers in this table represent the change in the column-integrated mixing ratios (i.e., the column density of the constituent divided by the SO_2 column denisty). Changes of less than 1% are not significant.

Changes in k_{205} seem to only affect sulfur molecules with an odd number of atoms, whereas changes in k_{207} affect all of the heavy sulfur molecules (and S_2Cl). Note again, however, that the S_2 abundance remains unchanged because the volcanic production rate for S_2 totally dominates over the production rate from all other photochemical means.

The highly speculative reaction R307 ($S_4 + Cl \rightarrow S_2Cl + S_2$) is responsible for producing most of the S_2Cl in our standard moderate-density model. The rate for this reaction has not been measured in the laboratory, and it is not even certain whether an appreciable energy barrier would exist. We conservatively assign the reaction a rate coefficient of 1.0×10^{-11} cm^3 s^{-1}, but realize that the rate coefficient could be considerably higher or lower than this value. Table B2 shows how our results would change for a factor-of-10 increase or decrease in k_{307}. Although the abundance of S_2Cl changes dramatically with such changes in k_{307}, few other of the potentially observable molecules are affected.

In all, the results seem to be less sensitive to changes in uncertain reaction rates than they are to changes in other uncertain parameters such as the eddy diffusion coefficient or total atmospheric density. One reason for this behavior is that the mixing ratios of the major parent volcanic species are kept constant at the lower boundary in our model, so that their abundances in the denser lower atmosphere have not been changed dramatically by these changes in the reaction rates. For example, S_2 and SO_2 are the major parent molecules for the sulfur and oxygen species in a Pele-type eruption. The photolysis loss rates for these molecules greatly exceeds their model production rates; thus, reasonable changes in most of the rate constants (other than the photolysis rates themselves) do not alter the abundance of S_2, SO_2, or any of the other major "observable" sulfur and oxygen molecules in the model as long as the volcanic supply rates for SO_2 and S_2 remain the same.

ACKNOWLEDGMENTS

The Caltech/JPL KINETICS code was developed jointly by Yuk L. Yung and Mark Allen, with assistance from many people over the years. We thank Franklin P. Mills for supplying absorption and photodissociation cross sections for several molecular species, Roger V. Yelle for supplying photoabsorption cross sections and J values for S_2 and for useful discussions regarding gravity waves, Michael E. Summers for supplying the background high-density model atmosphere, and Melissa McGrath for useful advice and suggestions. Comments from the two anonymous reviewers were very helpful in improving the manuscript. This paper represents Contribution Number 1104 from the Lunar and Planetary Institute, which is operated by the Universities Space Research Association. Support from the NASA Planetary Atmospheres Program is gratefully acknowledged.

REFERENCES

A'Hearn, M. F., P. D. Feldman, and D. G. Schleicher 1983. The discovery of S_2 in Comet IRAS-Araki-Alcock. *Astrophys. J.* **274**, L99–L103.

Allen, M., Y. L. Yung, and J. W. Waters 1981. Vertical transport and photochemistry in the terrestrial mesosphere and lower thermosphere (50–120 km). *J. Geophys. Res.* **86**, 3617–3627.

Atkinson, R., D. L. Baulch, R. A. Cox, R. F. Hampson, Jr., J. A. Kerr, M. J. Rossi, and J. Troe 1997. Evaluated kinetic and photochemical data for atmospheric chemistry. Supplement VI. IUPAC subcommittee on gas kinetic data evaluation for atmospheric chemistry. *J. Phys. Chem. Ref. Data* **26**, 1329–1499.

Austin, J. V., and D. B. Goldstein 1996. Direct numerical simulations of low-density atmospheric flow on Io. In *Molecular Physics and Hypersonic Flows* (M. Capitelli, Ed.), pp. 749–758. Kluwer Academic, Dordrecht/Norwell, MA.

Austin, J. V., and D. B. Goldstein 2000. Rarefied gas model of Io's sublimation-driven atmosphere. *Icarus* **148**, 370–383.

Bagenal, F., and J. D. Sullivan 1981. Direct plasma measurements in the Io torus and inner magnetosphere of Jupiter. *J. Geophys. Res.* **86**, 8447–8466.

Ballester, G. E., D. F. Strobel, H. W. Moos, and P. D. Feldman 1990. The atmospheric abundance of SO_2 on Io. *Icarus.* **88**, 1–23.

Ballester, G. E., M. A. McGrath, D. F. Strobel, X. Zhu, P. D. Feldman, and H. W. Moos 1994. Detection of the SO_2 atmosphere on Io with the Hubble Space Telescope. *Icarus* **111**, 2–17.

Ballester, G. E., J. T. Clarke, D. Rego, M. Combi, N. Larsen, J. Ajello, D. F. Strobel, N. M. Schneider, and M. McGrath 1996. Characteristics of Io's far-UV neutral oxygen and sulfur emissions derived from recent HST observations. *Bull. Am. Astron. Soc.* **28**, 1156.

Ballester, G. E., J. T. Clarke, M. Combi, D. F. Strobel, N. Larsen, M. McGrath, M. Lenigan, J. Ajello, N. M. Schneider, and D. Rego 1997. Io's far-ultraviolet emissions as observed with HST and IUE. *Bull. Am. Astron. Soc.* **29**, 980.

Ballester, G. E., P. D. Feldman, F. L. Roesler, H. W. Moos, R. J. Oliversen, R. C. Woodward, F. Scherb, W. H. Smyth, L. Ben Jaffel, D. F. Strobel, B. C. Wolven, and K. D. Retherford 1999. Lyman alpha observations of Io with STIS/HST. *Bull. Am. Astron. Soc.* **31**, 1193.

Basco, N., and A. E. Pearson 1967. Reactions of sulphur atoms in presence of carbon disulphide, carbonyl sulfide and nitric oxide. *Trans. Faraday Soc.* **63**, 2684–2694.

Baulch, D. L., J. Duxbury, S. J. Grant, and D. C. Montague 1981. Evaluated kinetic data for high temperature reactions. Volume 4. Homogeneous gas phase reactions of halogen- and cyanide-containing species. *J. Phys. Chem. Ref. Data.* **10**, Suppl.

Baulch, D. L., C. J. Cobos, R. A. Cox, P. Frank, G. Hayman, T. Just, J. A. Kerr, M. J. Pilling, J. Troe, R. W. Walker, and J. Warnatz 1994. Evaluated kinetic data for combustion modeling. *J. Phys. Chem. Ref. Data* **23**, 847–1033. [Eratta, *J. Phys. Chem. Ref. Data* **24**, 1609–1630.]

Belton, M. J. S., and 33 colleagues 1996. Galileo's first images of Jupiter and the Galilean satellites. *Science* **274**, 377–385.

Bhardwaj, A., and M. Michael 1999. On the excitation of Io's atmosphere by the photoelectrons: Application of the analytical yield spectral model of SO_2. *Geophys. Res. Lett.* **26**, 393–396.

Billmers, R. I., and A. L. Smith 1991. Ultraviolet-visible absorption spectra of equilibrium sulfur vapor: Molar absorptivity spectra of S_3 and S_4. *J. Phys. Chem.* **95**, 4242–4245.

Bouchez, A. H., M. E. Brown, and N. M. Schneider 2000. Eclipse spectroscopy of Io's atmosphere. *Icarus* **148**, 316–319.

Brewer, L., G. D. Brabson, and B. Meyer 1965. UV absorption spectrum of trapped S_2. *J. Chem. Phys.* **42**, 1385–1389.

Brown, R. A., D. E. Shemansky, and R. E. Johnson 1983. A deficiency of O III in the Io plasma torus. *Astrophys. J.* **264**, 309–323.

Cataldo, V., and L. Wilson 1999. The symmetrical shape of the Pillan and Pele volcanic plumes on Io as a constraint on eruption conditions. *Bull. Am. Astron. Soc.* **31**, 1164.

Chamberlain, J. W., and D. M. Hunten. 1987. *Theory of Planetary Atmospheres: An Introduction to Their Physics and Chemistry.* Academic Press, Orlando, Florida.

Chung, K., J. G. Calvert, and J. W. Bottenheim 1975. The photochemistry of sulfur dioxide excited within its first allowed band (3130 Å) and the "forbidden" band (3700-4000 Å). *Int. J. Chem. Kinetics* **71**, 161.

Clarke, J. T., J. Ajello, J. Luhmann, N. Schneider, and I. Kanik 1994. Hubble Space Telescope UV spectral observations of Io passing into eclipse. *J. Geophys. Res.* **99**, 8387–8402.

Cook, A. F., E. M. Shoemaker, B. A. Smith, G. E. Danielson, T. V. Johnson, and S. P. Synnott 1981. Volcanic origin of eruptive plumes on Io. *Science* **211**, 1419–1422.

Craven, W., and J. N. Murrell 1987. Trajectory studies of $S + O_2$ and $O + S_2$ collisions. *J. Chem. Soc. Faraday Trans. 2* **83**, 1733.

Davies, A. G., L. P. Keszthelyi, R. M. C. Lopes-Gautier, A. S. McEwen, W. D. Smythe, L. Soderblom, and R. W. Carlson 1999. Thermal signature, eruption

style and eruption evolution at Pele and Pillan patera on Io. *Lunar. Planet. Sci.* **30**, Abstract 1462.

Davies, A. G., L. P. Keszthelyi, D. A. Williams, and A. J. L. Harris 2000a. The lava lake at Pele: A comparison with terrestrial lava lakes. *Bull. Am. Astron. Soc.* **32**, 29.07.

Davies, A. G., R. Lopes-Gautier, W. D. Smythe, and R. W. Carlson 2000b. Silicate cooling model fits to Galileo NIMS data of volcanism on Io. *Icarus* **148**, 211–225.

de Almeida, A. A., and P. D. Singh 1986. Photodissociation lifetime of $^{32}S_2$ molecule in comets. *Earth, Moon, Planets* **36**, 117–125.

DeMore, W. B., S. P. Sander, D. M. Golden, R. F. Hampson, M. J. Kurylo, C. J. Howard, A. R. Ravishankara, C. E. Kolb, and M. J. Molina 1997. *Chemical Kinetics and Photochemical Data for Use in Stratospheric Modeling. Evaluation Number 12*. JPL Publication 97-4, Jet Propulsion Laboratory, Pasadena, CA.

Elbanowski, M. 1970. The kinetics of recombination of S_2 molecules formed during the flash photolysis of sulphur vapour. *Roczniki Chem.* **44**, 801–807.

Eska, V., U. von Zahn, and J. M. C. Plane 1999. The terrestrial potassium layer (75–110 km) between 71°S and 54°N: Observations and modeling. *J. Geophys. Res.* **104**, 17,173–17,186.

Fegley, B., Jr., and M. Yu. Zolotov 2000. Chemistry of sodium, potassium, and chlorine in volcanic gases on Io. *Icarus* **148**, 193–210.

Feldman, P. D., D. F. Strobel, H. W. Moos, K. D. Retherford, B. C. Wolven, M. A. McGrath, F. L. Roesler, R. C. Woodward, R. J. Oliversen, and G. E. Ballester 2000a. Lyman-α imaging of the SO_2 distribution on Io. *Geophys. Res. Lett.* **27**, 1787–1790.

Feldman, P. D., T. B. Ake, A. F. Berman, H. W. Moos, D. J. Sahnow, D. F. Strobel, H. A. Weaver, P. R. Young, and the FUSE Solar System Team 2000b. Detection of chlorine ions in the FUSE spectrum of the Io plasma torus. *Bull. Am. Astron. Soc.* **32**, 34.01.

Fowles, P., M. deSorgo, A. J. Yarwood, O. P. Strausz, and H. E. Gunning 1967. The reactions of sulfur atoms. IX. The flash photolysis of carbonyl sulfide and the reactions of $S(^1D)$ atoms with hydrogen and methane. *J. Amer. Chem. Soc.* **89**, 1352–1362.

Geissler, P. E., A. S. McEwen, L. Keszthelyi, R. Lopes-Gautier, J. Granahan, and D. P. Simonelli 1999a. Global color variations on Io. *Icarus* **140**, 265–282.

Geissler, P. E., A. S. McEwen, W. Ip, M. J. S. Belton, T. V. Johnson, W. H. Smyth, and A. P. Ingersoll 1999b. Galileo imaging of atmospheric emissions from Io. *Science* **285**, 870–874.

Geissler, P. E., A. S. McEwen, C. Phillips, L. Keszthelyi, E. Turtle, M. Milazzo, R. Lopes-Gautier, D. P. Simonelli, D. A. Williams, and the Galileo Imaging Team 2000. New results on Io's color and composition. *Lunar Planet. Sci.* **31**, Abstract 1968.

Gladstone, G. R., M. Allen, and Y. L. Yung 1996. Hydrocarbon photochemistry in the upper atmosphere of Jupiter. *Icarus* **119**, 1–52.

Goumri, A., D. Lasko, J.-D. R. Rocha, E. Francis, and P. Marshall 1993. Investigation of the gas-phase kinetics of the reaction $K + SO_2 + Ar$. *J. Phys. Chem.* **97**, 5295–5297.

Grillo, A., R. Reed, and M. W. Slack 1979. Infrared measurements of sulfur dioxide thermal decomposition rate in shock waves. *J. Chem. Phys.* **70**, 1634–1636.

Hapke, B. 1979. Io's surface and environs: A magmatic-volatile model. *Geophys. Res. Lett.* **6**, 799–802.

Hapke, B. 1989. The surface of Io: A new model. *Icarus* **79**, 56–74.

Hapke, B., and F. Graham 1989. Spectral properties of condensed phases of disulfur monoxide, polysulfur oxide, and irradiated sulfur. *Icarus* **79**, 47–55.

Helmer, M., and J. M. C. Plane 1993. A study of the reaction $NaO_2 + O \rightarrow NaO + O_2$: Implications for the chemistry of sodium in the upper atmosphere. *J. Geophys. Res.* **98**, 23,207–23,222.

Hendrix, A. R., C. A. Barth, and C. W. Hord 1999. Io's patchy atmosphere as measured by the Galileo Ultraviolet Spectrometer. *J. Geophys. Res.* **104**, 11,817–11,826.

Herron, J. T., and R. E. Huie 1980. Rate constants at 298 K for the reactions $SO + SO + M \rightarrow (SO)_2 + M$ and $SO + (SO)_2 \rightarrow SO_2 + S_2O$. *Chem. Phys. Lett.* **76**, 322–324.

Hopkins, A. G., S. Tang, and C. W. Brown 1973. Infrared and Raman spectra of the low-temperature products from discharged sulfur dioxide. *J. Am. Chem. Soc.* **95**, 3486–3490.

Hunten, D. M. 1985. Blowoff of an atmosphere and possible application to Io. *Geophys. Res. Lett.* **12**, 271–273.

Ingersoll, A. P. 1989. Io meteorology: How atmospheric pressure is controlled locally by volcanos and surface frosts. *Icarus* **81**, 298–313.

Ingersoll, A. P., M. E. Summers, and S. G. Schlipf 1985. Supersonic meteorology of Io: Sublimation driven flow of SO_2. *Icarus* **64**, 375–390.

Jacob, A., and C. A. Winkler 1972. Kinetics of the reactions of oxygen atoms and nitrogen atoms with sulfur trioxide. *J. Chem. Soc. Faraday Trans. 1* **68**, 2077–2082.

Jensen, D. E., and G. A. Jones 1978. Reaction rate coefficients for flame calculations. *Combust. Flame.* **32**, 1–34.

Johnson, R. E. 1997. Polar "caps" on Ganymede and Io revisited. *Icarus* **128**, 469–471.

Kargel, J. S., P. Delmelle, and D. B. Nash 1999. Volcanogenic sulfur on Earth and Io: Composition and spectroscopy. *Icarus* **142**, 249–280.

Kim, S. J., H. F. A'Hearn, and S. M. Larson 1990. Multi-cycle fluorescence: Application to S_2 in Comet IRAS-Araki-Alcock 1983VII. *Icarus* **87**, 440–451.

Krasnopolsky, V. A. 1987. S_3 and S_4 absorption cross sections in the range of 340 to 600 nm and evaluation of the S_3 abundance in the lower atmosphere of Venus. *Adv. Space Res.* **7**, (12)25–(12)27.

Kumar, S. 1980. A model of the SO_2 atmosphere and ionosphere of Io. *Geophys. Res. Lett.* **7**, 9–12.

Kumar, S. 1982. Photochemistry of SO_2 in the atmosphere of Io and implications on atmospheric escape. *J. Geophys. Res.* **87**, 1677–1684.

Kumar, S. 1984. Sulfur and oxygen escape from Io and a lower limit to atmospheric SO_2 at Voyager 1 encounter. *J. Geophys. Res.* **89**, 7399–7406.

Kumar, S. 1985. The SO_2 atmosphere and ionosphere of Io: Ion chemistry, atmospheric escape, and models corresponding to the Pioneer 10 radio occultation measurements. *Icarus* **61**, 101–123.

Küppers, M., and N. M. Schneider 2000. Discovery of chlorine in the Io Torus. *Geophys. Res. Lett.* **27**, 513–516.

Langford, R. B., and G. A. Oldershaw 1972. Flash photolysis of H_2S. *J. Chem. Soc. Faraday Trans. 1* **68**, 1550–1558.

Langford, R. B., and G. A. Oldershaw 1973. Mechanism of sulphur formation in the flash photolysis of carbonyl sulphide. *J. Chem. Soc. Faraday Trans. 1* **69**, 1389–1397.

Lellouch, E. 1996. Io's atmosphere: Not yet understood (Urey Prize lecture). *Icarus* **124**, 1–21.

Lellouch, E., M. Belton, I. de Pater, S. Gulkis, and T. Encrenaz 1990. Io's atmosphere from microwave detection of SO_2. *Nature* **346**, 639–641.

Lellouch, E., M. Belton, I. de Pater, G. Paubert, S. Gulkis, and T. Encrenaz 1992. The structure, stability, and global distribution of Io's atmosphere. *Icarus* **98**, 271–295.

Lellouch, E., D. Strobel, M. Belton, G. Paubert, G. Ballester, and I. de Pater 1994. Millimeter wave observations of Io's atmosphere: new data and new models. *Bull. Am. Astron. Soc.* **26**, 1136.

Lellouch, E., D. F. Strobel, M. J. S. Belton, M. E. Summers, G. Paubert, and R. Moreno 1996. Detection of sulfur monoxide in Io's atmosphere. *Astrophys. J.* **459**, L107–L110.

Lindzen, R. S. 1971. Tides and gravity waves in the upper atmosphere. In *Mesospheric Models and Related Experiments* (G. Fiocco, Ed.), pp. 122–130. Reidel, Dordrecht.

Lopes-Gautier, R., A. S. McEwen, W. B. Smythe, P. E. Geissler, L. Kamp, A. G. Davies, J. R. Spencer, L. Keszthelyi, R. Carlson, F. E. Leader, R. Mehlman,

L. Soderblom, and the Galileo NIMS and SSI Teams 1999. Active volcanism on Io: Global distribution and variations in activity. *Icarus* **140**, 243–264.

Mallard, W. G., Y. Mirokhin, F. Westley, J. T. Herron, R. F. Hampson, and D. H. Frizzell 1998. *NIST Chemical Kinetics Database 17-2Q98*. National Inst. Standards and Tech., Gaithersburg, MD.

Martinez, R. I., and J. T. Herron 1983. Methylthiirane: Kinetic gas-phase titration of sulfur atoms in S_xO_y systems. *Int. J. Chem. Kinetics* **15**, 1127–1135.

McEwen, A. S., and L. A. Soderblom 1983. Two classes of volcanic plumes on Io. *Icarus* **55**, 191–217.

McEwen, A. S., L. Keszthelyi, P. Geissler, D. P. Simonelli, M. H. Carr, T. V. Johnson, K. P. Klaasen, H. H. Breneman, T. J. Jones, J. M. Kaufman, K. P. Magee, D. A. Senske, M. J. S. Belton, and G. Schubert 1998a. Active volcanism on Io as seen by Galileo SSI. *Icarus* **135**, 181–219.

McEwen, A. S., L. Keszthelyi, J. R. Spencer, G. Schubert, D. L. Matson, R. Lopes-Gautier, K. P. Klaasen, T. V. Johnson, J. W. Head, P. Geissler, S. Fagents, A. G. Davies, M. H. Carr, H. H. Breneman, and M. J. S. Belton 1998b. High-temperature silicate volcanism on Jupiter's moon Io. *Science* **281**, 87–90.

McEwen, A. S., and 25 colleagues 2000. Galileo at Io: Results from high-resolution imaging. *Science* **288**, 1193–1198.

McGrath, M. A., M. J. S. Belton, J. R. Spencer, and P. Sartoretti 2000. Spatially resolved spectroscopy of Io's Pele plume and SO_2 atmosphere. *Icarus* **146**, 476–493.

Meyer, B. 1964. Solid allotropes of sulfur. *Chem. Rev.* **64**, 429–451.

Meyer, B. 1976. Elemental sulfur. *Chem. Rev.* **76**, 367–388.

Meyer, B., and E. Shumacher 1960. Isolierung und Charakterisierung von S_2 in gefärbten Schwefelkindensaten bei tiefen Temperaturen. *Helv. Chim. Acta* **43**, 1333–1349.

Meyer, B., and T. Stroyer-Hansen 1972. Infrared spectra of S_4. *J. Phys. Chem.* **76**, 3968–3969.

Meyer, B., T. Stroyer-Hansen, and T. V. Oommen 1972. The visible spectrum of S_3 and S_4. *J. Molec. Spectrosc.* **42**, 335–343.

Michael, M., and A. Bhardwaj 2000. FUV emissions on Io: Role of Galileo-observed field-aligned energetic electrons. *Geophys. Res. Lett.* **27**, 3137–3140.

Mills, F. P. 1998. *I. Observations and Photochemical Modeling of the Venus Middle Atmosphere. II. Thermal Infrared Spectroscopy of Europa and Callisto*. Ph.D. thesis, California Institute of Technology, Pasadena, CA.

Moreno, M. A., W. I. Newman, and M. G. Kivelson 1985. Ion partitioning in the hot Io torus: The influence of S_2 outgassing. *J. Geophys. Res.* **90**, 12,065–12,072.

Moreno, M. A., G. Schubert, J. Baumgardner, M. G. Kivelson, and D. A. Paige 1991. Io's volcanic and sublimation atmospheres. *Icarus* **93**, 63–81.

Morgan, J. S., and C. B. Pilcher 1982. Plasma characteristics of the Io torus. *Astrophys. J.* **253**, 406–421.

Moses, J. I. 1996. SL9 impact chemistry: Long-term photochemical evolution. In *The Collision of Comet Shoemaker-Levy 9 and Jupiter* (K. S. Noll, H. A. Weaver, and P. D. Feldman, Eds.), pp. 243–268. Cambridge Univ. Press, Cambridge, UK.

Moses, J. I., and D. B. Nash 1991. Phase transformations and the spectral reflectance of solid sulfur: Can metastable sulfur allotropes exist on Io? *Icarus* **89**, 277–304.

Moses, J. I., M. Allen, and G. R. Gladstone 1995. Post-SL9 sulfur photochemistry on Jupiter. *Geophys. Res. Lett.* **22**, 1597–1600.

Moses, J. I., E. Lellouch, B. Bézard, G. R. Gladstone, H. Feuchtgruber, and M. Allen 2000. Photochemistry of Saturn's atmosphere. II. Effects of an influx of external oxygen. *Icarus* **145**, 166–202.

Moses, J. I., M. Yu. Zolotov, and B. Fegley, Jr. 2002. Alkali and halogen photochemistry in a volcanically driven atmosphere on Io. *Icarus* **156**, 107–135.

Muller, C. H., III, K. Schofield, M. Steinberg, and H. P. Broida 1979. Sulfur chemistry in flames. *Symp. Int. Combust. Proc.* **17**, 867–879.

Murrells, T. P. 1988. Elementary reactions of the SCl radical. Part II. Rate constants and mechanisms of the reactions of SCl with NO_2, NO, O_2, $O(^3P)$, and $N(^4S)$. *J. Chem. Soc. Faraday Trans. 2* **84**, 85–94.

Nelson, R. M., and B. W. Hapke 1978. Spectral reflectivities of the Galilean satellites and Titan, 0.32 to 0.86 micrometers. *Icarus* **36**, 304–329.

Nelson, R. M., W. D. Smythe, B. W. Hapke, and A. J. Cohen 1990. On the effects of x-rays on the color of elemental sulfur: Implications for Jupiter's satellite Io. *Icarus* **85**, 326–334.

Nicholas, J. E., C. A. Amodio, and M. J. Baker 1979. Kinetics and mechanism of the decomposition of H_2S CH_3SH and $(CH_3)_2S$ in a radio-frequency pulse discharge. *J. Chem. Soc. Faraday Trans. 1*. **75**, 1868–1875.

Pearl, J., R. Hanel, V. Kunde, W. Maguire, K. Fox, S. Gupta, C. Ponnamperuma, and F. Raulin 1979. Identification of gaseous SO_2 and new upper limits for other gases on Io. *Nature* **280**, 755–758.

Plane, J. M. C., and M. Helmer 1994. Laboratory studies of the chemistry of meteoric metals. In *Research in Chemical Kinetics*, Vol. 2 (R. G. Compton and G. Hancock, Eds.), pp. 313–367. Elsevier, New York.

Plane, J. M. C., and D. Husain 1986. Determination of the absolute rate constant for the reaction $O + NaO \rightarrow Na + O_2$ by time-resolved atomic chemiluminescence at $\lambda = 589$ nm $[Na(3^2P_J) \rightarrow Na(3^2S_{1/2}) + h\nu]$. *J. Chem. Soc. Faraday Trans. 2* **82**, 2047–2052.

Plane, J. M. C., C.-F. Nien, M. R. Allen, and M. Helmer 1993. A kinetic investigation of the reactions $Na + O_3$ and $NaO + O_3$ over the temperature range 207–377 K. *J. Phys. Chem.* **97**, 4459–4467.

Radford, H. E., and F. O. Rice 1960. Green and purple sulfur: Electron-spin resonance studies. *J. Chem. Phys.* **33**, 774–776.

Rajasekhar, B., J. M. C. Plane, and L. Bartolotti 1989. Determination of the absolute photolysis cross section of sodium superoxide at 230 K: Evidence for the formation of sodium tetroxide in the gas phase. *J. Phys. Chem.* **93**, 7399–7404.

Reid, R. C., J. M. Prausnitz, and B. E. Poling, 1987. *The Properties of Gases and Liquids*. McGraw–Hill, Boston, MA.

Retherford, K. D., H. W. Moos, D. F. Strobel, B. C. Wolven, and F. L. Roesler 2000a. Io's equatorial spots: Morphology of neutral UV emissions. *J. Geophys. Res.* **105**, 27,157–27,165.

Retherford, K. D., P. D. Feldman, H. W. Moos, D. F. Strobel, B. C. Wolven, R. J. Oliversen, M. A. McGrath, F. L. Roesler, F. Scherb, G. E. Ballester, W. H. Smyth, and F. Bagenal 2000b. Io's UV aurora: Detection of neutral hydrogen and neutral chlorine. *Bull. Am. Astron, Soc.* **32**, 34.06.

Rice, F. O., and C. Sparrow 1953. Purple sulfur, a new allotropic form. *J. Am. Chem. Soc.* **75**, 848–850.

Rice, F. O., and J. Ditter 1953. Green sulfur, a new allotropic form. *J. Am. Chem. Soc.* **75**, 6066–6067.

Rice, F. O., and R. B. Ingalls 1959. Absorption spectra of some active species. *J. Am. Chem. Soc.* **81**, 1856–1859.

Roesler, F. L., H. W. Moos, R. J. Oliversen, R. C. Woodward, Jr., K. D. Retherford, F. Scherb, M. A. McGrath, W. H. Smyth, P. D. Feldman, and D. F. Strobel 1999. Far-ultraviolet imaging spectroscopy of Io's atmosphere with HST/STIS. *Science* **283**, 353–357.

Sagan, C. 1979, Sulphur flows on Io. *Nature* **280**, 750–753.

Sartoretti, P., M. A. McGrath, and F. Paresce 1994. Disk-resolved imaging of Io with the Hubble Space Telescope. *Icarus* **108**, 272–284.

Sartoretti, P., M. J. S. Belton, and M. A. McGrath 1996. SO_2 distributions on Io. *Icarus* **122**, 273–287.

Saur, J., F. M. Neubauer, D. F. Strobel, and M. E. Summers 2000. Io's ultraviolet aurora: Remote sensing of Io's interaction. *Geophys. Res. Lett.* **27**, 2893–2896.

Schenk, P. W., and R. Steudel 1965. New findings in the chemistry of the lower oxides of sulfur. *Angew. Chem. Intern. Ed. Engl.* **4**, 402–409.

Schenk, P. W., and R. Steudel 1968. Oxides of sulphur. In *Inorganic Sulphur Chemistry* (G. Nickless, Ed.), pp. 367–418. Elsevier, Amsterdam.

Schneider, N. M., W. H. Smyth, and M. A. McGrath 1989. Io's atmosphere and neutral clouds. In *Time-Variable Phenomena in the Jovian System*

(M. J. S. Belton, R. A. West, and J. Rahe, Eds.), pp. 75–99. NASA SP-494, Washington, DC.

Schneider, N. M., A. H. Park, and M. E. Kuppers 2000. Spectroscopic studies of the Io torus during Galileo encounters: Remote plasma diagnostics and the detection of Cl^{++}. *Bull. Am. Astron. Soc.* **32**, 35.03.

Schofield, K., and M. Steinberg 1992. Sodium/sulfur chemical behavior in fuel-rich and -lean flames. *J. Phys. Chem* **96**, 715–726.

Shemansky, D. E. 1987. Ratio of oxygen to sulfur in the Io plasma torus. *J. Geophys. Res.* **92**, 6141–6146.

Shemansky, D. E. 1988. Energy branching in the Io plasma torus: The failure of neutral cloud theory. *J. Geophys. Res.* **93**, 1773–1784.

Shi, Y., and P. Marshall 1991. A kinetic study of the recombination reaction Na $+SO_2+$ Ar. *J. Phys. Chem.* **95**, 1654–1658.

Sill, G. T., and R. N. Clark 1982. Composition of the surfaces of the Galilean satellites. In *Satellites of Jupiter* (D. Morrison, Ed.), pp. 174–212. Univ. of Arizona Press, Tucson.

Singleton, D. L., and R. J. Cvetanović 1988. Evaluated chemical kinetic data for the reactions of atomic oxygen $O(^3P)$ with sulfur containing compounds. *J. Phys. Chem. Ref. Data* **17**, 1377–1437.

Smith, R. A., and D. F. Strobel 1985. Energy partitioning in the Io plasma torus. *J. Geophys. Res.* **90**, 9469–9493.

Smith, B. A., and 21 colleagues 1979. The Jupiter system through the eyes of Voyager 1. *Science* **204**, 951–972.

Smythe, W. D., S. Kieffer, L. Kamp, R. Lopes, S. Douté, R. Carlson, and the Galileo NIMS Team 2000. Models of volcanic plumes on Io: results and observations. *EOS* **81**, S288.

Soderblom, L., T. Johnson, D. Morrison, E. Danielson, B. Smith, J. Veverka, A. Cook, C. Sagan, P. Kupferman, D. Pieri, J. Mosher, C. Avis, J. Gradie, and T. Clancy 1980. Spectrophotometry of Io: Preliminary Voyager 1 results. *Geophys. Res. Lett.* **7**, 963–966.

Spencer, J. R., and N. M. Schneider 1996. Io on the eve of the Galileo mission. *Annu. Rev. Earth Planet Sci.* **24**, 125–190.

Spencer, J. R., A. S. McEwen, M. A. McGrath, P. Sartoretti, D. B. Nash, K. S. Noll, and D. Gilmore 1997a. Volcanic resurfacing of Io: Post-repair HST imaging. *Icarus* **127**, 221–237.

Spencer, J. R., P. Sartoretti, G. E. Ballester, A. S. McEwen, J. T. Clarke, and M. A. McGrath 1997b. The Pele plume (Io): Observations with the Hubble Space Telescope. *Geophys. Res. Lett.* **24**, 2471–2474.

Spencer, J. R., K. L. Jessup, M. A. McGrath, G. E. Ballester, and R. Yelle 2000. Discovery of gaseous S_2 in Io's Pele plume. *Science* **288**, 1208–1210.

Steudel, R., G. Holdt, and A. T. Young 1986. On the colors of Jupiter's satellite Io: Irradiation of solid sulfur at 77 K. *J. Geophys. Res.* **91**, 4971–4977.

Strobel, D. F., and B. C. Wolven 2001. The atmosphere of Io: Abundances and sources of sulfur dioxide and atomic hydrogen. *Astrophys. Space Sci.* **277**, 271–287.

Strobel, D. F., X. Zhu, and M. E. Summers 1994. On the vertical thermal structure of Io's atmosphere. *Icarus* **111**, 18–30.

Summers, M. E. 1985. *Theoretical Studies of Io's Atmosphere.* Ph.D. thesis, California Institute of Technology, Pasadena, CA.

Summers, M. E., and D. F. Strobel 1996. Photochemistry and vertical transport in Io's atmosphere and ionosphere. *Icarus* **120**, 290–316.

Summers, M. E., D. F. Strobel, Y. L. Yung, J. T. Trauger, and F. Mills 1989. The structure of Io's thermal corona and implications for atmospheric escape. *Astrophys. J.* **343**, 468–480.

Trafton, L. 2000. Search for proton aurora and ambient hydrogen on Io. *Astron. J.* **120**, 488–495.

Trafton, L. M., J. J. Caldwell, C. Barnet, and C. C. Cunningham 1996. The gaseous sulfur dioxide abundance over Io's leading and trailing hemispheres: HST spectra of Io's $C^1B_2 - X^1A_1$ band of SO_2 near 2100 Å. *Astrophys. J.* **456**, 384–392.

Tsang, S.-Y., and C. W. Brown 1975. Raman spectra of matrix isolated S_2O. Evidence of the formation of S_3 and SO_2 from S_2O. *Inorg. Chem.* **14**, 2856–2858.

Tsang, W., and R. F. Hampson 1986. Chemical kinetic data base for combustion chemistry. Part 1. Methane and related compounds. *J. Phys. Chem. Ref. Data* **15**, 1087–1279.

Vogt, R. E., W. R. Cook, A. C. Cummings, T. L. Garrard, N. Gehrels, E. C. Stone, J. H. Trainor, A. W. Schardt, T. Conlon, N. Lal, and F. B. McDonald 1979. Voyager 1: Energetic ions and electrons in the Jovian magnetosphere. *Science* **204**, 1003–1007.

Wong, M. C., and R. E. Johnson 1995. The effect of plasma heating on sublimation-driven flow in Io's atmosphere. *Icarus* **115**, 109–118.

Wong, M. C., and R. E. Johnson 1996. A three-dimensional azimuthally symmetric model atmosphere for Io. 1. Photochemistry and the accumulation of a nightside atmosphere. *J. Geophys. Res.* **101**, 23,243–23,254.

Wong, M. C., and W. H. Smyth 2000. Model calculations for Io's atmosphere at eastern and western elongations. *Icarus* **146**, 60–74.

Young, A. T. 1984. No sulfur flows on Io. *Icarus* **58**, 197–226.

Yung, Y. L., and W. B. Demore 1982. Photochemistry of the stratosphere of Venus—Implications for atmospheric evolution. *Icarus* **51**, 199–247.

Yung, Y. L., M. Allen, and J. P. Pinto 1984. Photochemistry of the atmosphere of Titan: Comparison between model and observations. *Astrophys. J. Suppl. Ser.* **55**, 465–506.

Zolotov, M. Yu., and B. Fegley, Jr. 1998a. Volcanic origin of disulfur monoxide (S_2O) on Io. *Icarus* **133**, 293–297.

Zolotov, M. Yu., and B. Fegley, Jr. 1998b. Volcanic production of sulfur monoxide (SO) on Io. *Icarus* **132**, 431–434.

Zolotov, M. Yu., and B. Fegley, Jr. 1999. Oxidation state of volcanic gases and the interior of Io. *Icarus* **141**, 40–52.

Zolotov, M. Yu., and B. Fegley, Jr. 2000a. Eruption conditions of Pele volcano on Io inferred from chemistry of its volcanic plume. *Geophys. Res. Lett.* **27**, 2789–2792.

Zolotov, M. Yu., and B. Fegley, Jr. 2000b. Eruption conditions of Pele volcano on Io inferred from chemistry of its volcanic plume. *Lunar Planet. Sci.* **31**, 2098.